Development of an electrochemical surface-enhanced Raman spectroscopy DNA

aptamer biosensor for rapid detection of protein biomarkers of disease

By

Scott Gerald Harroun

A Thesis Submitted to Saint Mary's University, Halifax, Nova Scotia
in Partial Fulfillment of the Requirements for the
Degree of Master of Science in Applied Science

27 August 2014, Halifax, Nova Scotia

Approved:	Dr. Christa Brosseau	
	Supervisor	
	Department of Chemistry	
Approved:	Dr. Jan K. Rainey	
	External Examiner	
	Department of Biochemistry & Molecular Biology	
	Dalhousie University	
Approved:	Dr. Jason Masuda	
	Supervisory Committee Member	
	Department of Chemistry	
Approved:	Dr. Timothy Frasier	
	Supervisory Committee Member	
	Department of Biology	
Approved:	Dr. Diane Crocker	
	Chair of Thesis Defence	
	Graduate Studies Representative	

Date: 27 August 2014

Table of Contents

Abstract

Development of an electrochemical surface-enhanced Raman spectroscopy DNA aptamer biosensor for rapid detection of protein biomarkers of disease

By

Scott Gerald Harroun

Electrochemical surface-enhanced Raman spectroscopy (EC-SERS) is a vibrational spectroscopic method involving detection of a target molecule at a metal nanostructured surface to which a potential has been applied. EC-SERS can lower limits of detection, even relative to SERS, which is itself an improvement over conventional Raman spectroscopy. DNA aptamers are oligonucleotides engineered to bind a target molecule with high specificity and high affinity. Advantages of using aptamers instead of antibodies to bind a target molecule include time and temperature stability, *in vitro* synthesis, ease of handling and storage, and low cost. Thiolated DNA aptamers are immobilised onto Ag nanoparticles (AgNP) by the formation of a Ag-S bond. The aptamer-modified AgNP electrodes are then used for detection of target proteins: immunoglobulin E (IgE), cytochrome c (cyt c) and catalase-peroxidase (KatG), which are all biomarkers indicative of various health conditions. IgE is produced as a response to various allergens. Cyt c is a biomarker for diseases of the liver and kidney, and KatG is a biomarker for tuberculosis. This project uses EC-SERS of aptamer-modified AgNP electrodes for detection of these biomarker proteins. The overall goal is the eventual development of a low-cost and portable point of care diagnostic device that can be used in developing nation settings, such as South Africa.

27 August 2014

Acknowledgements

List of Abbreviations

6-MHA	6-mercaptohexanoic acid
6-MH	6-mercapto-1-hexanol
11-MUD	11-mercapto-1-undecanol
12-MDA	12-merpcatododecanoic acid
2-TU	2-Thiouracil
4-ABT	4-aminobenzenethiol
5cHS	Five coordinate high-spin
6cLS	Six coordinate low-spin
A	Adenine
Ag/AgCl	Silver chloride electrode
AgNP	Silver nanoparticle
AFM	Atomic force microscopy
AIDS	Acquired immunodeficiency syndrome
Apt	aptamer
ATN	Acute tubular necrosis
ATP	Adenosine triphosphate
ATR-FTIR	Attenuated total reflection infrared spectroscopy
AuNP	Gold Nanoparticle
C	Cytosine
CAD	Canadian dollar
CE	Chemical enhancement
CV	Cyclic voltammetry or cyclic voltammogram
Cyt c	Cytochrome c
dimesna	2,2'-dithio-bis-ethanesulfonate
DMDS	Dimethyl disulfide
DMS	Dimethyl sulfide
DMSO	Dimethyl sulfoxide
DNA	Deoxyribonucleic acid
DPhDS	diphenyl disulfide
DPhS	diphenyl sulfide
DPyDS	2,2'-dipyridyl disulfide
dsDNA	Double-stranded DNA
EC-SERS	Electrochemical surface-enhanced Raman spectroscopy
EC-SERRS	Electrochemical surface-enhanced resonance Raman spectroscopy
EDC	1-Ethyl-3-(3-dimethylaminopropyl)carbodiimide
EF	Enhancement factor
EIS	Electrochemical impedance spectroscopy
ELISA	Enzyme-linked immunosorbent assay
EM	Electromagnetic enhancement
ESAT6	6kDa Early Secretory Antigen
FWHM	Full width at half maximum
G	Guanine
Hb	Hemoglobin
HCA	Hierarchical cluster analysis

HEPES	4-(2-hydroxyethyl)-1-piperazineethanesulfonic acid
HIV	Human immunodeficiency virus
ICP-MS	Inductively coupled plasma mass spectrometry
IgE	Immunoglobulin E
IgG	Immunoglobulin G
INH	Isoniazid
KatG	Catalase-peroxidase
K_D	Dissociation constant
LAH	lipoic acid histamide derivative
LAM	Lipoarabinomannan
LOD	Limit of detection
LSPR	Localised surface plasmon resonance
LSV	Linear sweep voltammetry
MAC	*Mycobacterium avium* complex
Mb	Myoglobin
MB	Methylene blue
MDR-TB	Multi-Drug-Resistant Tuberculosis
MES	2-mercaptoethanesulfonate
mesna	2-sulfanylethanesulfonate
MM	methyl mercaptide
MTB	*Mycobacterium tuberculosis*
NIR	Near-infrared
ocp	Open circuit potential
PB	Phosphate buffer
PCA	Principal component analysis
PCR	Polymerase chain reaction
PDGF	Platelet-derived growth factor
PhSH	Phenyl mercaptan
POC	Point of care
PySH	2-mercaptopyridine
PZC	Potential of zero charge
RNA	Ribonucleic acid
rpm	Rotations per minute
RR	Resonance Raman
RT-PCR	Reverse transcription polymerase chain reaction
SAM	Self-assembled monolayer
sat.	Saturated
SELEX	Systematic evolution of ligands by exponential enrichment
SERS	Surface-enhanced Raman spectroscopy
SERRS	Surface-enhanced resonance Raman spectroscopy
SPE	Screen printed carbon electrode
ssDNA	Single-stranded DNA
SWV	Square wave voltammetry
T	Thymine
TB	Tuberculosis
TBA	Thrombin binding aptamer

UN	United Nations
USD	United States dollar
UV	Ultraviolet
UV-vis	Ultraviolet-visible
WHO	World Health Organization

List of Figures

List of Tables

Chapter 1: Introduction

1.1 Preamble

Tuberculosis is a global health problem that affects many people around the world, particularly in Sub-Saharan Africa. In fact, it is second only to HIV/AIDS in terms of deaths caused by a single infectious agent. The main diagnostic method used for low-resource settings is smear microscopy. Due to the long wait times for providing a result to the patient, many simply abandon their treatment and carry on with their lives, spreading tuberculosis to their family and co-workers.

By developing an aptamer-based biosensor using electrochemical surface-enhanced Raman spectroscopy (EC-SERS), it may be possible to provide a rapid diagnosis to the patient at the point of care, drastically reducing wait times and the need for a laboratory-based diagnostic method. EC-SERS is well suited for this sort of analysis, because the technology can readily be made portable. Furthermore, aptamer-based biosensors have many advantages, particularily over traditional antibody-based biosensors, including high binding affinity, low cost, longer shelf life and resistance to high temperature.

1.2 Objectives of this thesis

The overall goal of this project is to develop a DNA aptamer-based EC-SERS biosensor for rapid detection and diagnosis of tuberculosis at the point of care, particularily in developing nation settings. Within the thesis itself, the following goals were targeted:

- Aptamer-based detection of target proteins using their respective aptamers.

- Detection of immunoglobulin E (IgE) and cytochrome c (cyt c) using aptamers already available in the literature.

- Detection of the tuberculosis biomarker protein catalase-peroxidase (KatG) using an aptamer developed by the Blackburn group at the University of Cape Town.

- Detection of target proteins using EC-SERS as a primary method, along with cyclic voltammetry as a supplimentrary method.

- Optimisation of the aptasensor.

- Control studies with non-target proteins.

- Detection of proteins in the nanomolar to picomolar range.

1.3 Scope of this thesis

This thesis consists of eight chapters. Chapter 1 introduces the project and states its objectives and scope. Chapter 2 consists of a literature review of tuberculosis, point of care diagnsotics, SERS and DNA aptamers for biosensing, and an overview of the target proteins. Chapter 3 provides background theory for the spectroscopic and electrochemical methods used for analysis, along with DNA aptasensor development (SELEX, sulfur-

metal bonding and alkanethiol backfilling). Chapter 4 lists the instrumentation and reagents used, along with experimental procedures.

Experimental results are presented in Chapters 5 and 6. In Chapter 5, the two model proteins are discussed: IgE and cyt c. The chapter begins with attempted EC-SERS detection of IgE, followed by electrochemical and ATR-FTIR detection. Next, cyt c is detected using EC-SERS and CV. The aptasensor is optimised, followed by control studies, quantitative detection and detection in synthetic urine. In Chapter 6, preliminary experiments for detection of KatG are presented. Lastly, conclusions and future work are presented in Chapters 7 and 8, respectively.

Chapter 2: Literature Review

2.1 Introduction

The purpose of this section is to first provide the reader with a general overview of the state of tuberculosis infection around the world, particularly in sub-Saharan Africa. The role of point of care (POC) diagnostics to meet the need for rapid diagnosis of tuberculosis is discussed. The advantages of using DNA aptamers compared to antibodies for detection are explored. A survey of the literature of aptamer-based detection focuses on SERS and electrochemical methods. The target proteins for this study, cytochrome c (cyt c), catalase-peroxidase (KatG) and immunoglobulin E (IgE) are discussed, along with previous Raman and electrochemical characterisations and aptamer-based detection strategies used for other proteins.

2.2 Tuberculosis

Tuberculosis (TB) is caused by *Mycobacterium tuberculosis* (MTB), a bacterium. Typically, MTB bacteria will attack the lungs, but can also attack any part of the body, including the kidney, spine and brain. TB is a serious disease that is fatal if not treated properly. TB spreads through the air from one person to another; the various modes of transmission of TB bacteria into the air from a person infected with TB in the lungs or throat can include coughing, sneezing, singing or simply sbanding. TB cannot be spread by shaking someone's hand, sharing food or drink, touching bed linens or toilet seats, sharing toothbrushes or kissing [1].

There are two types of TB-related conditions: latent TB infection and TB disease. Latent TB infection occurs when people breathe in TB bacteria and become infected, but their body is able to prevent the bacteria from growing. Latent TB infection occurs for most people who become infected, and the bacteria live in the body without making people feel sick or causing other symptoms. Those who have latent TB infection cannot spread TB bacteria to others. However, if the TB bacteria become active in the body and the host immune system is unable to stop them from multiplying, the bacteria can cause active TB disease [1]. People with TB disease will exhibit symptoms such as a bad cough that lasts three weeks or longer, cough with sputum (phlegm) and blood, chest pain, loss of appetite, weakness or fatigue, weight loss, fever, chills and night sweats [1-2]. TB infection can become TB disease within a few weeks, or it can remain latent for years until the immune system becomes comprised for another reason, such as due to HIV infection [1].

Tuberculosis is one of the major health concerns worldwide, which often goes relatively unnoticed in developed nations. In 2006, the majority of new TB cases were in Southeast Asia, but the highest incidence and mortality rate occurs in sub-Saharan Africa. Multi-Drug-Resistant Tuberculosis (MDR-TB) is a cause for the growing number of cases of TB in Eastern Europe [3]. TB is second only to HIV/AIDS as the greatest killer worldwide due to a single infectious agent. For example, in 2012, 8.6 million people became infected with TB, and 1.3 million died from TB infection. Over 95% of these deaths occurred in low- and middle-income countries. Furthermore, it is among the top three causes of death for women aged 15 to 44 in developing countries. In the same year,

approximately 530,000 children were infected with TB, including 74,000 non-immunocompromised (HIV-negative) children who died from it. Due to their weakened immune system, TB is one of the leading killers of people infected with HIV, for whom it is the cause of one fifth of all deaths [2].

There are some good signs, however. The estimated number of people becoming ill each year with tuberculosis is declining, albeit at a very slow rate. The TB death rate dropped by 45% between 1990 and 2012, and an estimated 22 million lives have been saved through the use of DOTS (Directly Observed Treatment, Short-Course) and the Stop TB Strategy. Both programmes are recommended by the WHO [2]. As an example, much success in the fight against TB has been achieved in Cambodia. Twenty years ago, Cambodia had one of the highest rates of TB, along with a healthcare system weakened by poverty and conflict. The situation was drastically improved by transitioning from a hospital-based system to one at the level of primary healthcare centers. Data has shown that from 2002 to 2011, the Cambodian rate of TB infection decreased from 15.1 to 8.17 per 1000 people. Cambodia is now on track to meet the UN Millennium Development Goal of halving the prevalence and mortality of TB by 2015, compared to 1990 levels [4]. Nonetheless, TB remains a major global health problem.

Certain risk factors make someone more likely to develop TB disease if infected with TB bacteria. These factors include HIV infection, recent infection with TB bacteria (<2 years), abuse of alcohol or drugs, incorrect treatment of TB in the past, or other health problems than can affect the immune system, such as diabetes [1]. Among these

factors, co-infection with HIV stands out as the biggest concern. TB and HIV are both major public health issues in Sub-Saharan Africa, and often these two diseases occur together. In 2012, at least one third of people living with HIV were also infected with latent TB [2]. Moreover, people living with HIV and latent TB are 30 times more likely for it to develop into active TB disease, compared to people without HIV [2]. Together, TB and HIV form a deadly combination, where each disease speeds the progress of the other. For example, someone who is infected with both HIV and TB is more likely to become sick with active TB, and in 2012 about 320,000 people died of HIV-associated TB. In 2012, there were approximately 1.1 million new cases of HIV and TB together; 75% of these people were living in Africa [2].

A study in the Khayelitsha township, near Cape Town, South Africa has found that there are numerous advantages to the integration of TB and HIV primary care. Benefits include the merging of patient folders currently kept at separate locations, better contact between caregivers, optimization of human and financial resources, and improved overall care for patients. One drawback is the increased contact between patients with active TB and highly susceptible HIV-infected patients [5]. Surely such risks can be mitigated by developing a portable point-of-care device, where testing and diagnosis can be brought to the patient. Moreover, the eventual development of a multi-targeted device could be used to test simultaneously for TB, HIV and other infectious diseases, thereby saving resources in terms of labour and equipment.

2.3 Point of care diagnostics

Point of care (POC) diagnostics allow the test to be undertaken at wherever the patient is to be treated; be it a hospital, local clinic or their own home. POC devices are typically cost effective, provide a rapid result, and are portable and simple to use. Commonly used POC diagnostic methods include blood glucose monitors and home pregnancy tests. While POC testing can sometimes cost more than traditional laboratory based methods of detection, POC tests have the potential to indirectly lower medical costs, and allow for rapid life-or-death decision making. Consider hospital admissions, where a suspected myocardial infraction could be determined rapidly to be simple indigestion. Similarly, home diagnosis for streptococcal pharyngitis (strep throat) in children would save many doctor visits, and reduce transmission. Accurate *and* rapid distinction between rhinoviral and upper respiratory bacterial infections would diminish the untold numbers of antibiotic prescriptions that are written inappropriately; a widespread practice which contributes to antibiotic resistance. Novel POC testing methods are also being developed specifically for resource-limited settings that use microfluidics without moving parts or power sources, passive capillary force or active suction to replace pump or injection components, paper patterned with hydrophobic material to allow precise control of flow, electrochemical measurement on paper-based devices, transport of fluid through thread by capillary action, and measurements made with widely available electronics, such as mobile phones, portable music players or laptops, without additional modifications [6]. In all of these cases, relatively cheap (i.e. paper) and widely available and portable technology (i.e. mobile phones) are used instead of highly specialised and expensive laboratory equipment.

POC diagnostics have great potential to improve healthcare for the treatment of infectious diseases, particularly in low resource settings. These regions typically have inadequate infrastructure, and access to quality and timely medical care is often a challenge. POC testing can often be simple enough to be used at the primary care level and in remote settings that lack a laboratory. Additionally, such tests will allow patients to test themselves in the privacy of their own homes, which is well-suited for stigmatised diseases such as HIV [7]. There is no universally accepted definition of point of care diagnostic testing, but some agreed upon critical elements include rapid disease determination and communication of results to guide clinical decisions, and completion of testing and follow-up measures at the same clinical encounter. "Rapid" can range from seconds to several hours, but could be best described as "while the patient waits". It has also been recognised that POC testing can occur over a continuum of settings of increasing complexity: homes, community centres, local clinics, peripheral laboratories and hospitals. In all of these settings, the use of a central laboratory is not required [7].

Smear microscopy remains the most commonly used method for TB diagnosis in TB endemic countries. The method is fast if a microscope is available, relatively cheap and has high specificity. However, it has low sensitivity (ca. 50-60%), and it is even less sensitive in children, patients co-infected with HIV, and in patients with extrapulmonary TB. The method can be improved by using a fluorescent molecule for staining, but this step significantly increases the costs [8].

One major concern about conventional laboratory testing for TB (smear microscopy and culture) is that long turn-around times (typically weeks) and delays to diagnosis result in patients who end up abandoning testing and/or treatment [7-8]. This concern has been investigated in the Ntcheu District of Malawi. This region had previously been assessed to have access to adequate healthcare and laboratory facilities. Despite this relatively good situation, 19 of 157 new smear-positive TB patients did not continue with medical treatment. The interviewers were able to locate 5 of the patients, along with 14 caregivers for those who had died. The respondents said that a major factor contributing to illness and death was the delay for receiving the sputum smear results. Some did not even receive the result until several days, or even weeks, *after* the patient had died. This statement was confirmed by healthcare workers, who could attest to the difficulties in transporting samples and communicating the results. For others, challenges included travel costs to and from the hospital, fear of death in the hospital and inability to cover additional expenses incurred at the hospital, such as food and drugs. Since many people who live in sub-Saharan Africa do not have their own private transportation, it is often the case that the patient is brought to the hospital carried on someone's shoulder, in a stretcher, or on a bed tied to a car or bus, since there is no other option available. Furthermore, other patients state that they could not be admitted to the hospital without a family member who could stay there to care for their needs. Another barrier to treatment was the stigma of the association of TB with HIV/AIDS. National guidelines in Malawi recommend that smear-negative patients with persistent symptoms be assessed by chest radiography. Despite that fact that a functioning and free X-ray service is available at the hospital, and that the quality of laboratory results had

been independently verified, patients with persistent symptoms were often deemed to have unreliable false-negative laboratory results [9].

It is imperative for a device to be developed for the rapid detection and diagnosis of TB at the patient point of care. It has also been noted that improved accuracy of diagnosis will replace treatment based on empirical evidence, which will reduce unnecessary treatment and exposure to expensive drugs and their side effects [8].

The polymerase chain reaction (PCR)-based device Xpert MTB/RIF is being implemented in many countries for TB testing. A recent study has conducted a comprehensive analysis of the instrument. It was determined that its use at the point of care by non-specialised personnel is feasible; its use led to higher rates of treatment initiation, lower rates of patient dropout, and lower rates of empirical-evidence-based patient dropout compared to when smear-microscopy and chest radiography are available [10]. When testing was done using smear microscopy, 67% of patients began treatment on the same day. This number improved to 90% when Xpert MTB/RIF was used [8]. However, several drawbacks were also associated with the device, including no clinically important changes in long-term morbidity and cost effectiveness [10]. It has been noted that the placement of very expensive equipment in healthcare facilities in rural Africa will be a very difficult task. Such locations often have unreliable electricity or none at all, and poorly trained, underpaid and often illiterate staff [11]. The instrument itself is expensive, costing $17,000 USD, and even with a reduced price for low resource settings, each cassette for analysis still costs about $10 [8, 11]. Furthermore, maintaining the

device has also been an issue, since repair technicians may not be available. According to the Bill and Melinda Gates Foundation, the average yearly budget for individual healthcare clinics in South Africa is around $5000 [12]. Testing large volumes of people with suspected tuberculosis will put substantial pressure on already financially strained healthcare systems [11]. Additionally, there is still room for improvement in the sensitivity of the device, as shown in Table 1.

Table 1. Reported sensitivity of Xpert MTB/RIF TB diagnosis method [8].

Patient Type	Approximate Sensitivity
Smear-positive	98%
Smear-negative	75%
Smear-negative, HIV-positive	50%

The Xpert MTB/RIF method of detection cannot diagnosis isoniazid-resistance. Isoniazid is a commonly used drug for treatment of tuberculosis that is ineffective against Multi-Drug-Resistant Tuberculosis (MDR-TB). It is imperative to note that in some settings, 80% of MDR-TB is transmitted person-to-person [8]. MDR-TB has been detected in nearly all countries surveyed [2]. There is no doubt that accurate and rapid TB diagnosis is critical for stopping the stopping transmission of the disease and saving lives.

Sputum samples are used for smear microscopy testing for TB. However, this method does not work for patients who do not produce sufficient sputum, such as those who are HIV-positive and children, both of which exhibit a resulting smear-negative analysis. For this reason, attention has been focused on other biological samples that are more readily available, such as exhaled breath, stool, blood and urine. In particular, urine

is attractive because it is sterile, has a less complex matrix compared to sputum or serum, and TB-specific proteins and DNA can be found in the urine of infected patients. In addition, urine is simpler to collect, collection is pain free and safer for low resource settings, where sanitary collection of blood may not be possible. [8, 13]. A recent study in KwaZulu-Natal, South Africa examined a commercially available lateral-flow assay 'strip test' for the detection of the TB biomarker lipoarabinomannan (LAM) in urine samples from newly-diagnosed HIV-infected adults. It was found that the method gave similar results to sputum smear microscopy, and suffered from low sensitivity when used alone, but there was improved sensitivity when the two methods were used together [14]. Surely, an improvement in detection strategies for TB biomarkers in urine can improve patient outcomes.

2.4 Surface-enhanced Raman spectroscopy for biosensing

Raman spectroscopy, which is based on inelastic scattering of light, is a useful method for biosensing due to its ability to analyse aqueous samples. Its limitations, such as weak signal intensity, can be improved by using surface-enhanced Raman spectroscopy (SERS), which is an ideal technique for a device for rapid diagnosis of TB at the POC. Raman spectroscopy is a similar and complimentary method to infrared spectroscopy (IR). Both IR and Raman spectroscopy provide a molecular fingerprint for a target molecule, which is useful for detection in a complex sample. One benefit of using Raman spectroscopy over IR is that it is possible to analyse aqueous samples, which is more difficult to do using IR, due to the strong absorption band of water. One detriment, however, is that Raman spectra of dilute samples are typically very weak or non-existent

due to the inherently weak Raman scattering effect. Collection of Raman spectra on a metal nanostructured surface, typically Ag or Au, allows for significant signal enhancement; giving rise to the name surface-enhanced Raman spectroscopy. Linking a receptor (antibody or aptamer) onto the SERS-active surface allows for separation and detection of a target molecule in a complex sample. Further details regarding SERS are provided in Chapter 3.

2.5 DNA aptamers for biosensing

Biosensors typically have two elements: a biological recognition elements (enzymes, antibodies, receptors, etc.) and a transducer or signalling component (optical, electrochemical, etc.) [15-16]. Aptamers are specific nucleic acid sequences, typically DNA, that bind target molecules with high specificity and high affinity. Biosensors that use aptamers as their biorecognition element have been called "aptasensors". In fact, aptamers have even been described as "chemical antibodies" [15]. Indeed, the very name "aptamer" comes from the Latin *aptus,* which means "to fit" [17]. The following pages give a brief overview of why aptamers are advantageous over antibodies, followed by a survey of the literature of SERS and electrochemical based aptasensors. The theory and methodology for the Systematic Evolution of Ligands by Exponential Enrichment (SELEX) process for the selection of aptamers against target molecules is covered in Chapter 3. A diagram showing the widespread use of aptamers for various applications is shown in Figure 1.
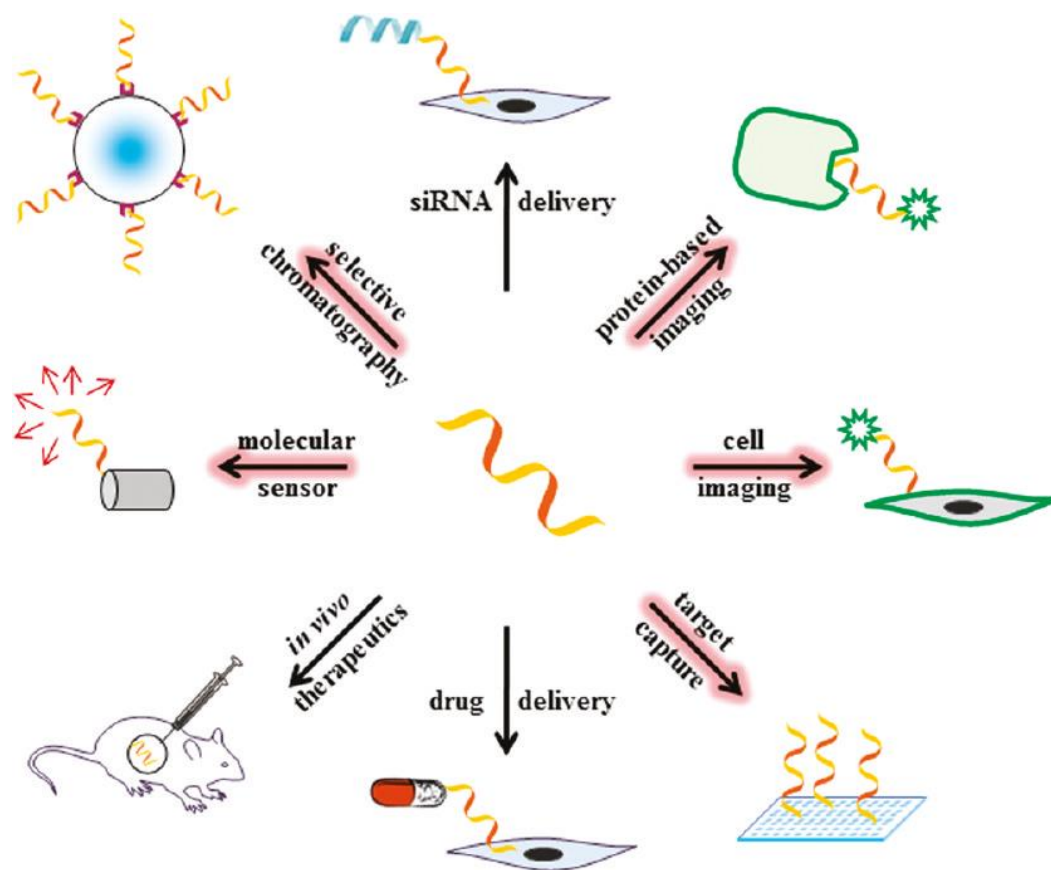
Figure 1. Use of aptamers for numerous analytical and biological applications. Bioanalytical applications of aptamers are highlighted Reprinted with permission from Anton B. Iliuk, Lianghai Hu, and W. Andy Tao, *Anal. Chem.* **2011**, *83*(12), 4440-4452. Copyright 2011 American Chemical Society.

2.5.1 Aptamers versus antibodies

Antibodies are very commonly used for biosensing, including both research and commercial applications [16, 18]; however, there are many advantages to using aptamers instead. Aptamers can be synthesised *in vitro*, while antibodies must be made *in vivo,* usually using cell lines or live animals [15, 19]. As a result, it is difficult if not impossible

to generate antibodies for molecules that do not generate an immunogenic response in the host or for molecules that are highly toxic [15-16, 19-20]. Aptamers can be generated for any target, including inorganic ions, amino acids, small organic molecules, nucleic acids, metabolites, drugs, proteins and whole cells/organisms [15-16, 19-20]. Additionally, *in vivo* synthesis of antibodies can suffer from batch-to-batch variation [16, 19]. Once the aptamer sequence has been identified, it can be mass produced with a high degree of uniformity [15-16, 18]. Aptamers can be designed to work best under highly specific conditions, such as in a non-physiological buffer [19], high temperature or extreme pH [15], or for *in vivo* detection strategies since aptamer-based sensors typically generate low immunological response in the host organism [18]. Aptamers can have high specificity and affinity [15-16, 18-19] that can surpass even that of antibodies [20]. Aptamers can be handled much more easily, have a longer shelf-life and typically have overall greater stability than antibodies, which are sensitive to temperature and subject to irreversible denaturation [15-16, 18-19]. Denatured aptamers can be easily regenerated and reused without losing their binding capacity [18]. Additionally, due to their relatively simple structure (compared to antibodies), aptamers can be modified as needed for specific applications, such as adding reporter molecules or tags, or incorporating a sulfur atom for immobilisation onto a metal surface [15-16, 19]. Self-assembled monolayers (SAM), such as thiolated DNA aptamers, are seeing increased use for electrochemical biosensors [21]. Due to their small size, aptamers may achieve a higher surface density when immobilised onto a substrate [16]. Lastly, while the SELEX process to generate aptamers can take 2 to 3 months, generation of antibodies can take much longer, requiring at least 3

to 6 months [22]. Once the ideal sequence is identified, chemical synthesis of the aptamer can be completed in just a few hours.

While touting the many benefits of aptamers over antibodies, it is also important to consider the disadvantages and areas needing further exploration associated with aptamer based biosensing. The majority of aptamers developed have been DNA aptamers, but RNA aptamers have also been explored. RNA aptamer stability is an issue, but modified bases could be used to overcome this problem. So far, few aptamer studies have been relevant for clinically important targets. Aptamer-based biosensing needs to move from proof-of-concept studies to real world applications. More detailed characterisation of DNA aptamers and a better understanding of the fundamental chemistry of aptamer-target binding are also needed to move toward practical developments. DNA is highly negatively charged, which can allow for non-specific electrostatic interaction with non-target molecules [16]. Additionally, aptamers can be vulnerable to nuclease attack. Aptamer stability can be improved by chemical modification, but such changes can impact the affinity and specificity of the aptamer for its target [20].

2.5.2 Label-based SERS aptasensors

The scope of this project does not include sensors employing SERS labels. Nonetheless, there has been much work in the area of DNA aptamer SERS biosensing using label-based assays, and as such it is worth reviewing. SERS is a distance-dependant phenomenon; the closer a molecule is to the metal nanostructured surface, the

more intense its SERS signal will be. Label-based methods often rely on a conformational change of the DNA aptamer after binding to the target molecule. A Raman label (reporter) molecule is attached to the aptamer, and its signal intensity changes when the change in conformation (after binding the target molecule) brings the label molecule closer to/further away from the surface. In other designs, the reporter molecule is displaced entirely from the aptamer. The choice of Raman reporter molecule is important because it must give an intense and distinct SERS spectrum. Common Raman reporter molecules include cyanine dye (Cy5) and methylene blue (MB).

In one recent study, an aptasensor was developed for the detection of cocaine in aqueous solution. When the aptamer binds the cocaine molecule, the change in conformation of the oligonucleotide brings a tetramethylrhodamine moiety (Raman reporter) closer to the Ag surface, thereby increasing its SERS signal intensity [23]. Another aptamer-based method for detection of adenosine has been reported. A gold nanoparticle (AuNP) is decorated with 4-aminobenzenethiol (4-ABT), and attached to the end of the aptamer. A change in conformation after binding adenosine brings the 4-ABT-AuNP into close proximity with the Au surface, thereby increasing the SERS signal intensity of 4-ABT [24]. In another study, a method for the detection of adenosine triphosphate (ATP) has been developed. dsDNA is attached to a AuNP with the Raman reporter molecule malachite green isocyanate, which gives a strong SERS signal. Introduction of ATP to the system displaces one strand of ssDNA from the dsDNA connected to the AuNP-Raman reporter, while the ATP binds to the remaining

immobilised ssDNA strand. The decrease in SERS signal is proportional to the amount of ATP present [25].

Another study reports placing the label on the target molecule instead of the aptamer. In this case, the target hormone vasopressin was labelled with 5-carboxytetramethylrhodamine. This method uses large-area Raman mapping and aptamer functionalised Au nanopillars to detect vasopressin in the picomolar concentration range [26]. While a very good biosensing assay for vasopressin was developed, the labelling step makes such a methodology impractical for cost-effective point-of-care and portable biosensing.

Thrombin is a commonly used model protein for aptasensors, and several label based methods have been reported for its detection. One surface-enhanced resonance Raman spectroscopy (SERRS) study for detection of thrombin used methylene blue (MB) attached to the thrombin binding aptamer (TBA). Introduction of thrombin displaces the aptamer from the surface, thereby decreasing the SERRS signal of MB [27]. A similar methodology was used with Au nanowires and the Raman reporter molecule Cy5, which resulted in a 10x lowering of the limit of detection. Additionally, this aptasensor could also be used for detection of Pb^{2+} and Hg^{2+} ions [28]. Finally, another report takes advantage of the electrostatic interaction between thrombin binding aptamer and crystal violet. An increase in thrombin concentration was found to cause an increase in the crystal violet SERS signal [29].

"Sandwich" type aptasensors have also been developed. This sort of assay first uses aptamers to bind the target molecule to a surface (heterogeneous type) or colloidal nanoparticle (homogeneous type). Another nanoparticle modified with both aptamer and the Raman reporter is then introduced to the system. This modified nanoparticle then binds the previously immobilised aptamer-target complex, thereby creating a sandwich. One study uses both heterogeneous and homogeneous style systems with the Raman reporter 5,5-dithiobis(2-nitrobenzoic acid) to detect staphylococcal enterotoxin B. Interestingly, this study uses an aptamer composed of amino acids instead of nucleic acids [30]. Other sandwich aptasensors of the heterogeneous and homogeneous styles have been developed for detection of thrombin [31-32]. Finally, another aptasensor of the homogeneous style used aptamer-modified magnetic nanoparticles in solution, which avoids the potentially time-consuming step of immobilisation onto a surface. The magnetic sandwich is then collected on the wall of a PCR tube using a magnet, for which SERS spectra are then collected for the Raman reporter molecule [33].

2.5.3 Label-free SERS aptasensors

Direct, or label-free, SERS-based detection using aptamers offers numerous advantages over indirect methods. Instead of detecting the strong SERS signal of the Raman reporter molecule, the spectral change based on the detection of the analyte molecule is observed directly. Changes in the spectrum can be based on changes in aptamer conformation identified by changes in band position or intensity, or identification of distinct spectral features of the target molecule itself [34-36]. SERS can provide an advantage in multiplexed biosensing because Raman bands typically have

narrow spectral bandwidths, which minimises overlap between multiple banda. One of the great benefits of Raman spectroscopy and SERS is that the spectrum provides a unique chemical fingerprint for identification of the target molecule. Label-free methods also tend to have less preparation steps, and therefore take less time for analysis. Additionally, due to the enhancement effect of the metal nanostructured surface, a high signal response can be generated for a small amount of analyte [37]. Label-based methods can also be problematic because the label can affect the active site of a biomolecule, which often results in a need for additional efforts to increase the specificity of the sensing method (aptamer or antibody) [38]. The labelling modification step can also be costly. These advantages directly relate to label-free biosensing using SERS; general benefits of SERS are covered in later sections.

While there are many benefits, there are also some disadvantages associated with label-free SERS-based biosensing that are worth noting. SERS is a surface phenomenon; therefore, target molecules must be adsorbed onto the surface. Molecules with high affinity for surfaces, such as thiols, will easily be detected since they readily stick to the metal surface. The same cannot be said for all molecules. Fortunately this issue is overcome by the high affinity of the target molecule for its specific aptamer, which after immobilisation essentially *is* the surface. Another inherent drawback of label-free SERS detection is the small Raman cross section of some analytes. While most molecules should be able to produce SERS signal since most have Raman-active vibrations, not all molecules give *good* SERS spectra. For some analytes, it is simply not possible to detect them at low concentration due to poor light scattering [39]. High laser power can be used

to compensate for low signal intensity, but the increase in power can also cause degradation of the sample [36]. Lastly, there is also the balance of sensitivity and reproducibility. SERS "hot spots" can give extreme signal enhancements, but they tend to be highly localised. This concern is not just limited to label-free biosensing. Development of novel plasmonic nanostructures with both high SERS enhancement and structural reproducibility will therefore play an important part in the future of label-free SERS-based biosensing [39].

Negri *et al.* have published several recent papers where they have used SERS for direct detection of the binding of influenza nucleoprotein to its DNA-aptamer. In their studies, the aptamer-covered substrate was treated with buffer and control virus nucleoprotein (respiratory syncytial virus, RSV), which resulted in no significant spectral differences when compared to the bare aptamer. However, when treated with influenza nucleoprotein, significant spectral differences were observed. Some differences were indicative of a change in conformation, such as changes in band wavenumber and intensity relative to other bands. Additionally, new bands were observed that were associated with protein. The binding of the influenza nucleoprotein by the DNA-aptamer is further validated by the use of AFM to monitor changes in surface morphology after being the target protein. Lastly, the authors used principal component analysis (PCA) scores and dendrograms produced by hierarchical cluster analysis (HCA), which were able to distinguish between aptamer spectra with and without protein with 100% accuracy [34, 40].

In another notable SERS study, Neumann *et al.* reported direct detection of platelet-derived growth factor (PDGF) and cocaine. In their study, it was observed that DNA-aptamer spectra are very reproducible, even after exposure to control molecules. However, treatment with the target molecule resulted in significant spectral differences. Moreover, these differences were found to be irreproducible. They propose that these differences are based on the variation of conformations that can occur in the SAM of the DNA-aptamer after treatment with the target molecule. Differing results were obtained for the two systems used in their study. Anti-PDGF aptamer and anti-PDGF treated with lysozyme showed no spectral change, while significant differences were observed when anti-PDGF was treated with PDGF protein. Similarly, the anti-cocaine aptamer gave highly reproducible spectra. However, spectral irreproducibility was observed after the system was treated with cocaine, benzocaine and caffeine. Nonetheless, the spectral differences observed when the aptamer was treated with cocaine were greater than when it was treated with the two non-target analytes, suggesting greater binding of cocaine than the other species [41].

Recent studies demonstrate the usefulness of SERS for detection of the binding of target molecules to DNA-aptamer in complex media. In one study, an aptamer-based SERS method of detection is used to detect ricin B chain in fruit juices and milk. Ricin is a protein toxin that can be used as a bioterror agent. The A chain is responsible for enzymatic activity; the B chain is responsible for delivering the former into the target cell. Similar to the previously mentioned studies, this method of detection is based on interpretation of spectral differences before and after binding of the target molecule by

the aptamer. They also report that if the aptamer is functionalised onto the SERS substrate beforehand, and then the total analysis time is less than 40 minutes [42]. In a follow up report, a better aptamer sequence for ricin was developed. Not only was the method better than the previous report, but it also was superior to a commercially available ELISA kit for detection of ricin [43]. In a more recent study, the authors used a similar method to detect *Bacillus anthracis* (anthrax) spores in orange juice. The aptamer sequence they used had previously been found to also bind similar bacterial spores. In their study, *B. mycoides* was used as a non-target spore. While the aptamer did bind this non-target analyte, they reported a spectral difference between *B. anthracis* and *B. mycoides* that could be distinguished by PCA [44]. Their work highlights the ability of SERS to generate a molecular fingerprint for each chemical species. Similar methodologies were also used in another study. In this case, a single aptamer was used for SERS detection of four pesticides in apple juice [45]. Another group has also reported aptamer-based SERS detection of the commonly used organophosphate insecticide malathion in tap water [46]. Another group has reported a microfluidic SERS aptasensor for detection of the nephrotic mycotoxin ochratoxin A, which poses a public health risk because it has been detected in foods. Their method demonstrates how SERS aptasensors can be designed such that only a very small sample volume is required, which is relevant to point-of-care and portable diagnostics [47].

Another series of papers studied the thrombin binding aptamer (TBA). In one study, both TBA and thiolated TBA on AgNPs were characterised by normal Raman spectroscopy and SERS. In this work, it was found that the thiolated and non-thiolated

aptamer gave similar spectra. However, they found that SERS spectra for both are markedly different from their Raman spectra [48]. Two reports highlight the use of this aptamer for direct SERS detection of thrombin. In both studies, bands characteristic of protein are observed, which are distinct from the SERS spectra of the nucleic acid aptamer. When a control protein was introduced, no significant spectral changes were observed [35-36].

2.5.4 Electrochemical methods

Electrochemical aptasensors are prepared in a similar manner to those used for SERS-based detection. Typically the thiolated aptamer is immobilised onto a Ag or Au surface by formation of a covalent M-S bond. To prevent non-specific adsorption of non-target and matrix molecules onto the surface, an alkanethiol blocking molecule is often used to fill any gaps on the surface not covered by the aptamer SAM. Electrochemical aptasensors are typically based on three types of changes: configurational change, conformational change and conductivity change. Configurational change systems are based on the assembly or dissociation of the aptamer. Examples for each include the formation of a sandwich structure (aptamer-analyte-aptamer) or the elimination of previously formed intramolecular Watson-Crick interactions resulting in a change from dsDNA to ssDNA, respectively. Systems based on conformational change have a simpler design, since the only change occurring is a conformational change of the aptamer after binding. These systems are advantageous because they can usually be used for repeat measurements, but they are disadvantageous because this type of biosensor only works if the aptamer undergoes significant conformational change upon binding the target

molecule. Finally, systems based on conductivity change, as their name suggests, are based on a change in conductivity of the aptamer before and after binding the target molecule [18].

In one report, cyclic voltammetry (CV) was used for detection of the protein lysozyme. A SAM of thiolated DNA aptamer is immobilised onto the Au working electrode, followed by adsorption of the blocking molecule 6-mercapto-1-hexanol. Detection of lysozyme is based on changes in CV measurements before and after binding the protein. Two redox probe ions were explored: $[Fe(CN)_6]^{3-}$ and $[Ru(NH_3)_6]^{3+}$. When $[Fe(CN)_6]^{3-}$ was used, the current of the aptamer-protein complex was greater than just the aptamer alone. However, reproducible results could not be obtained. When $[Ru(NH_3)_6]^{3+}$ was used, it was possible to make quantitative measurements. Electrostatic interaction allows the positively charged $[Ru(NH_3)_6]^{3+}$ to balance the three negatively charged phosphate residues at physiological pH. As a result, binding of the positively charged lysozyme neutralises some of the negatively charged phosphate backbone, thereby allowing $[Ru(NH_3)_6]^{3+}$ to bind only where lysozyme has not. This change in the surface chemistry results in a decrease in the measured current [49].

Another study used a similar setup for detection of the cancer biomarker protein angiogenin. In this case, the redox probe was $[Fe(CN)_6]^{3-}$. The method of detection used was square wave voltammetry (SWV), but the binding step was also confirmed by CV and electrochemical impedance spectroscopy (EIS) measurements. This method was found to have a good linear range from 0.01 to 30 nM. Control proteins at 100 nM

concentration (lysozyme, thrombin and Hb) were found to give very minimal change in signal. Additionally, this method was able to reproduce the results for clinical samples with high accuracy [50]. A similar system was prepared for detection of lysozyme, but instead impedance spectroscopy was used for analysis [51].

2.6 Target proteins

The three target protein systems studied in this project were immunoglobulin E, cytochrome c and catalase-peroxidase. The following sections give a brief overview of their role in human disease, and previous methods to detect these proteins using aptamer-based assays.

2.6.1 Immunoglobulin E

The immunoglobulin E (IgE) antibody is among the first molecules produced by the immune system in response to antigens that cause asthma and allergies. IgE production is increased during allergic reactions [52]. In healthy people, the concentration of IgE in serum is about 150 ng/mL. Certain parasitic diseases and hyper-IgE syndrome may cause its concentration to increase by up to three orders of magnitude. The concentration of IgE is about 10 times higher than the normal level for individuals with increased risk of developing allergies, and its concentration increases by 1000x for individuals who are showing symptoms of allergic reaction [53]. Accordingly, detection of IgE antibody may be useful for clinical analyses.

The sequence of the anti-IgE aptamer for binding human IgE protein was first reported by Wiegand *et al.* [54]. It has been named D17.4, but herein it will also be identified as anti-IgE. The structure of the anti-IgE aptamer has been thoroughly investigated by Katilius *et al.* [55]. Anti-IgE aptamer has been used for detection of IgE by various methods, including: quartz crystal microbalance [56-57], atomic force microscopy [58], surface plasmon resonance [59], fluorescence spectroscopy [60-61], impedance spectroscopy [62] and various voltammetric methods including sandwich assays [63-64] and electrochemical systems [65-68].

Some studies have used the standard D17.4 aptamer, while others use the sequence (D17.4ext) developed by Liss *et al.* which has an extension of four base pairs on the stem to increase the stability of the aptamer and its affinity for IgE [56]. In one report Khezrian *et al.*, the extended variant of anti-IgE is immobilised onto the electrode surface. Methylene blue (MB) was intercalated via specific interaction with the guanine bases of the aptamer. Binding of IgE by the aptamer releases the MB, which results in a decrease in band current measured by differential pulse voltammetry. Minimal non-specific interaction with control proteins was observed. Additionally, it was possible to detect IgE in serum samples, and measured concentrations were in agreement with analysis by ELISA [65]. In another report by Lee *et al.*, the standard D17.4 aptamer (ssDNA) binds competitively with IgE and the complementary DNA sequence of the aptamer. The complementary DNA strand has an additional guanine-rich section, which allows for intercalation with methylene blue. After binding, the biosensor is treated with MB. The measured current by square wave voltammetry (SWV) is equivalent to the

amount of intercalated DNA, which decreases as more IgE is bound (at higher concentrations) instead of the complementary DNA strand. This method was also found to be selective for IgE when high concentrations of control proteins were introduced [66]. Another electrochemical study using the anti-IgE aptamer involves a significantly extended sequence that binds the IgE relatively far from the electrode surface, which results in a decrease in measured current by SWV [67]. Finally, another study takes the approach of modifying the 3' terminus near the surface with a biotin group, which is used to bind streptavidin-modified alkaline phosphatase (the 5' terminus is immobilised onto the electrode). Detection is based on the conversion near the electrode surface of 1-naphthyl phosphatase to 1-naphthol, which is hindered by binding of the IgE antibody [68].

2.6.2 Cytochrome c as a biomarker

Cytochrome c (cyt c) participates in the mitochondrial electron-transport chain of the inner mitochondrial membrane. The heme group of cyt c acts as a redox intermediate to shuttle electrons between Complex III and Complex IV. Apoptosis is programmed cell death; when cells detect an apoptotic stimulus (DNA damage, metabolic stress or unfolded proteins), the apoptotic pathway is triggered, which causes mitochondrial cyt c to be released into the cytosol [69]. After cyt c has been released, it commits the cell to die by either a rapid apoptotic mechanism involving caspase activation, or through a slower necrotic process due to a collapse of the electron transport mechanism. This process generates oxygen free radicals and decreases production of ATP, thereby causing the cell to die [70].

Studies have linked increased levels of cyt c in urine and serum to various health conditions. Based on studies in rodents, cyt c has been identified as a biomarker for drug-induced liver injury from acetaminophen in both serum and urine samples [71]. One clinical study reported that cyt c was undetectable (<50 pg/mL) in the control group serum, but in patients suffering from chronic hepatitis C the median concentration of cyt c increased to 600 pg/mL (48 pM) [72]. Another clinical study looked at several different diseases of the liver. The normal concentration of cyt c, along with concentrations in serum measured for patients suffering from various liver conditions are shown in Table 2. The normal concentration is under 10 pM, but in some cases it increases significantly as a result of these various diseases of the liver [73].

Table 2. Concentrations of cytochrome c in patients suffering from liver conditions [73].

Condition	Number of patients	Mean [cyt c] (pg/mL)	[cyt c] in pM	Increase (x healthy)
Healthy (control)	9	112 (0-200)	9.04	-
Acute hepatitis	12	3040 (265–12098)	245	27.1
Chronic hepatitis	30	255 (0–550)	20.6	2.28
Chronic hepatitis with acute aggravation	6	749 (0–2036)	60.5	6.69
Liver cirrhosis	30	441 (46–2800)	35.6	3.94
Hepatocellular carcinoma (liver cancer)	30	323 (19–1000)	26.1	2.89
Fulminant hepatitis (liver failure)	15	10686 (1800–25 900)	862.89	95.5

The psychostimulant methamphetamine and the anti-HIV agent betulinic acid have been found to increase the levels of cyt c in rat brains by 61% and 50%, respectively [74]. This finding supports previous suggestions that cyt c could also serve

as a biomarker for mild brain injury [73]. In another clinical study using a Western blot assay, no cyt c was detected in human urine for healthy patients, but it was detected in patients suffering from acute tubular necrosis (ATN), which can be brought on by hypotension (low blood pressure) and the use of nephrotoxic drugs, which are known to cause kidney damage. No concentration was given for the patients suffering from ATN [75]. When human cancer cell lines are exposed to aspirin, cyt c is released from the mitochondria of these cells. This result suggests that aspirin plays an important role in the apoptotic mechanism to kill cancerous cells [76]. Accordingly, novel methods for detection of cyt c may be useful for this and other cancer research explorations.

2.6.3 SERS and Electrochemistry of Cytochrome c

The first time electrochemical surface-enhanced Raman spectroscopy (EC-SERS) was applied to the analysis of complex biomolecules was for an investigation of sperm whale myoglobin (Mb) and tuna cyt c, which took advantage of the tendency of proteins to adsorb onto metal surfaces. EC-SERS analysis was done in a solution of 0.1 M Na_2SO_4. The spectrum observed at -0.6 V vs. SCE showed very high signal-to-noise ratios. The spectrum was characteristic of the heme chromophore, but no vibrations associated with the protein amino acids were observed. Strong SERS spectra could be collected at concentrations as low as 100 nM. The bands in the spectrum indicated that at -0.6 V, the heme Fe is in its low-spin reduced state, Fe(II), indicating reduction at the Ag electrode since its normal oxidation state in solution is Fe(III). When the potential was stepped more positive to -0.2 V a decrease in spectral intensity was observed. Additionally, band positions indicated that cyt c was reoxidised to its low-spin Fe(III)

state. It was also proposed that while Mb is likely denatured at the Ag surface, cyt c is not because its spectra remain reproducible after oxidation and reduction cycles [77]. Their analysis used 514.5 and 457.9 nm excitation, both of which ought to give resonance Raman enhancement in addition to SERS, due to the position of the absorption maxima for cyt c. In its absorption spectrum, ferrocytochrome c has two major bands, the Soret band at 416 nm and the β band at 530 nm. Ferricytochrome c has three major bands, the Soret band at 416 nm, the α band at 550 nm and the β band at 520 nm [78]. Another recent study has also used UV/vis for a spectroelectrochemical analysis of cyt c and other redox proteins [79].

Cyt c has been well characterised by resonance Raman spectroscopy, non-resonant SERS, and UV resonance Raman spectroscopy [80-82]. In the non-resonant SERS study, spectra were collected using a 632.8 nm laser focused on a Ag rod working electrode. By using the non-resonant laser wavelength, it was possible to observe the amino acid features of the protein. Among other amino acids, cyt c contains tryptophan, tyrosine and phenylalanine residues, all of which were detected. In accordance with previous results, cyt c was found to remain in its native state at potentials more positive than -0.7 V vs. Ag/AgCl. However, partial unfolding was observed at -0.8 V, due to the detection of the amide III band. Spectroscopic results indicate that the heme could be adopting a more parallel orientation to the electrode surface, or that its distance from the surface could be increasing [81].

A surface-enhanced resonance Raman spectroscopy (SERRS) study of cyt c immobilised on a 2-mercaptoethanesulfonate (MES) monolayer on Ag has also been conducted. Cyt c is known to electrostatically adsorb at neutral pH onto negatively charged alkanethiol monolayers (i.e. carboxylate or sulfonate group) so MES is suitable as a linkage monolayer. EC-SERRS spectra were collected at potentials ranging from -500 to +100 mV vs. Ag/AgCl, with measurements at 100 mV increments. A potential of -500 mV will safely reduce the protein without denaturing it. It is suggested that application of a negative charge to the electrode surface may be responsible for the increase in intensity of the cyt c bands. At a potential of 0 mV, the heme iron is oxidised to Fe^{3+}, but the protein remains in the native six coordinate low-spin (6cLS) configuration around the central Fe^{3+}. Further increase of the potential to 100 mV results in the formation of the non-native five coordinate (5cHS) high spin configuration of the Fe^{3+} ion [83]. Another group looked at the voltammetric measurement of cyt c adsorption onto self-assembled monolayers (SAM). Cyt c was electrostatically adsorbed onto 16-mercaptohexanoic acid and covalently immobilised using 1-Ethyl-3-(3-dimethylaminopropyl)carbodiimide (EDC). [84-85]. Their work compared the electron transfer between the electrostatically and covalently immobilised cyt c. Additionally, the effect of the chain length of the alkanethiol was determined by comparison with 11-mercaptoundecanoic acid. Another SERRS study looked at the adsorption of cyt c onto several different alkanethiols. For cyt c electrostatic adsorption onto a series of alkanethiols with carboxylate headgroups, SERRS signal intensity for cyt c was found to decrease with an increase in chain length. However, cyt c could still be detected at a distance as large as 24 Å (C_{16}-SAM). Another interesting result was the effect of

the headgroup of the alkanethiol. For C_2-SAMs, the signal for cyt c on 2-mercaptoethanol was 220x weaker than that obtained for cyt c on mercaptoacetic acid. Furthermore, cyt c could not be detected on 11-mercapto-1-undecanol, but could be detected on 11-mercaptoundecanoic acid. Their results show that the headgroup of the alkanethiol SAM has a major impact on the nature of the electrostatic adsorption of cyt c [86].

2.6.4 Aptamer-based detection of cytochrome c

A 61-mer DNA aptamer was developed by Chinnapen and Sen for binding to cyt c protein. The aptamer is called CH6A, and will hereafter be referred to as anti-cyt. The aptamer sequence is 5'-AGT GTG AAA TAT CTA AAC TAA ATG TGG AGG GTG GGA CGG GAA GAA GTT TAT TTT TCA CAC T-3'. It was also reported that the affinity of the aptamer for cyt c increases in the presence of the iron-containing porphyrin, hemin. The dissociation constant (K_D) for DNA aptamer to cyt c was found to be 4.6 ± 0.6 µM, but in the presence of 10 µM hemin this value improves to 0.3 ± 0.2 µM. Their study suggests that hemin increases the strength of the DNA-cyt c interaction by inducing folding of the guanine-rich loop to form a G-quadruplex structure [87]. EC-SERS measurements of hemin on a Ag electrode have previously been reported in the range of -0.50 to +0.20 V using a 532 nm laser [88].

The anti-cyt aptamer has been used in several studies to detect the binding of cyt c protein. The methods, dynamic range and limits of detection are listed in Table 3. Note that the bio-barcode assay using PCR to generate the signal used a different DNA

sequence, but it is included for comparison since there are relatively few aptamer-based

detection studies of cyt c in the literature.

Table 3. Aptamer-based detection of cytochrome c protein.

Method	Dynamic Range	LOD	Control Biomolecules	Ref.
Capillary Chromatography	0.06-1 mg/mL	1 µM	Transferrin, serum albumin, IgG	[89]
Inductively coupled plasma mass spectrometry	0.1-20 nM	30 pM	Cysteine, glutathione, transferrin, lysozyme, thrombin, Mb, Hb, HSA	[90]
Bio-barcode assay	-	810 pM	-	[91]
Electrochemical impedance spectroscopy	50 pM-50 nM	63.2 pM	Fibrinogen, IgG, albumin	[92]
SERS, Raman reporter	1 nM-1 µM	2 nM	Hb, IgG	[93]

In the SERS study for detection of cyt c [93], a modified version of the aptamer is

employed. The same anti-cyt sequence is used, but with the addition of a third strand to

form a "triplex switch" with a Raman reporter molecule attached The Raman reporter is

carboxy-X-rhodamine. When cyt c is introduced to the system, it binds to the anti-cyt.

However, the anti-cyt is displaced from the AuNP surface, thereby causing the remaining

portion of the oligonucleotide to change its conformation and bring the reporter molecule

closer to the surface. Since SERS is a distance-dependent effect, closer proximity to the

surface results in signal enhancement for the Raman reporter molecule. Their method was

found to have a linear dynamic range of 1 nM to 1 µM, with a detection limit of 2 nM.

The aptamer was also found to be specific for binding cyt c. Signal response for the

control proteins hemoglobin (Hb) and immunoglobulin G (IgG) at 1 µM concentration

were found to be equivalent to the response of the blank solution (no protein) [93]. It is worth noting that all of the studies using the CH6A aptamer tested their assay with various control proteins, as shown in Table 1. In all of the systems, minimal or no signal was detected for the control proteins, indicating that the aptamer is highly specific for cyt c. However, in none of the studies were control studies conducted with a control aptamer. A control aptamer could be, for example, a random scrambled sequence of the anti-cyt, or it could be an unrelated aptamer used to detect another protein.

2.6.5 Catalase-peroxidase

There are many tuberculosis-derived biomolecules that can be found in urine and sputum that are indicative of infection. For the overall project, four TB biomarkers are being considered: 6kDa Early Secretory Antigen (ESAT6), catalase-peroxidase (KatG), lipoarabinomannan (LAM) and IS6110 DNA fragments. For the purposes of this thesis, only KatG was investigated. In addition to tuberculosis, KatG protein is also a known biomarker for *Mycobacterium avium* complex (MAC). MAC infection can be a severe complication of HIV, and it is becoming more common among non-HIV infected persons. Furthermore, MAC is as common as tuberculosis in some areas [94].

At the time of writing, there have been no SERS studies of KatG. There have, however, been several studies where the enzyme has been characterised by resonance Raman spectroscopy. The resonance Raman studies of KatG make comparison between wild type KatG, and its S315T mutant variation. The S315T mutation, where a serine residue is replaced by a threonine residue, is the most prevalent substitution, and it is

associated with resistance to the commonly used TB medication isoniazid (INH). In one study, the wild type and mutant proteins were characterised, along with determining the effects of pH and coordination of fluoride ion with the heme iron [95]. Another used resonance Raman (RR) spectroscopy to investigate the conformational differences of the wild type and mutant KatG, and found differences in the heme pocket stability of the two variants [96]. Another report used RR spectroscopy to study the reactions of KatG and KatG(S315T) have been reported, along with their INH complexes with two organic peroxides, *m*-chloroperoxybenzoic acid and peracetic acid. The mutant variation of the enzyme was found to have reduced catalytic activity [97]. A recent review article highlighted the existing Raman and crystallographic data for several catalase-peroxidases from *Mycobacterium tuberculosis* and other species [98]. In addition to these spectroscopic studies, there has also been redox potential measurements for KatG and KatG(S315T), using cyclic voltammetry, squarewave voltammetry and spectroelectrochemical measurements with a spectrophotometer. The results suggest that resistance to INH of KatG(S315T) is not brought about by changes in heme redox potential [99].

Unlike cyt c, there is currently no literature reporting an aptamer available for KatG. Aptamers specific for KatG were developed by members of the Dr. Jonathan Blackburn research group at the University of Cape Town in South Africa. Sequences and preparation of the anti-KatG aptamers will be discussed in the Materials & Methods section. Aptamers for other TB-specific antigens have been developed. Previously reported aptamers were specific for the CFP-10/ESAT-6 heterodimer protein

in sputum and MPT64 protein [100-101]. Developing aptamer-based methods of detection for TB biomarkers is a novel avenue of research that needs to be explored.

2.6.6 Control protein

Cyt c and KatG are both heme proteins. A cheap and abundant heme protein that can be used as a control in both the cyt c and KatG studies is hemoglobin (Hb). Several studies have previously reported the Raman of Hb and SERS of Hb on Ag and Au [102-104]. Hb has also been used in previous reports as a control protein for the anti-cyt aptamer [90, 105].

Chapter 3: Theory

3.1 Introduction

This section provides an overview of the techniques used in this project. First, Raman spectroscopy and its enhanced variants are covered. Next an overview of the electrochemical methods, principally cyclic voltammetry, is presented. The SELEX method used to select DNA aptamers is then discussed, followed by the thiol chemistry used to immobilise the aptamers onto the Ag nanoparticle surface used for SERS. Lastly, an overview of the characterisation of DNA aptasensors is presented.

3.2 Spectroscopic Methods

The main spectroscopic method used for this project is based on Raman scattering. However, as normal Raman spectroscopy suffers from several draw backs, several improved variants are used. These enhancements include surface-enhancement via metal nanostructures (SERS), along with resonance (SERRS) and electrochemical enhancements (EC-SERS).

3.2.1 Raman Spectroscopy

The technique of Raman spectroscopy is based on the inelastic scattering of monochromatic light. Inelastic scattering was predicted by Smekal in 1923 [105], but was not experimentally observed until 1928, when it was reported by Raman and Krishnan. [106]. Most scattered light is elastically scattered, with no net change in frequency of the radiation, which is known as Rayleigh scattering. About $1/10^6$ photons will be

inelastically scattered, thereafter having a change in frequency. The molecule is excited to a virtual excited state, and then falls back to a lower state, and the net difference in energy of the scattered light is measured. Those that fall back to a state that is higher than their initial state are said to undergo Stokes Raman scattering. Anti-Stokes Raman scattering occurs when the excited species fall back to a state that is lower than the initial state. The downside of Raman spectroscopy is that since relatively few photons are Stokes shifted, the Raman signal is inherently weak. Fluorescence is often much stronger than the weak Raman signal, particularly for conjugated organic molecules, which often attenuates the Raman spectrum. Nonetheless, Raman spectroscopy has some important advantages, such as the ability to analyse aqueous samples without significant spectral interference from water [107]. Accordingly, various techniques have been developed to enhance the weak Raman signal.

3.2.2 Surface-enhanced Raman spectroscopy (SERS)

Surface-enhanced Raman spectroscopy (SERS) was first reported by Fleischmann *et al*. when it was observed that pyridine adsorbed onto electrochemically roughened silver was observed to give an abnormally strong Raman signal that was potential dependant [108]. This large enhancement could not be simply attributed to an increase in surface concentration of pyridine at the surface, due to electrochemical roughening, and two theories were proposed. Jeanmaire and Van Duyne proposed that an electromagnetic effect gives rise to the SERS enhancement, [109] while Albrecht and Creighton proposed that a charge-transfer effect was the reason [110]. Both theories are now accepted as being contributors to the SERS enhancement.

The main contribution to SERS enhancement is from the electromagnetic effect (EM) [111]. Laser excitation of a roughened metal surface gives rise to a collective oscillation of conduction electrons in that surface, which generates a localised surface plasmon resonance (LSPR). An analyte adsorbed onto or in close proximity to this surface will have significant Raman signal enhancement. The EM mechanism typically gives enhancement factors (EF) of approximately 10^6-10^8, but can possibility contribute, an EF up to 10^{10}. EFs of up to 10^{14} are often quoted in the literature, especially for single molecule SERS, but there remains a wide variability in methods to measure the EF, which must be considered when comparing EFs [111]. The enhancement mechanism is dependent on the optical properties of the material, the size and shape of the nanostructured or roughened surface, and other factors, such the use of bimetallic structures and choice of laser excitation wavelength [112]. Only vibrations with a polarisability tensor that is perpendicular to the SERS-active surface will interact with the incident radiation, generating a band in the vibrational spectrum. This is known as the surface selection rule [112].

An interesting feature of EM enhancement is that this enhancement mechanism occurs close to the SERS-active surface without physical contact. Murray and Allara used a polymer layer to separate the Ag SERS-substrate from *p*-nitrobenzoic acid. The distance-dependant enhancement above the rough silver films was demonstrated, and the EM enhancement mechanism was found to have an effect within the range of 10 nm [113].

In addition to the EM enhancement, there is also a chemical enhancement (CE) mechanism based on charge transfer, According to Otto, "Certainly, without the EM mechanism there would be no signal, but the chemical mechanism determines what is observed." [114]. The CE mechanism typically contributes enhancement to the Raman spectrum by a factor of 10-100. More importantly, this mechanism determines which bands are observed [114]. The SERS spectrum gives information about both the adsorbate (analyte) and its environment (surface and solvent), particularly information about the enhancing nanoparticle, spatial orientation of the adsorbate, and the polarisation properties of the local electric field. It is often the case that molecules adsorbed onto a SERS-active surface give significantly different vibrational spectra from that of a neat sample (i.e. the normal Raman spectrum). There can be changes to both the frequency and intensity of the bands observed [112]. The charge transfer mechanism of adsorbed molecules is brought about by donor or acceptor orbitals which interact with the metal substrate. It should be noted that while all species ought to be able to undergo electromagnetic SERS enhancement, not all are able to be have the charge-transfer enhancement, since not all species can chemisorb onto the metal surface.

The best metals for SERS enhancement are the coinage metals: Ag, Au and Cu. Ag and Au are most commonly used because Cu can easily form an oxide layer, thereby preventing SERS. These metals work best for SERS because their optical constants lie in the spectral region of excitation used for Raman spectroscopy. However, since the enhancement properties can be modulated by the shape, size and external dielectric constant of the metals, poor enhancers in the visible region could provide good SERS

signal in the near-infrared (NIR) region of the spectrum [112]. Accordingly, Ni, Pt and Pd are sometimes used in SERS applications.

3.2.3 Resonance Raman spectroscopy and SERRS

Resonance Raman (RR) spectroscopy is a variant of Raman spectroscopy where the frequency of the incident laser is close to the energy of an electronic transition of the molecule being studied. This frequency can be measured using ultraviolet-visible (UV-vis) spectroscopy. When the laser beam frequency and the electronic transition align, the vibrational modes associated with that transition are enhanced significantly relative to other modes, which give an increased Raman signal intensity. RR spectroscopy is well suited for the study of complex systems, including biological samples. Typically a large molecule, such as a protein, will give a complicated Raman spectrum. However, using RR spectroscopy, only certain vibrations are enhanced due to the *resonance* of the incident laser and electronic transition, which can allow for easier identification of the target molecule. Those bands that are enhanced by the RR effect are typically much more intense than those generated by normal Raman scattering. A good example of RR spectroscopy is the case of hemoglobin (and heme proteins in general). When the Raman laser excitation wavelength is tuned to align with the electronic transition (UV-vis maximum) of the iron centre, it gives rise to a Raman spectrum associated with the modes of the tetrapyrrole-iron group (heme). One obvious advantage of RR spectroscopy is the enhanced the signal intensity, however there is also an increased risk of photodegradation of the analyte. Surface-enhanced Resonance Raman Spectroscopy

(SERRS) combines both RR spectroscopy and SERS, which leads to an increased signal intensity with contributions from both effects [112].

3.2.4 Electrochemical surface-enhanced Raman spectroscopy (EC-SERS)

Collecting SERS spectra at an electrified surface is often called "potential dependant SERS" or "electrochemical SERS". The latter is abbreviated as EC-SERS. The two components of SERS enhancement are the electromagnetic field enhancement (EM) and the chemical enhancement (CE), as discussed previously. Both of these enhancement mechanisms can be changed and improved by the application of an electrode potential. If the applied potential is more positive or negative than the inherent potential of zero charge (PZC) of the metal electrode, then it will affect the coverage and/or orientation of the species adsorbed on the surface. Change in coverage and/or orientation of the molecule may lead to a change in the observed SERS signal intensity. However, even when these changes do not occur, an applied potential may still increase the SERS signal intensity by a change of the bonding interaction between the molecule with the surface or nanostructured surface morphology. With so many factors to consider, EC-SERS is one of the most complicated SERS systems, but it also has numerous advantages, including increased signal enhancement. It also offers a lot of flexibility for analysis, because experimental conditions that affect both SERS and electrochemistry can be altered, such as electrode material, electrolyte, solvent, electrode potential and temperature [115].

EC-SERS has been used to study a variety of molecules, including nucleic acids. One study reported the normal Raman and EC-SERS spectra at Ag, Au and Cu electrodes

for 2-thiouracil (2-TU). Chemisorption onto Ag is most relevant for the context of this project. Adsorption onto the Ag electrode is via the formation of a Ag-S bond. Adsorption gives rise to several changes in the vibrational spectrum, including changes in band intensity and band position. The authors acknowledge that due to the complexity of the system, assignment of bands in the SERS spectrum can be open for debate. Based on the interpretation of the E-SER spectra, 2-TU remained anchored onto the Ag electrode while the potential was made more negative. However, the orientation on the Ag surface was found to be potential dependant, where at more negative potentials the orientation of 2-TU changes from a vertical to a tilted position [116]. Similar spectral interpretations have also been used to determine the potential dependant orientation of 3-(butyl-butoxycarbonyl)-1-methylpyridinium isomers at a AgNP electrode surface [117].

3.3 Electrochemistry

Two types of electrochemical methods were used in this project: cyclic voltammetry and linear sweep voltammetry.

3.3.1 Cyclic voltammetry

Cyclic voltammetry (CV) is the most popular technique for acquiring qualitative information about electrochemical reactions, and it is often the first experiment performed in electroanalytical studies. CV employs a linear potential scan of a stationary working electrode in an unstirred solution between two limit potentials. The potential scan uses a triangular waveform (Figure 2) for a single cycle or multiple cycles. During this potential sweep, the potentiostat measures the current which is plotted against the

applied potential. The resulting plot of i vs E is called a cyclic voltammogram [118-119]. An example CV is shown in Figure 3.
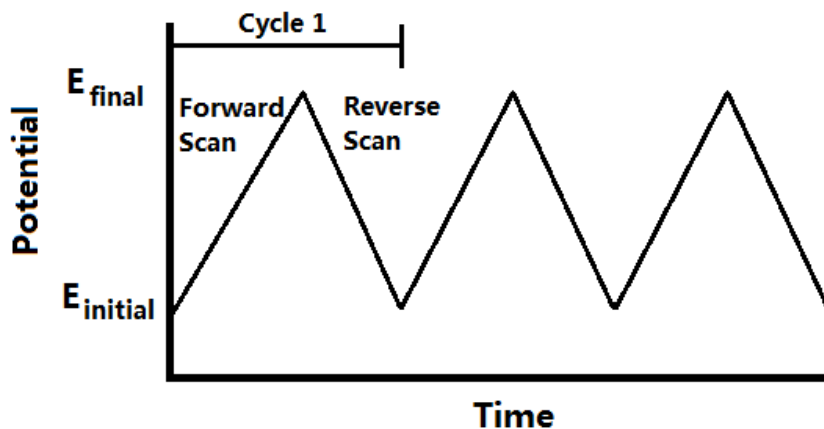
Figure 2. Triangular waveform of a potential-time excitation signal in a cyclic voltammetry measurement.
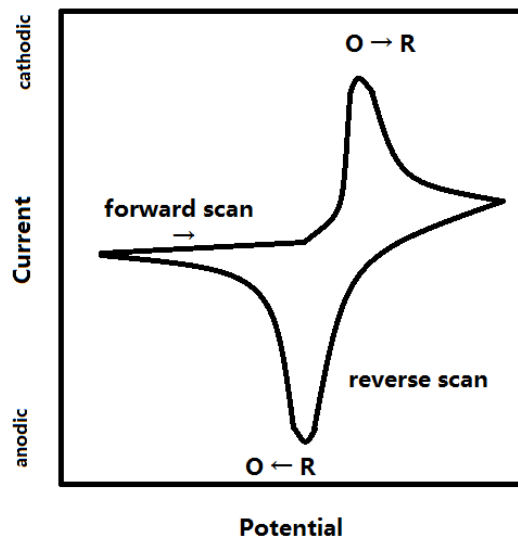
Figure 3. Typical cyclic voltammogram for a reversible oxidation/reduction reaction.

3.3.2 Linear sweep voltammetry

A linear sweep voltammogram (LSV) could be described as half of a cyclic voltammogram. The potential is swept from an initial potential to a final potential at a controlled scan rate, but it is not swept back as is done with a CV. LSV can be used as an analytical method, but it is not used as such for this project. Instead, it is used to avoid jumping directly from open circuit potential (ocp) to a desired potential [118, 119].

3.4 DNA Aptasensor Development

Aptamers are specific nucleic acid sequences that are able to bind a target molecule with high specificity and high affinity. The advantages of using aptamers instead of antibodies for biosensing, along with a survey of the relevant literature, are covered in Chapter 2. The word "aptamer" is derived from the Latin word *aptus*, which means "fitting" and the Greek word *meros,* meaning "particle". These short single stranded DNA or RNA oligomers have a wide variety of shapes, including stems, loops, bulges, hairpins, pseudoknots, triplexes and quadruplexes [120-121]. Their three dimensional structures allow them to bind a wide variety of targets, ranging from small molecules to whole organisms. The binding of the aptamer to a target is a result of structural compatibility, such as the stacking of aromatic rings, electrostatic and van der Waals interactions and hydrogen bonding. Furthermore, chemical modifications can be employed to improve the binding capability or stability of the aptamer, or to add new features, such as a Raman reporter or sulfur atom for surface immobilisation [120].

3.4.1 Systematic Evolution of Ligands by Exponential Enrichment (SELEX)

Combinatorial chemistry involves the synthesis and simultaneous screening of large libraries of structurally distinct but chemically related compounds to identify and isolate molecules with a specific function. Nucleic acids are attractive for this purpose because they are able to fold into defined secondary and tertiary structures. Once identified, they then can be easily amplified by PCR or in vitro transcription. A large amount of molecules (i.e. 10^{15} nucleic acid sequences) can be produced by chemical synthesis, and then screened in parallel [120].

In 1990 a new method was devised for the selection of RNA oligonucleotides that bind tightly and selectively to a specific non-nucleic acid target. Tuerk and Gold developed the method and called it Systematic Evolution of Ligands by Exponential enrichment (SELEX) [122]. Ellington and Szostak independently used a similar selection procedure to identify specific RNA molecules exhibiting the ability to fold into a stable three-dimensional structure to create a binding site for small organic dyes. Ellington and Szostak also contributed the term "aptamer", and DNA aptamers were also introduced by the same authors [123-124].

A typical SELEX process begins with a chemically synthesised random DNA oligonucleotide library containing 10^{13} to 10^{15} different sequences. For selection of DNA aptamers, the library can be used as is without any modifications. However, for selection of RNA aptamers, the DNA library must first be converted to an RNA library. The random oligonucleotide pool is then incubated directly with the target molecule. The

oligonucleotides that bind to the target are separated from those that are unbound or are weakly bound. The bound sequences are then eluted and amplified by PCR or RT-PCR. The resulting dsDNA must then be separated into relevant ssDNA. The newly formed pool of DNA is then used for another round of SELEX. After several rounds, the number of potential sequences is reduced to a much lower number relative to the initial oligonucleotide random pool. The number of rounds required can depend on the target features, concentration, the random oligonucleotide library, selection conditions, and ratio of target molecule to oligonucleotide and the efficiency of the partitioning methods. With each new round of SELEX, the stringency is increased in order to reduce the number of candidate sequences. This is achieved by lowering the target concentration or changing the binding and washing conditions. After the last round of SELEX, the PCR products are cloned to obtain the individual aptamers. Their binding features are then studied in order to determine the affinity and specificity of the prospective aptamers. Lastly, mutation and truncation experiments can be used to determine which region of the sequence is responsible for binding. The selected aptamer(s) can then be modified as desired for their end use [120].

3.4.2 Self-assembled aptamer monolayers via metal-sulfur bonding

The SERS-based aptasensor design requires that the aptamer be immobilised onto the SERS-active substrate, which in this project is silver nanoparticles (AgNP). The commercially produced aptamer is modified with a disulfide protecting group for stability. In order for the aptamer to be immobilised onto the surface, the S-S bond must be broken and a Ag-S bond must be formed. Experimental observation of the Ag-S bond

and lack of a S-S bond is imperative because it confirms this essential step of spontaneous breaking of the S-S bond in the preparation of the aptasensor.

Several similar studies investigated how the S-S bond of aromatic disulfides breaks in the presence of Ag to form a Ag-S bond. Sandroff and Herschbach investigated diphenyl disulfide (DPhDS), diphenyl sulfide (DPhS) and phenyl mercaptan (PhSH). As expected, the Raman spectra of DPhDS and DPhS have many similarities. However, a band at 542 cm^{-1} was only observed in the DPhDS spectrum. This band was attributed to the S-S stretch. The SERS spectrum of DPhDS on Ag was found to be remarkably similar to that of PhSH on Ag. The S-S band was gone, but a new band at 246 cm^{-1} was observed, which is attributed to the Ag-S stretch. In both cases, identical mercaptides on silver were formed. Similar results were observed when the phenyl group was substituted for a benzyl group [125]. Venkataramanan *et al.* also reported similar results [126]. In a later study, Takahashi *et al.* conducted a similar investigation of DPhDS/PhSH and 2,2'-dipyridyl disulfide (DPyDS) with 2-mercaptopyridine (PySH). DPyDS/PySH were found to give similar results to the DPhDS/PhSH system under basic, neutral and acidic conditions. Sandroff and Herschbach proposed that the chemisorbed mercaptides have a flat orientation on the Ag surface, but Takahashi *et al.* propose that they have an upright orientation where the Ph-S and Py-S bond is perpendicular to the Ag surface [127].

Joo *et al.* used similar methods to look at a system of alkyl sulfides: dimethyl sulfide (DMS), dimethyl disulfide (DMDS) and methyl mercaptide (MM), along with their ethyl variants. Sandroff and Herschbach had originally proposed that the C-S bond

can be broken in the presence of Ag, but Joo *et al*. found that this was not the case for dimethyl sulfide. Similar to the findings of Sandroff and Herschbach, Joo *et al*. found that the S-S bond is cleaved in the presence of Ag, since the SERS spectrum of DMDS was found to be essentially identical to the SERS spectrum of MM [128]. Similar results were also observed for sodium 2-sulfanylethanesulfonate (mesna) and 2,2'-dithio-bis-ethanesulfonate (dimesna). For dimesna, the bands in the Raman spectrum at 511 and 532 cm^{-1} are attributed to the S-S stretch for two different conformers of the molecule. These bands are absent in the SERS spectrum of dimesna. Moreover, the SERS spectrum on Ag of dimesna is essentially the same as that of mesna in terms of band position and intensity. For both mesna and dimesna absorbed on Ag, the Ag-S stretch is reported as a weak band at 280 cm^{-1}. Just as the S-H bond of mesna is broken to form the Ag-S bond, so too is the S-S bond of dimesna. In both cases, identical thiolates are formed [129].

Another study looked at lipoic acid histamide derivative (LAH), which has a disulfide in its 1,2-dithiolane component. The S-S stretch was observed in the Raman spectrum at 508 cm^{-1}. This result is in agreement with the calculated spectrum of 3-ethyl-1,2-dithiolane, where this mode appears at 481 cm^{-1}. In the SERS spectrum of a self-assembled monolayer of LAH on a Ag electrode, the S-S band was not observed. A new broad band at 231-235 cm^{-1} was attributed to the formation of the Ag-S bond. Theoretical modelling of the molecule on a cluster of 8 Ag atoms revealed an optimised structure where the disulfide bridge has been broken, and replaced with bidentate bonding of both sulfur atoms with silver. The SERS band is in good agreement with the calculated bands for the Ag-S stretch at 249 and 252 cm^{-1}. EC-SERS spectra showed a slight downshift of

the wavenumber of the Ag-S bond between -0.60 and -0.90 V, which indicates the weakening of the Ag-S bond [130].

3.4.3 Alkanethiol backfilling

While the purpose of the formation of the Ag-S bond is to immobilise the DNA aptamer onto the Ag surface, it does not mean that the DNA cannot interact with the surface in another manner. Some DNA may also be interacting with the surface via the nitrogen-containing nucleotide bases. To prevent this interaction, a lateral thiol spacer molecule is used. The alkanethiol spacer molecule competes with the non-specifically adsorbed DNA bases for the Ag surface, thereby displacing the DNA. After treatment with the spacer molecule, a mixed monolayer of DNA and spacer will be formed, both immobilised via a metal-sulfur bond. This process is shown in Figure 4 [131]. In addition to displacing "extra" or non-specifically adsorbed DNA, the spacer molecule will occupy any gaps on the surface, thereby preventing non-specific interaction of non-target molecules in the matrix from interacting with the surface. This method has been used in previous studies. For example, Negri *et al.* used (1-Mercaptoundec-11-y)tetra-(ethyleneglycol) for a SERS-based aptasensor for influenza nucleoprotein, while Orcaña *et al.* used polyethylene glycol for an EIS-based aptasensor for cyt c [34, 92].
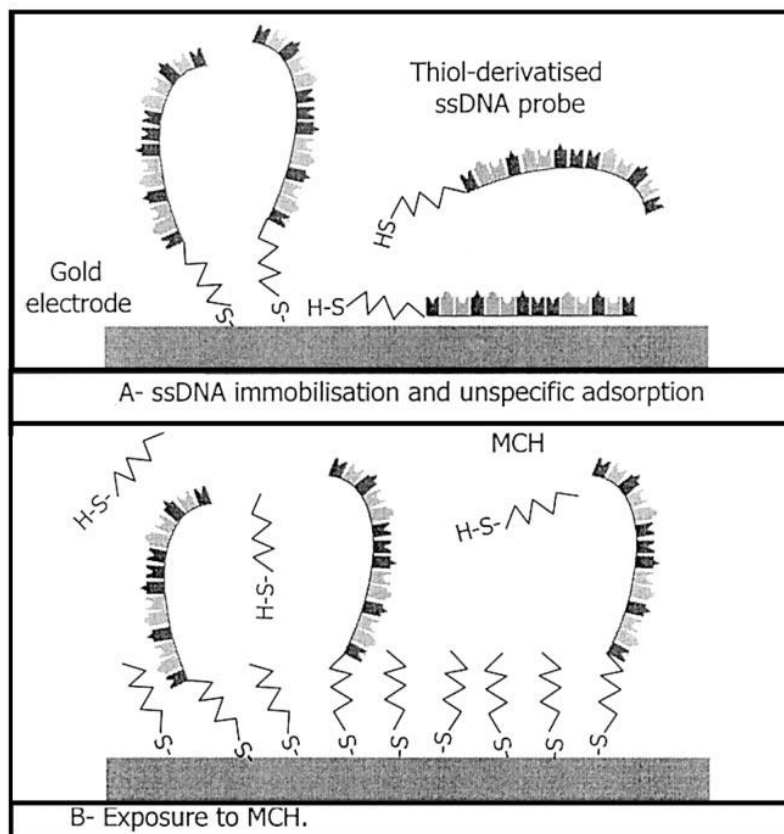
Figure 4. A) Immobilisation of ssDNA onto a Au electrode. The DNA interacts with the Au via the formation of a Au-S bond, and by interaction of the nitrogen of the nucleotide bases with the Au. B) Displacement of non-chemisorbed DNA by means of a mercaptohexanol spacer. (MCH) Reprinted from Biosensors and Bioelectronics, Vol 15, M.I Pividori, A Merkoçi, S Alegret, Electrochemical genosensor design: immobilisation of oligonucleotides onto transducer surfaces and detection methods, Pages 291-303, Copyright 2000, with permission from Elsevier.

3.5 Raman and SERS of DNA

DNA consists of three principle components: a negatively charged phosphodiester group, a five carbon deoxyribose sugar, and a nitrogenous base. The two purine bases are adenine (A) and guanine (G), and the two pyrimidine bases are cytosine (C) and thymine (T). DNA forms its double helix (dsDNA) via the hydrogen bonding interactions of Watson-Crick base pairing of A-T and C-G.

Otto *et al*. collected Raman and SERS spectra for the four DNA bases on Ag. As is the case with most chemical species, differences were observed between the Raman and SERS spectra. Some new bands were observed in the SERS spectrum, while others seen in the Raman spectra were not visible in the SERS spectra. The positions of some bands shifted as well, due to interaction with the surface. Nonetheless, by comparison with theoretical data, the authors were able to identify the vibrations for most of the bands. Raman and SERS were able to provide unique spectral fingerprints for each of the DNA bases [132].

Barhoumi *et al*. studied thiolated ssDNA and dsDNA on Au nanoshell-based SERS substrates. It was found that a thermal pre-treatment consisting of heating and rapid cooling before immobilisation onto the substrate resulted in much more uniform SERS spectra. It was also found that the dominant SERS bands were from adenine, followed by guanine, with weaker contributions from cytosine and thymine [133].

Dong *et al.* studied thiolated ssDNA and dsDNA on Au using EC-SERS. For both ssDNA and dsDNA, stronger band intensities were observed at more negative potentials. By interpreting the spectral data using the SERS surface selection rules, it was found that a vertical orientation of DNA is favoured at negative potentials. At more positive potentials, the DNA lies flat on the surface [134]. This finding is in agreement with a previous potential-dependant atomic force microscopy (AFM) study [135].

3.6 Raman and SERS of Proteins

Raman spectroscopy is a very useful technique to understand the overall structure of proteins, but it cannot provide detailed information like precise three-dimensional localisation of individual structural elements, such as peptides and other components. Most characteristic protein vibrational bands originate from the amide group, which are shown in Table 4.

Table 4. Characteristic protein Raman bands [136].

Name	Vibration	Wavenumber / cm^{-1}
Amide A	N-H stretching	~ 3500
Amide B	N-H stretching	~ 3100
Amide I	C=O stretching	1600-1690
Amide II	C-N stretching and N-H bending	1480-1580
Amide III	C-N stretching and N-H bending	1230-1300
Amide IV	OCN bending	625-770
Amide V	OOP NH bending	640-800
Amide VI	OOP C=O bending	540-600
Amide VII	Skeletal mode	200

The position of the amide I and III bands is indicative of the secondary structure of proteins. For α-helical proteins, these bands are found at 1662-1655 and 1272-1264 cm^{-1}, respectively. For proteins with β-sheet structure, they are found at 1674-1672 and 1242-

1227 cm^{-1}, respectively [136]. However, sometimes the amide I band is not observed in SERS spectra of proteins containing bulky amino acid side chains that increase its distance from the metal surface [137]. Raman and SERS spectra of human immunoglobulin G (IgG) have also given differing results. Amino acid residues that were in close contact with the silver electrode were observed, but not any amide backbone vibrations [138].

The spectral profile of proteins strongly depends on the wavelength of the laser excitation. When the wavelength matches the absorption range of a particular chromophore within the protein, a significant increase in signal intensity for this group is observed. In the case of heme proteins, resonance Raman spectra are obtained when the laser wavelength matches that of the porphyrin ring's absorption band. The electronic absorption spectrum of porphyrins have two maxima: the Soret band near 420 nm and the Q band around 550 nm. When 488 and 532 nm lasers were used for several heme proteins, significant RR enhancement was observed, with bands characteristic of the porphyrin heme centre. When the non-resonant 1064 nm laser was used, much weaker bands were observed [136]. When resonance Raman spectra are collected in combination with SERS, it is called SERRS. For heme proteins, nearly all of the SERRS bands are a result of the heme group itself, as opposed to the amino acids [139].

Chapter 4: Materials and Methods

4.1 Introduction

This section begins by giving an overview of the chemicals, DNA aptamers, proteins and other reagents used for this project. The instrumentation used for this project is covered as well, including the Raman spectrometers and the potentiostat/galvanostats. Next, the steps for the fabrication, characterisation and application of the biosensor are explained. The methods of detection, namely, electrochemical SERS and cyclic voltammetry are covered, followed by an overview of the data processing procedure.

4.2 Reagents

$AgNO_3$ (99.9995%), NaF (99.99%), $NaBH_4$ (≥99%), NaCl (99%), NaOH (99.99%), Tris-HCl (Trizma), $Ru(NH_3)_6Cl_3$ (98%), $K_4Fe(CN)_6$ (99.99%), 6-mercapto-1-hexanol (99%), 6-mercaptohexanoic acid (90%), 11-mercapto-1-undecanol (99%), 12-mercaptododecanoic acid (96 or 99%), equine heart cytochrome c (95%), human hemoglobin (lyophilised powder), porcine hemin (98.0%), and 4-(2-hydroxyethyl)-1-piperazineethanesulfonic acid (HEPES) were purchased from Sigma-Aldrich Corporation (St. Louis, MO, USA). KCl (≥99.0%), H_2SO_4 (95.0-98.0%) were purchased from Fisher Scientific (Fairlawn, NJ, USA). Purified human Immunoglobulin E (IgE) of ≥ 99% purity from serum (Myeloma, kappa & lambda) was purchased from Scripps Laboratories (San Diego, CA, USA). Lyophilised catalase-peroxidase (KatG) protein purified from a standard non-infectious *E. coli* strain was supplied by the Jonathan Blackburn laboratory at the Institute of Infectious Disease and Molecular Medicine, University of Cape Town, South Africa. K_2HPO_4 (≥98.0%) was purchased from Anachemia Canada (Montreal, QC,

Canada). KH_2PO_4 ($\geq99.0\%$) and trisodium citrate ($\geq99.0\%$) was purchased from ACP Chemicals (Montreal, QC, Canada). Na_2SO_4 ($\geq99.0\%$), $MgCl_2{\cdot}6H_2O$ ($\geq97\%$) and $(CH_3)_2SO$ ($\geq99.9\%$) were purchased from BDH Inc. (Toronto, ON, Canada). $CaCl_2{\cdot}2H_2O$ ($\geq99\%$) was purchased from Caledon Laboratories Ltd (Georgetown, ON, Canada). Citric acid ($\geq99\%$) was purchased from Alfa Aesar (Ward Hill, MA, USA). Triton X-100 was purchased from J. T. Baker Chemical Co. (Phillipsburg, NJ, USA). Synthetic urine solution (deionised water, 17-21% w/v urea, 6-10% NaCl w/v, 0.9 - 1.2% w/v $MgSO_4{\cdot}7H_2O$, < 1% w/v $CaCl_2$) was purchased from Ricca Chemical Company (Arlington, TX, USA). Ethanol (95%) was purchased from Commercial Alcohols (Brampton, ON, Canada). All reagents were used as received without further purification.

DNA aptamers with a 5' thiol modifier were synthesised by Integrated DNA Technologies, Inc. (Coralville, IA, USA). Instead of being synthesised with a HS- group, the aptamers are made with a HO-$(CH_2)_6$-S-S-$(CH_2)_6$- group for greater stability. Aptamer nomenclature is not yet standardised, but several naming formats have been used in the literature. The aptamer for thrombin has been called "thrombin binding aptamer", which then uses the acronym "TBA" [48]. Other reports have used the style "anti-X", such as "anti-influenza aptamer" and "anti-PDGF aptamer" [34, 41]. Other styles simply describe them, such as "the aptamer against ricin B chain" or "vasopressin-specific aptamer" [26, 42]. Lastly, many aptamers are given a letter/number style name, such as SS2-52 for a multiple pesticide binding aptamer [45]. For the purpose of this thesis, the aptamers will use the "anti-" format, with the target protein names abbreviated. The aptamer for immunoglobulin E is abbreviated as "anti-IgE" and the aptamer for

cytochrome c is abbreviated as "anti-cyt". The sequences for these aptamers were already available in the literature [140-141]. The aptamer for catalase-peroxidase is abbreviated as "anti-KatG". The sequence for anti-KatG was developed in the laboratory of Jonathan Blackburn at the University of Cape Town, South Africa. The sequences for the anti-IgE, anti-cyt and anti-KatG aptamers are listed in Table 5.

Table 5. The composition of the anti-IgE, anti-cyt and anti-KatG aptamers.

Aptamer	Sequence	Reference
anti-IgE	5'-HO-$(CH_2)_6$-S-S-$(CH_2)_6$-GGGGCACGTTTATCCGTCCCTCCTAGTGGCGTGCCCC-3'	140
anti-cyt	5'-HO-$(CH_2)_6$-S-S-$(CH_2)_6$-AGTGTGAAATATCTAAACTAAATGTGGAGG GTGGGACGGGAAGAAGTTTATTTTTCACACT-3'	141
anti-KatG	5'-HO-$(CH_2)_6$-S-S-$(CH_2)_6$-GCCTGTTGTGAGCCTCCTAACCCGAACAATCAAGG GGCCGAGGAACCGCGGCATGCTTATTCTTGTCTCC CTATAGTGAGTCGTATTA-3'	-

4.3 Instrumentation

4.3.1 Raman spectrometers

For most of the initial experiments of this project, a DeltaNu Advantage 785 Raman Spectrometer produced by DeltaNu (Laramie, WY, USA) was used. This instrument uses a diode laser with a wavelength of 785 nm as the excitation source. The spectrometer resolution is 4.0 cm^{-1}. Its laser power ranges from 2.93 to 55.9 mW. The spectrometer has an air-cooled CCD detector, and is connected to a laptop computer which uses NuSpec software for signal processing and the setting of spectral parameters. The software was also produced by DeltaNu.

For later studies, a DXR SmartRaman Raman spectrometer with a 180 Degree Sampling Accessory produced by Thermo Fisher Scientific Inc. (Madison, WI, USA) was used. The laser wavelength can be changed between visible 532 nm (diode-pumped, solid state) and near-infrared 780 nm (frequency-stabilised single mode diode laser). The high-resolution grating has a range of 1800-50 cm^{-1}, with a spectral resolution of 3.0 cm^{-1}. The full-range (low-resolution) grating for the 532 nm laser has a range of 3500-50 cm^{-1} and for the 780 nm it is 3300-50 cm^{-1}; the resolution is 5.0 cm^{-1}. The 532 and 780 nm lasers have power ranges of 1-10 and 10-150 mW, respectively.

4.3.2 Potentiostat/Galvanostat

Electrochemical measurements were completed using a WaveNow USB Potentiostat / Galvanostat produced by Pine Research Instrumentation (Durham, NC, USA). The instrument connects to a standard PC. The software for setting electrochemical parameters is Aftermath Data Organizer (version 1.2.4361), also produced by Pine Research Instrumentation. The electrodes used with the potentiostat were disposable screen printed carbon electrodes (SPE), also purchased from Pine Research Instrumentation. Built into the SPE is a 5 mm x 4 mm rectangular carbon working electrode, a Ag/AgCl reference electrode, and a carbon counter/auxiliary electrode. The electrodes are mounted in a mini USB cell cap for ease of use. The electrochemical cell is a standard glass vial with a total volume of approximately 20 mL. For most measurements, custom made small-volume (~5 mL) and flat-walled vials were used. A picture of this set-up is shown in Figure 5.

Figure 5. Photo of the setup used for EC-SERS, including the flat-walled vial, AgNP-modified screen printed electrode, and holder for connection to the potentiostat.

Some cyclic voltammetry (CV) measurements were made using a Model 263A Potentiostat/Galvanostat produced by Princeton Applied Research (Oakridge, TN, USA). The software for this instrument is Electrochemistry Power Suite 258, produced by the same company. This instrument also connects to a standard PC. These measurements used a gold working electrode, a Ag/AgCl/Sat. KCl reference electrode, and a Pt wire counter electrode. The working electrode was polished with alumina (0.05 µm) prior to use. The electrodes and a polishing kit (model PK-4 / MF-2060) were purchased from BASi Instruments (West Lafayette, IN, USA).

4.3.3 Electrochemical SERS setup

Electrochemical SERS (EC-SERS) measurements were made by coupling the Raman spectrometer with the potentiostat. The laser is focused onto the working electrode of a modified SPE in the electrochemical small-volume cell. Raman spectra can then be collected at the desired applied potential. In order to reduce interference in the spectra (i.e. interference from room light), Raman spectra must be collected in a darkened room. A diagram of this setup is shown in Figure 6.
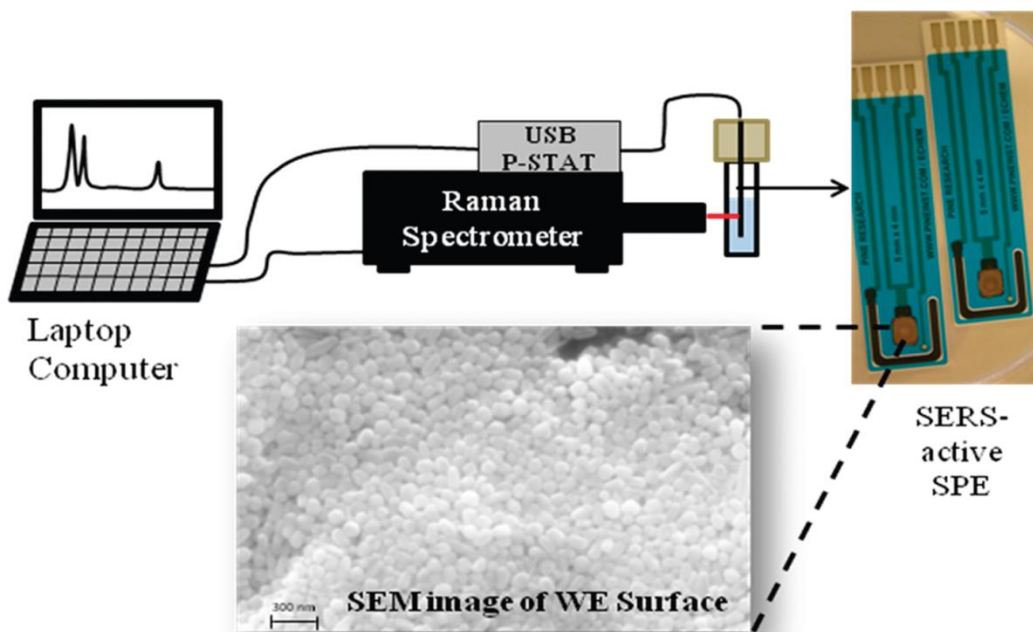
Figure 6. Schematic setup of the EC-SERS setup, coupling a Raman spectrometer with a portable potentiostat. The inset shows an SEM image of the AgNPs deposited onto the working electrode of a disposable screen printed electrode. Reproduced with permission from A. M. Robinson, S. G. Harroun, J. Bergman, C. L. Brosseau. *Anal. Chem.,* **2012,** *84,* 1760-1764. Copyright 2012 American Chemical Society.

4.3.4 Water purification system

For all prepared solutions and for rinsing the glassware and electrodes, a Milli-Q Direct 8 ultrapure water purification system was used. The system provides water with a resistivity of ≥ 18.2 MΩ cm. This instrument is produced by EMD Millipore Corporation (Billerica, MA, USA).

4.3.5 Infrared spectrometer

Attenuated total reflectance infrared (ATR-FTIR) spectroscopy measurements were made using a Vector 22 infrared spectrometer produced by Bruker (Billerica, MA, USA). It has a MIRacle Single Reflection HATR attachment produced by Pike Technologies (Madison, WI, USA).

4.3.6 UV-visible spectrophotometer

UV-visible spectrophotometry measurements were made using a Cary 50 Bio UV-visible spectrophotometer produced by Varian (Palo Alto, CA, USA) with a Xenon flash lamp.

4.4 Biosensor Preparation

The following subsections provide an overview of how the aptasensor (aptamer-biosensor) was prepared. The steps for building the biosensor include: preparation of Ag nanoparticles (AgNP) and deposition of them onto the electrode, immobilisation of the thiolated DNA aptamer onto the AgNPs via the formation of a Ag-S bond, followed by

alkanethiol backfilling. Lastly, the binding buffer solutions to induce binding of the target

protein to the aptamer are covered as well.

4.4.1 Silver Nanoparticles

Silver nanoparticles were prepared by two methods. One method is based on the

commonly used Lee-Meisel method [143]. Approximately 500 mL of deionised water

was added to a large beaker, to which 0.09 g of $AgNO_3$ was added. The $AgNO_3$ solution

was covered, stirred rapidly and brought to a vigorous boil. To the beaker, 10 mL of 1%

w/w trisodium citrate was added. The solution is boiled in the dark for 30 min, after

which it is removed from the heat, diluted to 400 mL (if required) and allowed to cool.

The colloidal suspension is then centrifuged in 1 mL aliquots for 10 minutes at ~3600

rpm. The centrifuge is of model type Galaxy 16, produced by VWR (Missassauga, ON,

Canada). The supernatant is removed, and another 1 mL aliquot of colloidal AgNP

suspension is added to the centrifuge tube; this process is repeated ten times. The

resultant colloidal silver pellet is used to prepare the AgNP-modified SPEs. AgNPs

prepared by this method are indicated in figure captions as "citrate reduced AgNPs".

The second procedure to prepare silver nanoparticles (AgNP) was adapted from

Zhao *et al*. [144]. The following were added to a 3 neck flat-bottom flask: 95.0 mL

ultrapure cold water, 1.0 mL of 0.1 M $AgNO_3$, 3.4 mL of 5% w/w trisodium citrate, 600

µL of 0.17 M citric acid and 200 µL of 0.1 mM $NaBH_4$. The solution is allowed to react

for 1 minute at room temperature, after which it is refluxed while boiling for 120 minutes.

The colloidal suspension of AgNP is centrifuged at a speed of ~8000 rpm in 14 tubes

containing 1430 µL of colloidal suspension each. After removal of the supernatant, pellets are collected in a single tube. The supernatant from the second centrifugation is removed, followed by dilution with ultrapure water to 50 µL. Three layers of 5 µL each are added to the working electrode of the disposable screen printed electrode. Other studies in our group found that these citrate/borohydride reduced AgNPs give a more reproducible signal than the citrate reduced Lee-Meisel AgNPs. AgNPs prepared by this improved method are indicated in figure captions as "citrate/borohydride reduced AgNPs".

For both methods, the concentrated AgNPs were deposited onto the electrode in an identical manner. Three successive 5 µL layers of AgNPs were drop-coated onto the working electrode of the screen printed electrodes. The preceding layer was allowed to dry in air before the next was added. The AgNPs were gently spread with the pipet tip to cover the entire working electrode surface.

4.4.2 Immobilisation of DNA-aptamer

The DNA aptamers were received from the manufacturer in the solid phase, and diluted to a concentration of 1 mM using pH 7.4 phosphate buffer (12.5 mM KH_2PO_4 and 29.3 mM K_2HPO_4). For each electrode prepared, a 10 µL aliquot of the aptamer solution was drop coated onto the AgNP surface, and allowed to dry overnight. The aptamer is immobilised onto the AgNPs through the spontaneous formation of a Ag-S bond. The concentration of aptamer was usually either 1 or 0.1 mM, as indicated. In some analyses, the aptamer was annealed prior to immobilisation. For this process, the aptamer solution

was palced in an Eppendorf tube in boiling water for five minutes, followed by rapid cooling (annealing) in an ice bath before deposition onto the AgNP electrodes.

4.4.3 Alkanethiol spacer backfilling

Two alkanethiol spacer molecules were used for this project: 12-mercaptododecanoic acid (12-MDA) and 11-mercapto-1-undecanol (11-MUD). The purpose of the spacer molecule is to displace residual DNA aptamer that is not immobilised via a Ag-S bond, promote upright orientation of the aptamer, and prevent non-specific interaction of non-target molecules with the biosensor surface. The spacer molecule solution was prepared in 95% ethanol. Aptamer-modified AgNP electrodes were incubated in the 1.0 or 0.1 mM ethanolic spacer solution for 2 hours, followed by light rinsing with ethanol and water.

4.4.4 Binding of protein samples

The proteins were prepared in pH 7.4 phosphate buffer or a specific binding buffer, as indicated. Immunoglobulin E (IgE) was prepared in pH 7.4 phosphate buffer (12.5 mM KH_2PO_4 and 29.3 mM K_2HPO_4) in tubes containing a 20 µL aliquot of 500 nM protein, which were then frozen for storage. To induce binding of protein to the anti-IgE aptamer, 10 µL of 3 mM $MgCl_2$ was added after the aptamer solution had thawed. Typically, 10 µL of the IgE/$MgCl_2$ solution was pipetted onto the anti-IgE biosensor, and allowed to react for 1 hour, followed by light rinsing with phosphate buffer and water.

Two methods were used for binding of the heme proteins to their respective aptamers. Initially, a 10 µL aliquot of the protein solution was drop-coated onto the aptamer-modified AgNP electrode. At lower concentrations, it was feasible to incubate the electrode in 7.0 mL of protein solution while stirring rapidly. For both methods, after 1 hour of binding, the electrode was lightly rinsed with phosphate buffer or binding buffer, followed by light rinsing with water. Cytochrome c was prepared in either phosphate buffer or binding buffer. The binding buffer for the anti-cyt aptamer contained: 50 mM Tris-HCl, 120 mM NaCl, 50 mM KCl, 1% DMSO, 0.03% Triton X-100, 10 µM $K_3Fe(CN)_6$ [141]. A similar procedure was used for the anti-KatG aptamer, where the binding buffer contained 20 mM HEPES (4-(2-hydroxyethyl)-1-piperazineethanesulfonic acid), 75 mM NaCl, 2 mM KCl, 2 mM $CaCl_2$ and 2 mM $MgCl_2$ [100]. After 1 hour, the electrodes were lightly rinsed with phosphate buffer or binding buffer, followed by rinsing with water. When the control protein hemoglobin was used, an identical procedure to what was used for the target protein was followed.

4.5 Detection of aptamer-protein complex formation

The main method of detection for this project is electrochemical SERS (EC-SERS). Additional measurements were conducted using cyclic voltammetry. The methodology used for the two methods are explained in the following subsections.

4.5.1 EC-SERS: cathodic and anodic scans

For this technique, the Raman spectra are collected on the aptamer-AgNP modified working electrode. The first spectrum collected without an applied potential is

simply a regular SERS spectrum. The lack of an applied potential is designated as ocp, for open-circuit potential. The first desired potential is applied (typically 0.0 V) while the EC-SERS spectrum is recorded. The process is repeated for the next potential (e.g. -0.1 V), and so on, until the spectrum at the final desired potential has been recorded. Typically, EC-SERS spectra are collected at ocp, and then from 0.0 to -1.0 V, in -0.1 V increments (cathodic scan). An anodic series can be collected after, typically from -1.0 to 0.0 V in +0.1 V increments. For the aptasensor or aptasensor-protein complex, spectra were typically collected for 30 s, at a power of 3 mW (for cyt c) or 7 mW (for KatG).

4.5.2 EC-SERS: Multiple spots collected at constant potential

One commonly known problem with SERS is that it suffers from irreproducible signal intensity. Even on a relatively uniform SERS substrate, SERS spectra can vary from one spot to the next due to slight changes in SERS enhancement and/or orientation of the adsorbed molecule on the surface. In order to minimise these spot-to-spot variations, multiple SERS spectra can be collected and then averaged using software. Typically, 10 or 30 spectra were collected. It is not practical for a POC device to collect multiple spectra (10 or more) at each applied potential, so multiple EC-SERS spectra are recorded at a single potential (often -0.7 V). This potential is chosen so that it is the optimal potential for EC-SERS detection of the target molecule. Instead of jumping from ocp to the desired potential directly, linear sweep voltammetry was used for a gradual potential sweep from 0.0 V to the desired potential. For example, a linear sweep from 0.0 to -0.7 V at a scan rate of 2.3 mVs^{-1} takes approximately five minutes.

4.5.3 Cyclic Voltammetry

Cyclic voltammetry was used in this project as a supplementary analysis method. It is convenient since the same electrode can be used as is used for EC-SERS measurements. In some cases, CVs were collected after the cathodic and anodic EC-SERS spectra were collected. In other cases, CVs were recorded without first having performed EC-SERS, in order to guarantee the integrity of the results, as the EC-SERS analysis may have changed the surface characteristics. For some measurements, a traditional three electrode electrochemical cell was used instead of the disposable screen printed carbon electrodes (SPE). For this method, a gold working electrode, Ag/AgCl/Sat. KCl reference electrode, and a Pt wire counter electrode were used.

4.6 Signal Processing

Raman spectral data were processed using Origin 9 software, produced by OriginLab Corporation (Northampton, MA, USA). Data from the Raman spectrometers were saved as a .CSV (comma-separated values) file type, and imported into Origin. All spectra are normalised for the selected laser power and spectral acquisition time. For a single Raman or SERS spectrum, plotting is straightforward. For a series of EC-SERS spectra measured at different potentials, they are plotted in an overlay style with space added between each spectrum to prevent overlap of bands. When spectra are smoothed, typically the Adjacent Averaging method with 8 points is used. Cyclic voltammograms are also plotted using Origin 9 software. The data is copied from the electrochemical software (Aftermath) into Origin 9.

Chapter 5: Model Proteins - Immunoglobulin E and cytochrome c

5.1 Introduction

Immunoglobulin E (IgE) is one of the first antibodies produced by the immune system to counter antigens causing asthma and allergic reactions, and its concentration in the body increases accordingly during these conditions [52-53]. Rapid detection of IgE may therefore be useful for clinical analyses. Cytochrome c (cyt c) is a biomarker protein for various diseases of the liver and other conditions, as discussed in Chapter 2. It also serves as a model protein for the development of an EC-SERS system for detection of the tuberculosis biomarker, catalase-peroxidase. In this chapter, EC-SERS is used for the development of an aptamer-based method for detection of IgE in phosphate buffer, and cyt c in buffers and urine. This research is novel in its own right, and the knowledge gained here will expedite the development of the tuberculosis aptasensor for point of care diagnostics. This first phase of the project was conducted while the aptamer for the tuberculosis biomarker KatG was being developed at the University of Cape Town, South Africa.

5.2 EC-SERS of anti-IgE aptamer

The aptamer specific for immunoglobulin E antibody (IgE) was developed by Wiegand *et al*. [140]. For the purposes of this thesis, it is identified as anti-IgE. To characterise the aptamer, 10 μL of 1 mM anti-IgE was drop coated onto a citrate reduced AgNP electrode, and allowed to dry overnight. Light rinsing with several milliliters of phosphate buffer and ultrapure water was done to remove any excess aptamer on the

surface that had not been immobilised via the formation of a Ag-S bond. EC-SERS spectra were collected at ocp and over the potential range of 0.0 to -1.0 V, shown in Figure 7. After a 2 hour incubation of a newly prepared aptamer-modified electrode in 1 mM 12-mercaptododecanoic acid (12-MDA) in ethanol, followed by rinsing in ethanol and water, a similar series of EC-SERS spectra were obtained, shown in Figure 8. EC-SERS spectra of the alkanethiol spacer 12-MDA on AgNPs only (no aptamer) are shown in Figure 9. Detailed discussion of the spectra follows in subsequent sections.
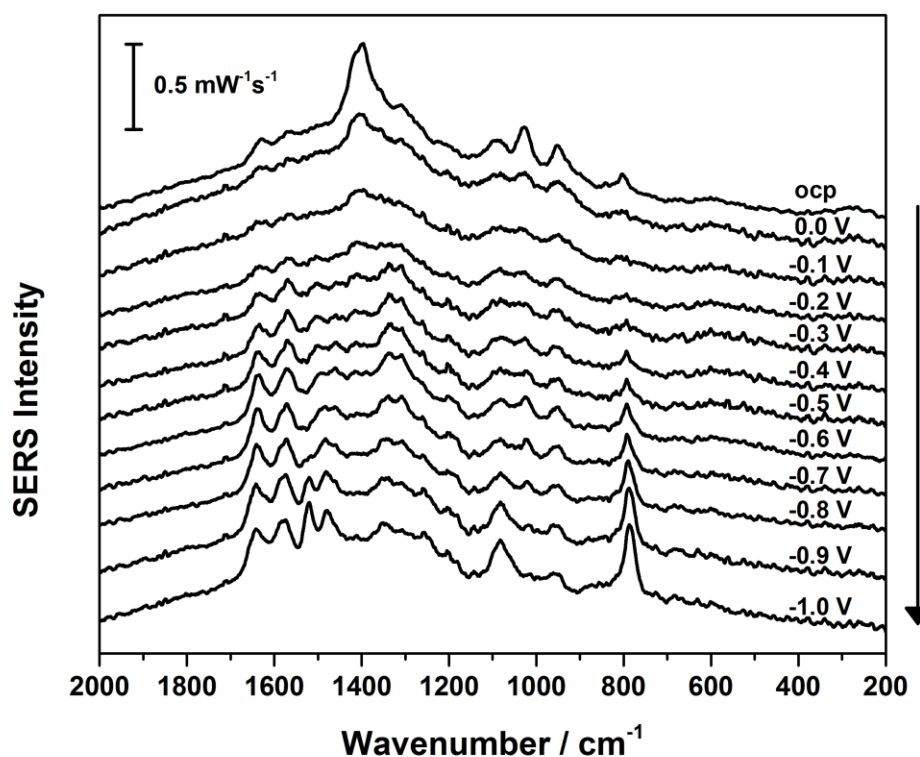
Figure 7. EC-SERS of 10 μL of 1 mM anti-IgE aptamer on a citrate reduced AgNP electrode in 0.1 M NaF. Laser power = 46.5 mW, collection time = 60 s, wavelength = 785 nm.
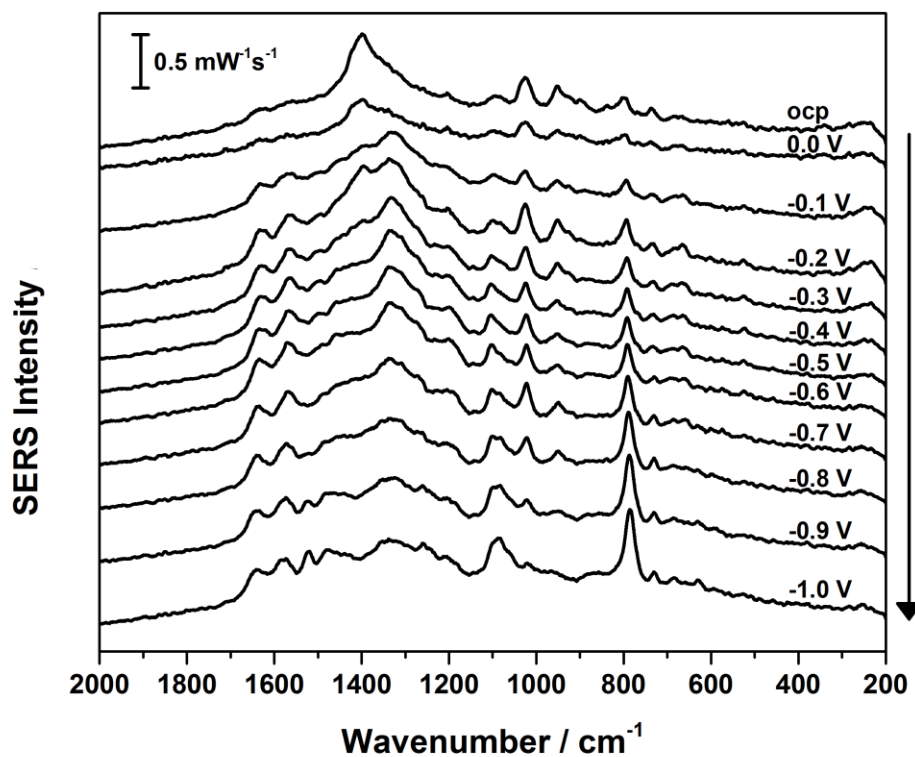
Figure 8. EC-SERS of 10 μL of 1 mM anti-IgE aptamer + 1 mM 12-MDA on a citrate reduced AgNP electrode in 0.1 M NaF. Laser power = 46.5 mW, collection time = 60 s, wavelength = 785 nm.
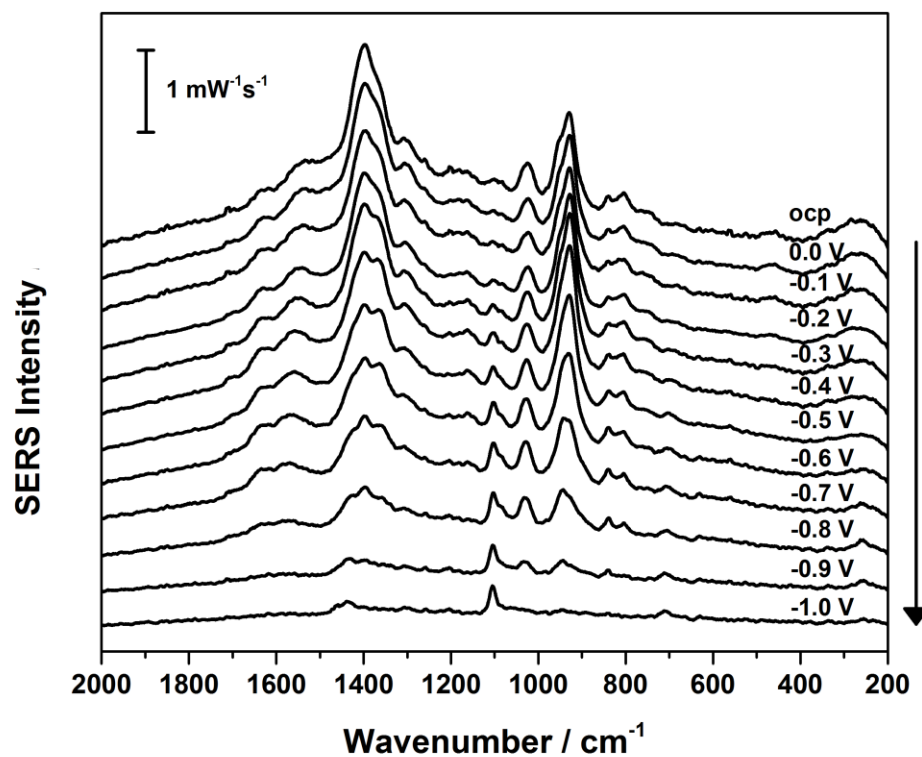
Figure 9. EC-SERS of 1 mM 12-MDA on a citrate reduced AgNP electrode in 0.1 M NaF. Laser power = 46.5 mW, collection time = 60 s, wavelength = 785 nm.

5.3 Attempted EC-SERS detection of IgE protein

The AgNP + anti-IgE + 12-MDA aptasensor was used for EC-SERS detection of IgE protein from a 10 μL aliquot of 0.5 μM IgE protein + 3 mM MgCl$_2$. The purpose of the Mg^{2+} is to induce binding of the IgE to the anti-IgE aptamer. After a reaction time of 1 hour, EC-SERS spectra were collected in a similar manner to what had been done for the previous trials without IgE protein, shown in Figure 10.

Shown in Figure 11 are comparisons of each component of the aptasensor system recorded at -1.0 V: anti-IgE, 12-MDA, anti-IgE + 12-MDA, and anti-IgE + 12-MDA + IgE. No significant changes are observed between the aptamer spectra with and without 12-MDA. The dominant band in the EC-SERS spectrum of the aptamer is the 785 cm^{-1} band with contributions from both cytosine and adenine. Compared to the cyt c and KatG aptamers (discussed in later sections), the 731 cm^{-1} band for adenine is relatively weak. This difference can be attributed to the increased distance from the AgNP surface for adenine in the anti-IgE aptamer. Since SERS is a distance-dependant phenomenon, molecules that are closest to the AgNP surface will receive the most intense signal enhancement.

When the spectra of anti-IgE + 12-MDA with/without IgE protein are compared, it is clear that no IgE protein was detected in the spectrum. There are no major changes of band intensity or position, and no new bands appear in the EC-SERS spectrum. This same result was observed over several trials, where only the anti-IgE aptamer could be

detected, but not its target protein. In another analysis (data not shown), EC-SERS spectra could not even be collected for IgE protein alone on a AgNP electrode.
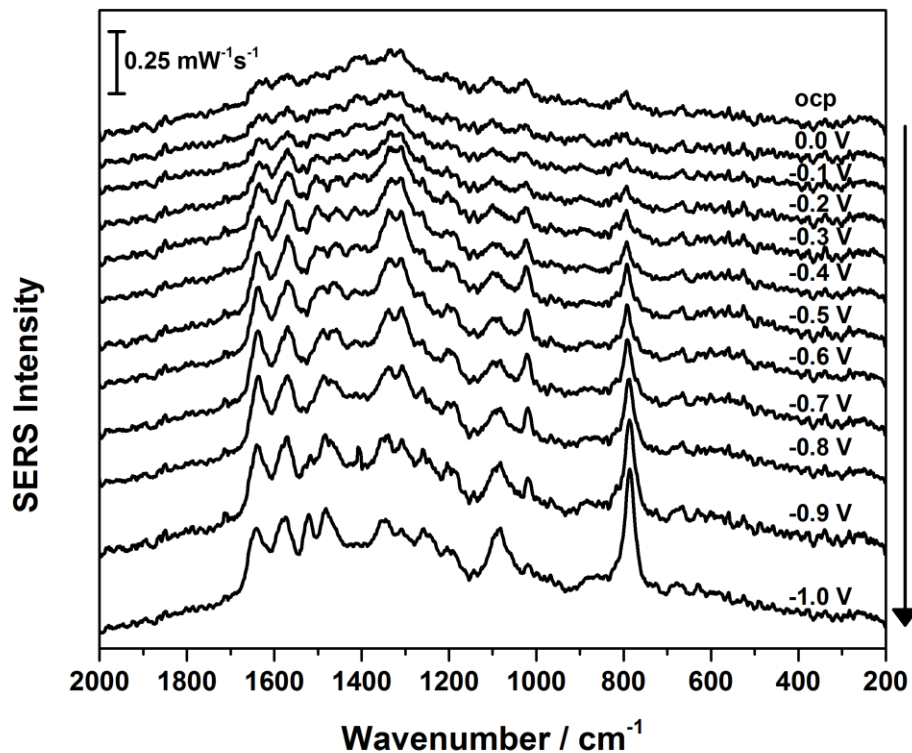
Figure 10. EC-SERS of 10 μL of 1 mM anti-IgE aptamer + 1 mM 12-MDA + 10 μL of 0.5 μM IgE protein + 3 mM $MgCl_2$ on a citrate reduced AgNP electrode in 0.1 M NaF. Laser power = 46.5 mW, collection time = 60 s, wavelength = 785 nm.
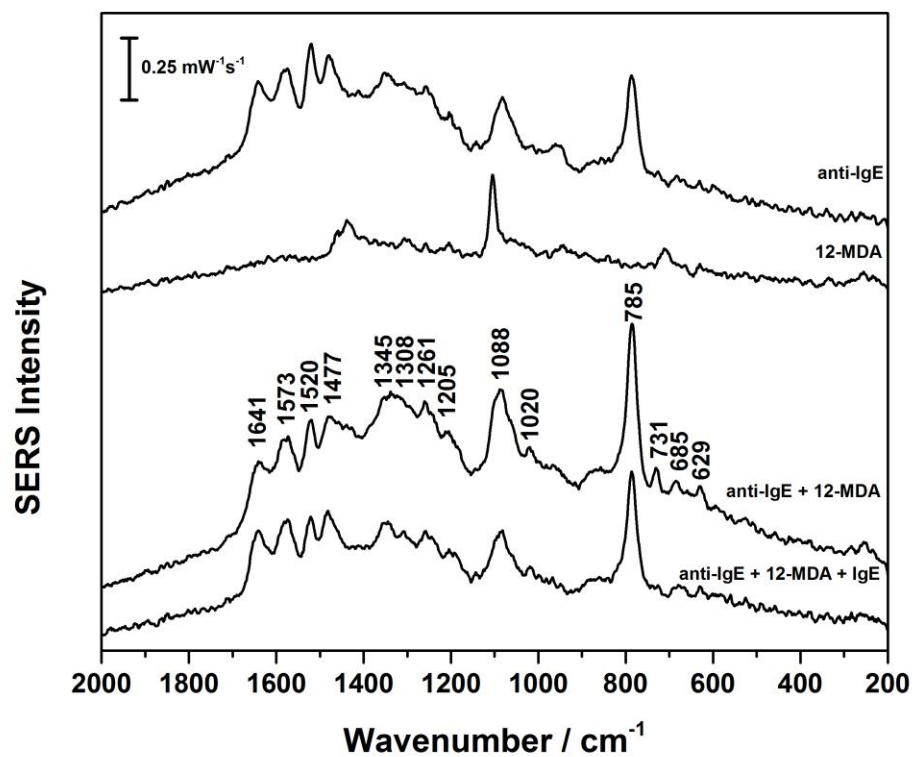
Figure 11. Comparison of spectra collected at -1.0 V from Figures 7-10.

5.4 ATR-FTIR spectroscopy of IgE protein

In order to confirm that IgE protein is indeed in the sample, ATR-FTIR spectroscopy was used to analyse the protein solution. The spectrum (Figure 12) recorded for 0.5 µM IgE in phosphate buffer does indeed show protein bands. The amide I band with contributions from ν(C=O), ν(C-N), and δ(N-H) mode is observed at 1651 cm^{-1}. The amide II band with contributions from δ(N-H) and ν(C-N) is observed at 1539 cm^{-1}. The band at 1741 cm^{-1} for ν(C=O) is indicative of amino acids [154]. The ATR-FTIR spectrum shows that it is indeed possible to collect a vibrational spectrum for the IgE protein at a concentration of 0.5 µM.
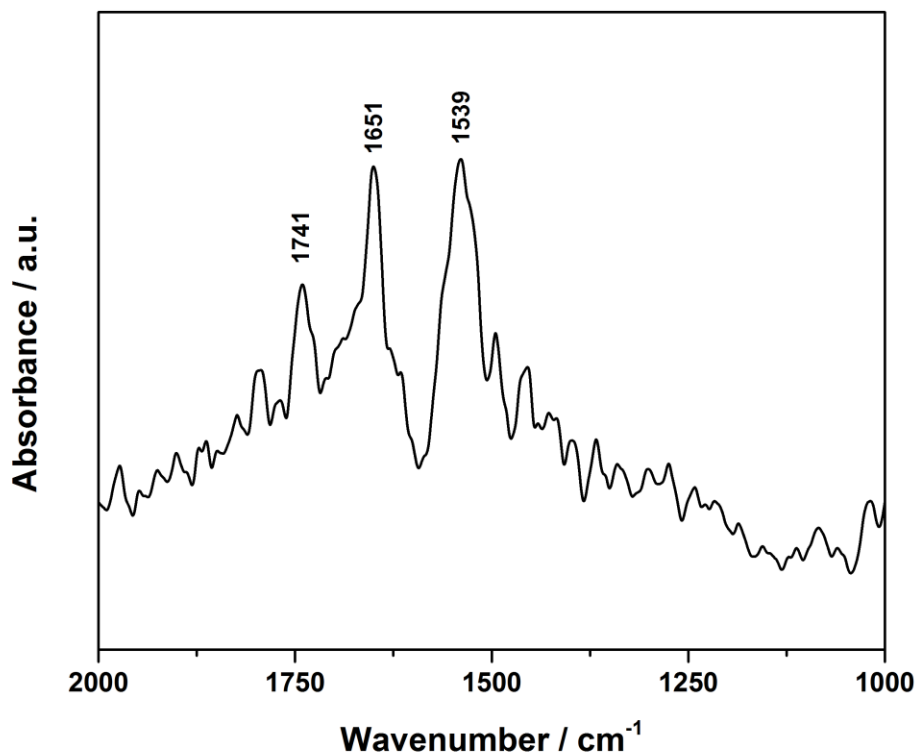
Figure 12. ATR-FTIR spectrum of IgE protein (20 µL of 0.5 µM) in phosphate buffer.

5.5 Electrochemical detection of IgE

It was not possible to detect IgE protein using the EC-SERS aptasensor setup, nor as just the protein non-specifically adsorbed onto the AgNPs. The ATR-FTIR results showed that protein is indeed present in the sample. In order to test if the aptasensor was indeed working, cyclic voltammetry was used. A three electrode system was used for the analysis, which consisted of a Au working electrode, onto which the aptamer and 12-MDA were immobilised, a Pt wire counter electrode, and a Ag/AgCl (KCl sat.) reference. The electrodes were immersed in a solution containing 1 mM $K_3Fe(CN)_6$ in phosphate buffer for all analyses. After the polishing step, the aptamer/spacer functionalised Au electrode was prepared in a similar manner to the EC-SERS AgNP electrodes. One other difference was that the incubation step in 12-MDA was for only 20 minutes in 50 μM solution. The purpose of the $K_3Fe(CN)_6$ is to act as a redox probe. As the Au surface becomes increasingly covered (i.e. insulated), less electron transfer is able to occur, thereby resulting in a decrease in measured current. These results are shown in Figure 13. Changes are observed at each step of the aptasensor preparation. When the Au electrode is treated with anti-IgE aptamer, the measured current of the CV decreases due to the insulating effect of the DNA SAM. Similarly, after the electrode is immersed in 12-MDA, a larger decrease in measured current is observed. Finally, an even lower current is measured after the anti-IgE/12-MDA modified Au electrode is treated with IgE. This result suggests that IgE is indeed binding to the aptamer, but so far, the EC-SERS method has not been able to detect it.
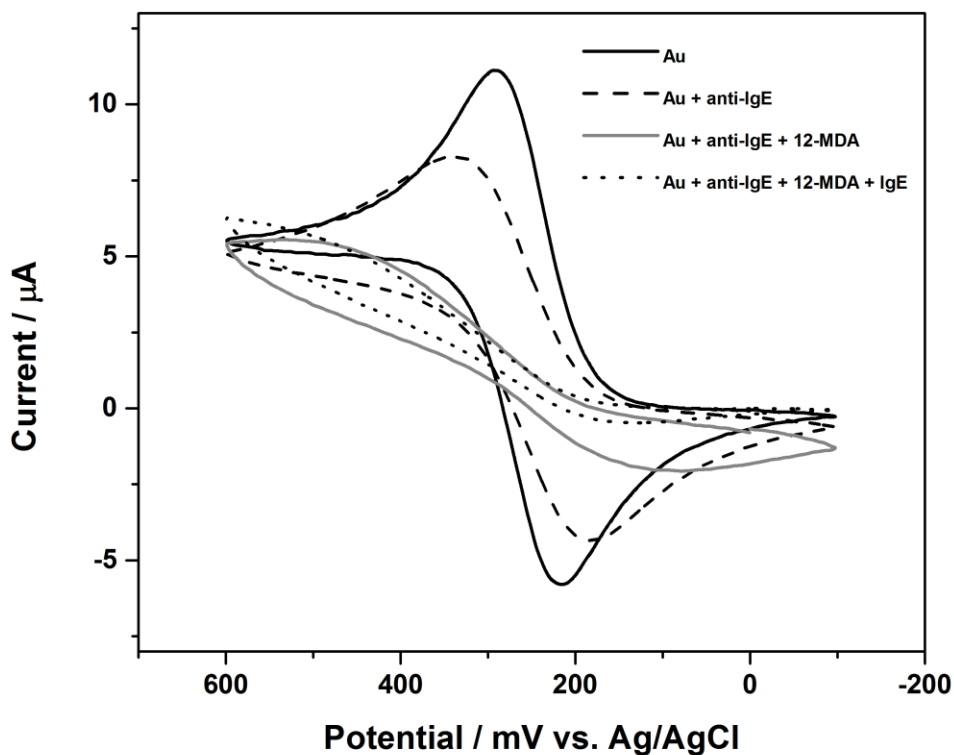
Figure 13. Cyclic voltammetry detection of IgE binding to anti-IgE aptamer on Au working electrode in 1 mM $K_3Fe(CN)_6$ + phosphate buffer. Pt counter electrode and Ag/AgCl (KCl sat.) reference electrode. Scan rate = 20 mVs^{-1}.

5.6 Concentration of anti-IgE

Ten spectra were collected and averaged for the anti-IgE aptamer over the concentration range of 1 to 0.001 mM (Figure 14). It may be the case that the 1 mM anti-IgE results in the formation of an aptasensor with such a high concentration of aptamer that it simply overwhelms the IgE spectrum, and additionally, prevents optimised binding

to the surface. Good EC-SERS spectra were obtained for the 0.1 and 0.01 mM anti-IgE solutions, which means that preparation of the aptasensor using costly 1 mM anti-IgE is not necessary.
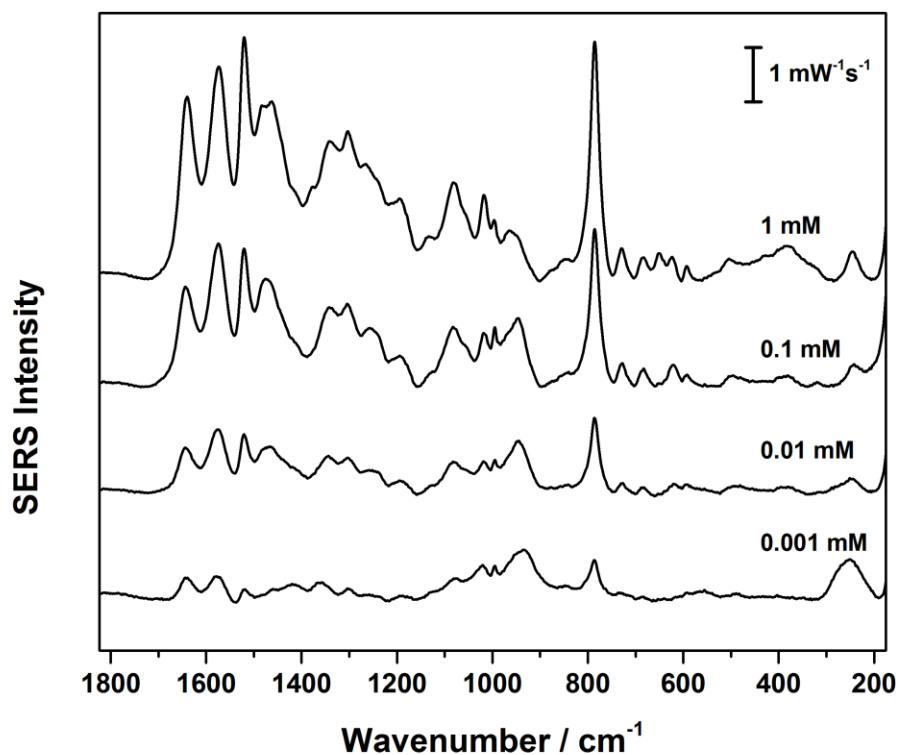
Figure 14. Averaged EC-SERS spectra (10 spots) recorded at -1.0 V of 10 µL of anti-IgE aptamer on citrate/borohydride reduced AgNP electrodes in 0.1 M NaF. Collection time = 30 s. 532 nm wavelength: laser power = 3 mW.

5.7 Laser Wavelength: Near IR or visible light excitation?

For the previously shown EC-SERS spectra, a bench top Raman spectrometer with a 785 nm laser was used. For the majority of this project (cyt c and KatG sections), another Raman spectrometer was used, which has switchable laser wavelengths of 780 and 532 nm. Additionally, this instrument allows for greater precision in terms of focusing on the electrode surface. In order to determine the optimal wavelength, spectra were collected using the visible 532 nm laser and the near-infrared (NIR) 780 nm laser, as shown in Figure 15. For this analysis, 10 spectra were collected at different spots while the potential was held constant at -1.0 V (LSV: 2 mVs^{-1} sweep from 0.0 to -0.7 V first) and then averaged. The 780 nm laser gives similar results that nonetheless compare favourably with the results of the 785 nm laser (Figure 7). However, the difference is very likely because a higher quality instrument was used for the 780 nm spectra. Even better signal was observed when the visible 532 nm laser was used. Accordingly, the 532 nm laser was used for all later analyses. Band assigned is shown in Table 6.
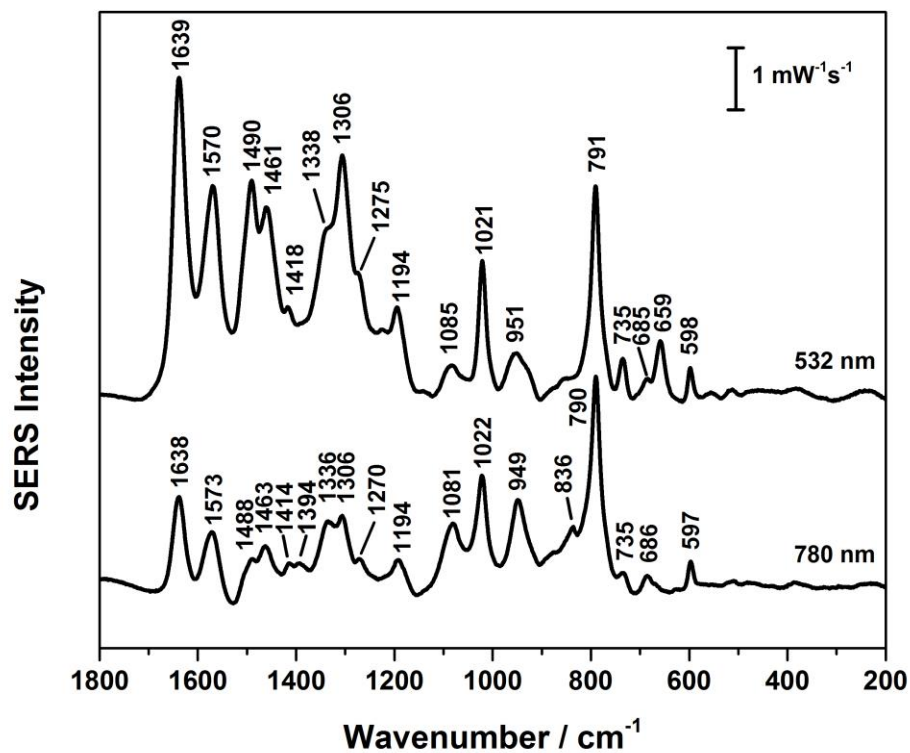
Figure 15. Averaged EC-SERS spectra (10 spots) recorded at -0.7 V for 10 μL of 0.1 mM anti-IgE aptamer on citrate/borohydride reduced AgNP electrodes in 0.1 M NaF. For 532 nm laser excitation: power = 10 mW, collection time = 30 s, . For 780 nm laser excitation: power = 50 mW, collection time = 30 s, 780 nm averaged spectrum multiplied by 5 for ease of visual comparison.

Table 6. Band assignment for the anti-IgE aptamer on AgNPs.

Wavenumber / cm^{-1}		Assignment	Reference
780 nm	532 nm		
1638	1639	Ring stretching of guanine or ν(C=O)	34, 132, 145
1573	1570	Ring stretching of guanine and adenine	134
1488	1490	Adenine, thymine, cytosine	133
1463	1461	Ring breathing of adenine	34, 134, 146
1414	1418	CH_2 deformation (?)	48
1394	-	CH_2 deformation	34, 48
1336	1338	Adenine (mixed modes)	34, 134, 146
1306	1306	ν(C-O-C) of adenine or ν(C-NH$_2$) of cytosine	145, 147
1270	1275	Ring stretching + CH bending of thymine	34, 48, 132
1194	1194	Cytosine and adenine (mixed modes)	132
1081	1085	DNA backbone (PO$_2^-$ stretch)	133, 148
1022	1021	NH$_2$ rock of adenine	146
949	951	Deoxyribose	134
836	-	C-O-P-O-C	149
790	791	Ring breathing of cytosine and thymine	34, 133
735	735	Ring breathing of adenine	34, 132, 133, 146, 147
686	685	Guanine or ν(C-S)	34, 133, 148
-	659	ν(C-S)	34, 125, 128, 150, 151
597	598	Ag-S-C-C$_{trans}$	152
-	557	Ag-S-C-C$_{gauche}$ or cytosine	132, 152
510	512	Guanine (mixed modes)	132
~230	243	ν(Ag-S)	125, 126, 130

5.8 Conclusion for IgE aptamer studies

The studies of the anti-IgE aptamer have not yielded a working EC-SERS aptasensor for IgE protein. Despite this unsuccessful endeavour, much useful information has been gained. The CV results show that the aptamer is indeed binding IgE, but this binding was not detected by EC-SERS. EC-SERS studies of the aptamer itself have revealed that the 12-MDA alkanethiol spacer does not interfere with the aptamer spectrum. The visible 532 nm laser excitation gives better spectra than the NIR 780 nm one. Lastly, the major bands in the EC-SERS spectra of the anti-IgE aptamer have been assigned to their DNA modes of vibration.

The IgE protein may not have been detected because it gives a weak Raman/SERS spectrum itself, or because of the distance from the surface of the protein in the aptamer-protein complex. If the former problem is indeed the case, other studies involving proteins that are stronger Raman scatterers may be more fruitful. For this reason, cytochrome c, a protein containing a Raman active heme group, was chosen for the subsequent model protein studies.

5.9 Normal Raman spectroscopy of cytochrome c protein

The first step of the aptamer-based detection of cytochrome c protein (cyt c) phase of the project was to collect normal Raman spectra of cyt c, and determine which laser wavelength is best for this purpose. The two available laser excitations were the visible 532 nm and near-infrared (NIR) 780 nm lasers. The UV-visible spectrum of 10 μM cyt c is shown in Figure 16, which is in agreement with previous results in the literature [80]. The band at approximately 530 nm suggests that resonance Raman enhancement ought to be obtained when the 532 nm wavelength laser is used, which is consistent with previous resonance Raman studies of cyt c [80, 153]. A Raman laser near 409 nm might give even greater resonance enhancement, but only 532 and 780 nm lasers were available.
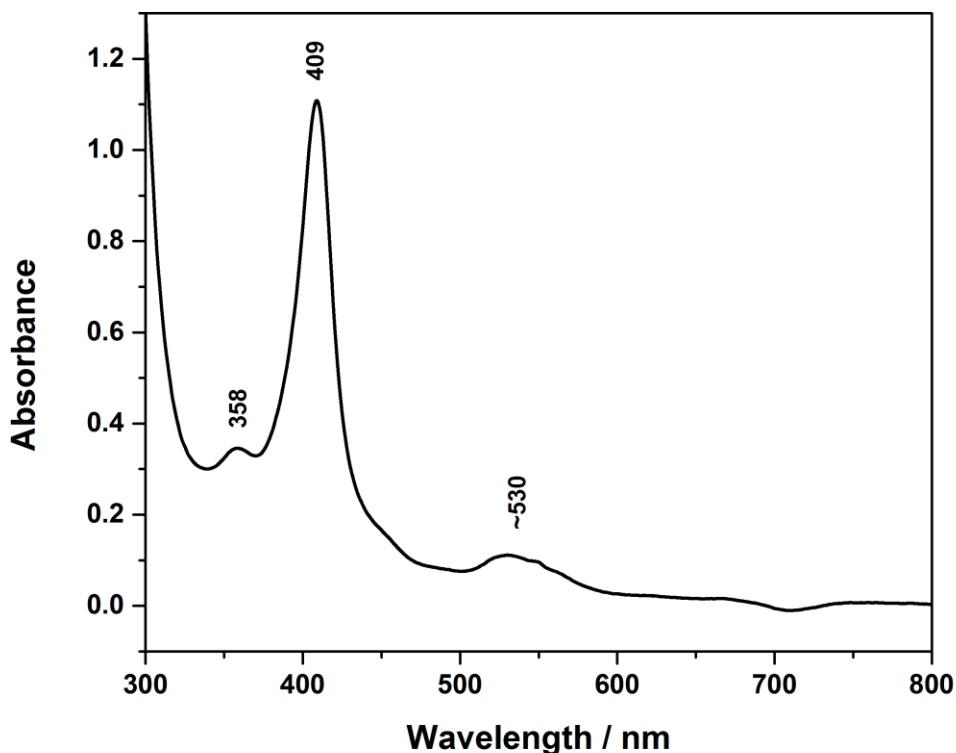
Figure 16. UV-vis spectrum of 10 μM cyt c.

The Raman spectra recorded using the 532 and 780 nm lasers are shown in Figure 17. The 532 nm spectrum has more vibrational information than the 780 nm spectrum, and nearly all bands that appear in both spectra are more intense in the 532 nm spectrum. The assignments for these bands are given in Table 7. Most of the band assignments can be attributed to the porphyrin modes of the heme group.
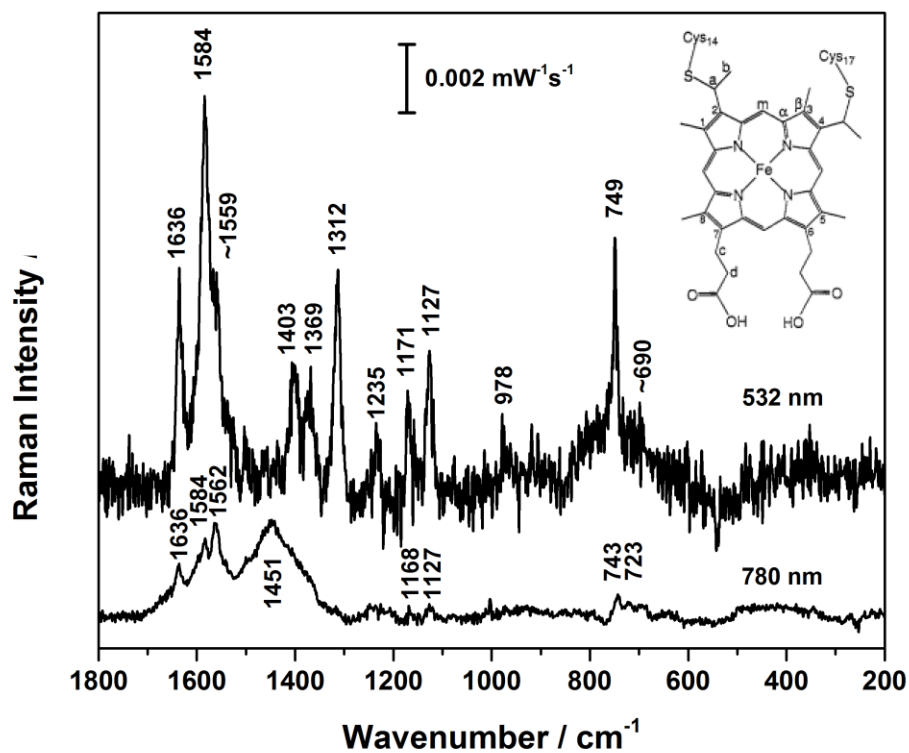
Figure 17. Raman spectra of bulk cyt c recorded using 532 nm (10 mW, 120 s) and 780 nm (100 mW, 120 s) laser excitation. The labelled molecular structure of the heme moiety of cyt c is included for reference. Reproduced with permission from S. Hu, I. K. Morris, J. P. Singh, K. M. Smith, T. G. Spiro. *J. Am. Chem. Soc.,* **1993,** *115,* 12446-12458. Copyright 1993 American Chemical Society.

Table 7. Band assignment for Raman of bulk cyt c protein.

Band / cm^{-1} (532 nm)	Band / cm^{-1} (780 nm)	Assignment	Reference
1636	1636	$\nu(C_\alpha - C_m)_{asym}$, Fe^{3+} 6cLS	[80, 83]
1584	1584	$\nu(C_\alpha C_m)_{asym}$	[136]
1559	1562	$\nu(C_\alpha - C_m)_{asym}$, Fe^{3+} 5cLS	[83]
-	1451	$\delta(CH_2)$ wag prop	[81]
1403	-	ν(pyr quarter-ring)	[83]
1369	-	ν(pyr half ring)$_{sym}$, Fe^{2+}	[83]
1312	-	$\nu(C_\alpha C_\beta)$	[136]
1235	-	$\delta(C_m{-}H)$	[83]
1171	1168	ν(pyr half ring)$_{sym}$	[83]
1127	1127	$\nu(C_\alpha N)$	[136]
978	-	Amide III	[81]
749	743	ν(pyr breathing); $\nu(C_\alpha C_\beta)$	[136]
-	723	pyr fold$_{asym}$	[80]
~690	-	ν(pyr deform)sym, or $\nu(C_aS)$	[81, 136]

5.10 EC-SERS of cytochrome c protein

EC-SERS spectra of equine cytochrome c protein (cyt c) in solution were recorded at open circuit potential (ocp), and over the potential range of 0.0 to -1.0 V (-0.1 V increments) vs. Ag/AgCl. EC-SERS spectra were first collected for 5 μM cyt c in 0.05 M NaF at a citrate reduced AgNP electrode (shown in the Appendix Figure A1). At a midway point through the project, there were concerns that fluoride ion may be forming a Fe-F bond with the heme iron centre of the cyt c, as reported in the literature. [157-159] It is not known whether this difference could affect the binding of cyt c to the DNA aptamer. However, as a precaution, some experiments were repeated and later ones were conducted using 0.03 M Na_2SO_4 as the supporting electrolyte instead. EC-SERS spectra were collected for 10 μM cyt c in 0.03 M Na_2SO_4, shown in Figure 18. Band assignments

are given in Table 8. In both cases, the EC-SERS signal intensity was found to increase significantly in the range of -0.7 to -1.0 V.
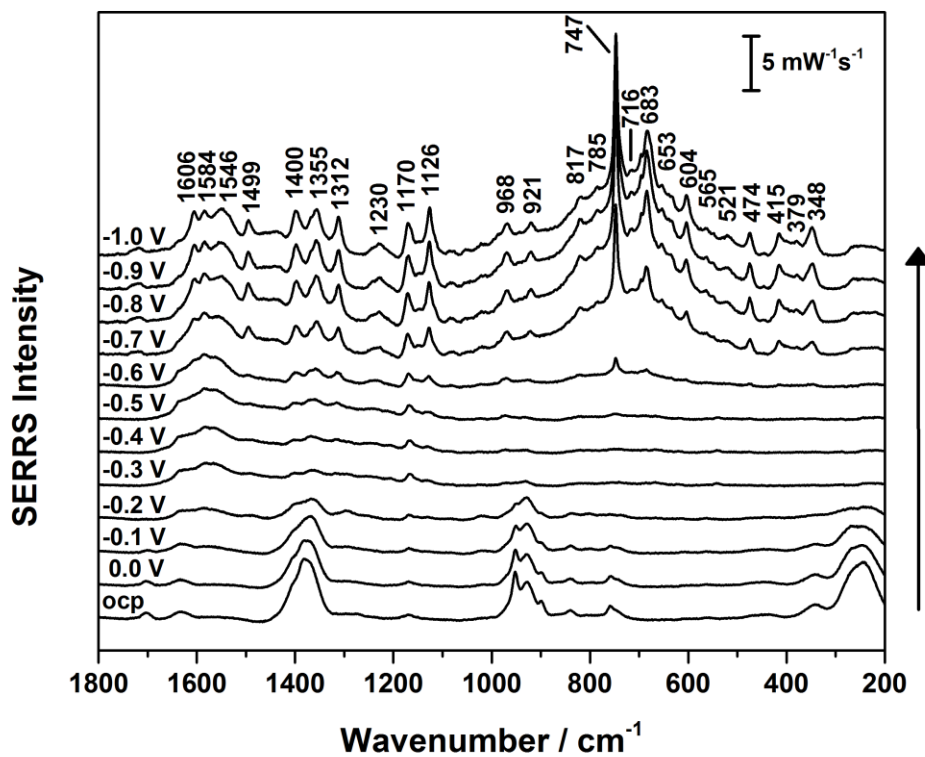
Figure 18. EC-SERRS 10 μM cyt c solution in 0.03 M Na$_2$SO$_4$ at a citrate/borohydride reduced AgNP electrode collected at ocp, and over the cathodic potential range of 0.0 to -1.0 V vs Ag/AgCl. Laser power = 10 mW, collection time = 30 s, wavelength = 532 nm.

Table 8. Partial band assignment for 10 µM cyt c solution in 0.03 M Na_2SO_4 at a citrate/borohydride reduced AgNP electrode.

Band / cm⁻¹	Assignment	Reference
1606	$\nu(C_\alpha - C_m)_{asym}$ (1636 cm⁻¹) Reduction from 6cLS Fe^{3+} to 5cHS Fe^{2+}	[81]
1584	$\nu(C_\alpha C_m)_{asym}$	[136]
1546	Mode not clear, but indicates Fe^{2+}	[81]
1499	$\nu(C_\alpha - C_m)$sym	[83]
1400	ν(pyr quarter-ring)	[83]
1355	?	-
1312	$\nu(C_\alpha C_\beta)$ $\delta(CH_2)$ wag	[81, 136]
1230	$\delta(C_m-H)$	[83]
1170	ν(pyr half ring)$_{sym}$	[83]
1126	$\nu(C_\alpha N)$	[136]
968	$\nu(C_c C_d)$ prop	[81]
921	?	-
817	?	-
785	?	-
747	ν(pyr breathing); $\nu(C_\alpha C_\beta)$	[136]
716	Mode not clear, but indicates Fe^{2+}	[81]
683	$\nu(C_a S)$	[81]
653	Pyr fold$_{asym}$	[80]
604	?	-
565	?	-
521	?	-
474	?	-
415	?	-
379	$\delta(C_b C_c C_d)$prop	[81]
348	δ(prop), Fe^{3+} or pyr swivel	[80-81]

Many new bands appear in the EC-SERRS spectra of cyt c (Figure 18) when compared with the normal resonance Raman spectrum (532 nm, Figure 17). Some of these bands are assigned based on data available in the literature, whereas others cannot be identified with certainty. Nonetheless, there are some reoccurring bands, such as the pyr breathing band at 748 cm^{-1}. A thorough study of the cyt c Raman and EC-SERS spectra are not necessary at this point because, as is shown later, not all of these bands appear in the spectra of cyt c bound to the anti-cyt DNA aptamer. Accordingly, cyt c marker bands will be chosen from those observed for the aptamer-protein complex.

The next step involved detection of non-specifically adsorbed cyt c on a citrate reduced AgNP electrode (analysis in 0.1 M NaF only), instead of simply analysing a solution of bulk cyt c with added electrolyte. For this analysis, 20 μL of 10 μM cyt c protein was drop-coated onto the AgNP electrode, and left to incubate for 1 hour at room temperature before lightly rinsing with phosphate buffer. EC-SERS spectra were collected in 0.1 M NaF electrolyte. While the band intensities were significantly weaker, as would be expected, the spectral profile of the adsorbed cyt c was similar to what was recorded for the protein solution. The same bands were observed, and signal enhancement was best at potentials more negative than -0.6 V. The cathodic and anodic scans are shown in Figure 19.
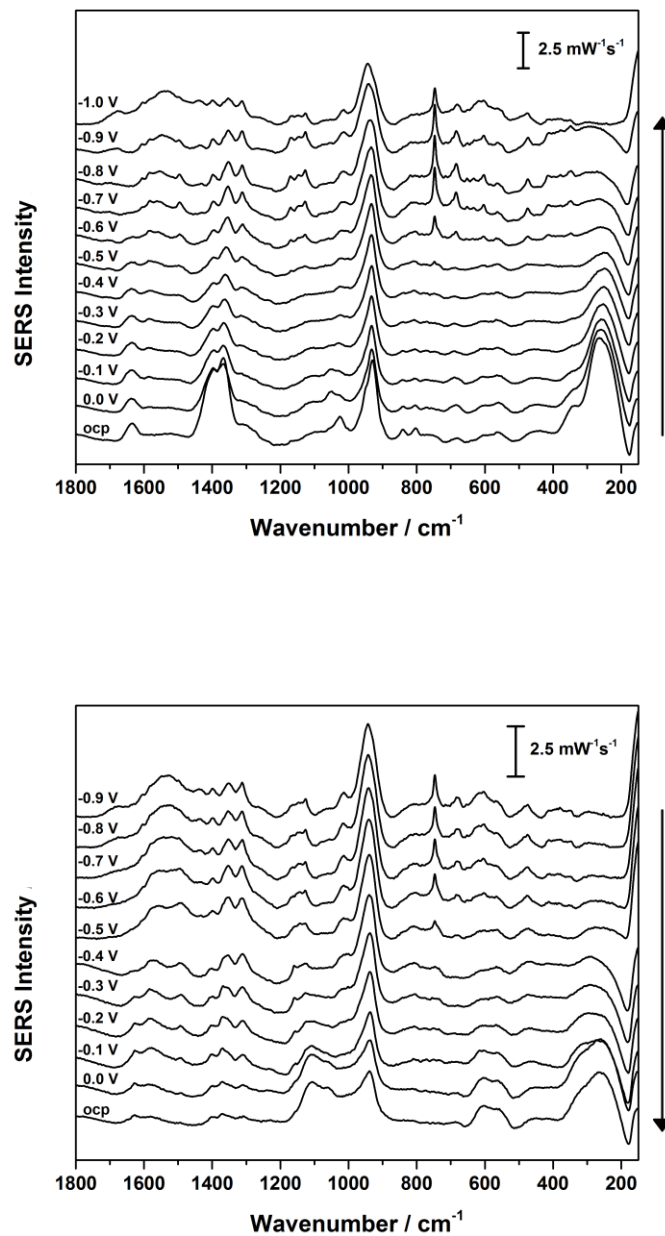
Figure 19. EC-SERS spectra (Top: cathodic scan; bottom: anodic scan) of 20 μL of 10 μM cyt c non-specifically adsorbed onto a citrate reduced AgNP electrode in 0.1 M NaF. Laser power = 3 mW, collection time = 30 s, wavelength = 532 nm.

In the cathodic scan (Figure 19, top), it was observed that the strongest cyt c band (748 cm^{-1}) reaches a maximum at -0.7 and -0.8 V, but decreases slightly thereafter. There was no improvement in the anodic scan (Figure 19, bottom) when the applied potential was stepped back to more positive values.

5.11 EC-SERS of anti-cytochrome c aptamer

The anti-cytochrome c aptamer (anti-cyt) was previously developed by Chinnapen *et al.* [87]. Full experimental preparation details are provided in Chapter 4. In order to characterise the aptamer, 10 µL of 1 mM anti-cyt was drop coated onto a citrate reduced AgNP electrode, and allowed to dry overnight. Light rinsing with several milliliters of phosphate buffer and ultrapure water was done to remove any excess aptamer on the surface that had not been immobilised via the formation of a Ag-S bond. EC-SERS spectra were collected in electrolyte in a similar manner to what had been done for the non-specifically adsorbed cyt c protein; spectra are shown in Figure 20. At ocp and over the potential range of 0.0 to -0.2 V, the citrate used in the AgNP synthesis dominates the spectra. The characteristic DNA bands begin to increase in signal intensity as the potential is stepped more negative. Minimal changes in intensity are observed over the potential range of -0.7 to -1.0 V. In the anodic scan, a slight decrease in signal intensity is observed as the applied potential is stepped back to more positive values.

The EC-SERS spectrum for anti-cyt recorded at -0.7 V (cathodic scan) is shown in Figure 21, with all major bands labelled. The band assignments are listed in Table 9.
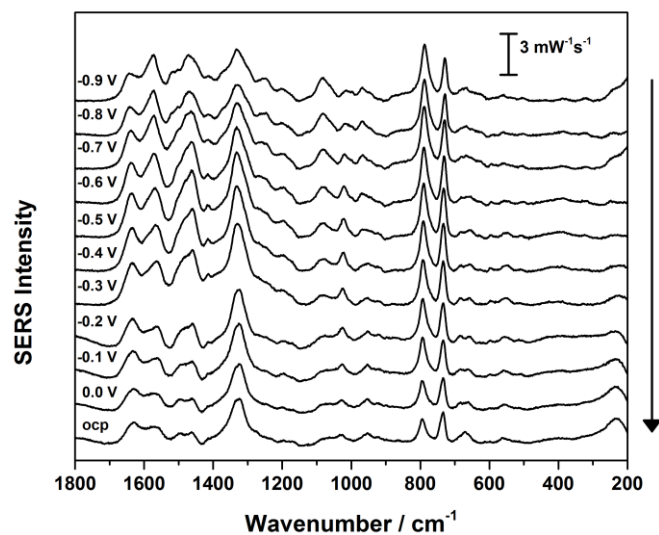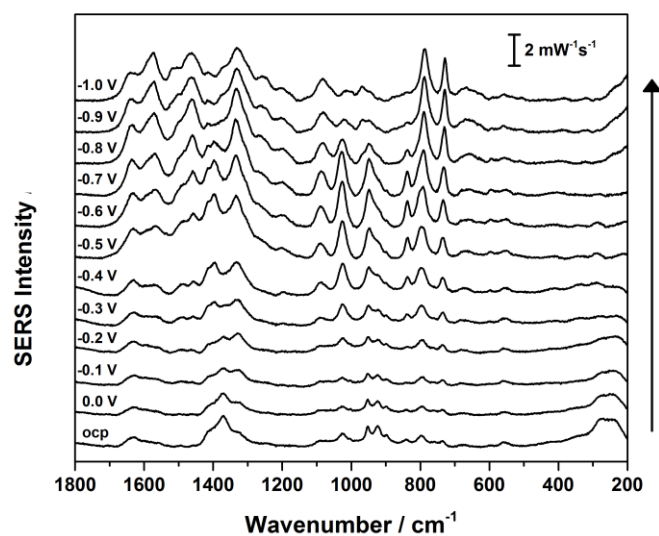
Figure 20. EC-SERS spectra (Top: cathodic scan; bottom: anodic scan) of 10 μL of 1 mM anti-cyt aptamer on a citrate reduced AgNP electrode in 0.1 M NaF. Laser power = 3 mW, collection time = 30 s, wavelength = 532 nm.
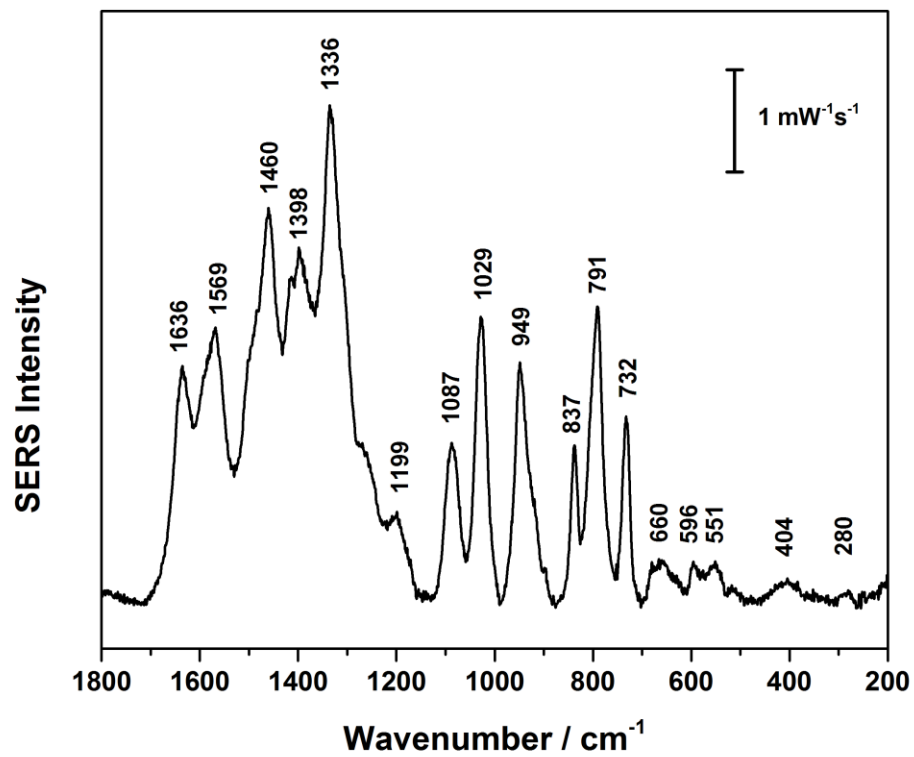
Figure 21. EC-SERS spectrum of 10 μL of 1 mM anti-cyt aptamer on a citrate reduced AgNP electrode in 0.1 M NaF recorded at -0.7 V (cathodic). Laser power = 3 mW, collection time = 30 s, wavelength = 532 nm.

Table 9: Band assignment for the anti-cyt aptamer on AgNPs.

Band / cm^{-1}	Assignment	Reference
1636	Ring stretching of guanine or ν(C=O)	[34, 132, 145]
1569	Ring stretching of guanine and adenine	[134]
1460	Ring breathing of adenine	[34, 134, 146]
1398	CH_2 deformation	[34, 48]
1336	Adenine (mixed modes)	[34, 134, 146]
1199	Cytosine and adenine (mixed modes)	[132]
1087	DNA backbone (PO_2^- stretch)	[133, 148]
1029	NH_2 rock of adenine	[146]
949	Deoxyribose	[134]
837	C-O-P-O-C	[149]
791	Ring breathing of cytosine and thymine	[34, 133]
732	Ring breathing of adenine	[34, 132-133, 146-147]
660	ν(C-S)	[34, 125, 128, 150-151]
596	Ag-S-C-C$_{trans}$	[152]
551	Ag-S-C-C$_{gauche}$ or cytosine	[40, 152]
404	?	-
280	ν(Ag-S)	[129]

Immobilisation of the aptamer onto the AgNPs ought to give rise to a ν(Ag-S) band. A relatively weak band is observed at 280 cm^{-1}. The position of this band is usually reported around 250 cm^{-1} [125-126, 130], but in one study it was found at 280 cm^{-1} [129]. Formation of the Ag-S bond would necessarily be coincident with the breaking of the S-S bond, previously reported in the range 504-542 cm^{-1} [125-128]. The vibrational mode giving rise to the weak band observed at 551 cm^{-1} is not certain, but assigning it to a S-S stretch would not be unreasonable. Some residual non-specifically adsorbed aptamer may be on the surface giving rise to a S-S band. However, the low wavenumber of the ν(C-S) band at 660 cm^{-1} suggests the formation of a Ag-S bond. In the Raman spectrum of cysteine, the ν(C-S) band is observed at 690 cm^{-1}, but after adsorption onto Ag, the band broadens and downshifts to 670 cm^{-1} in the SERS spectrum, which indicates the

formation of a strong Ag-S bond [151]. If the Ag-S bond has indeed been formed, then the 551 cm^{-1} may be simply from cytosine [132] or from the Ag-S-C-C moiety [152].

Before beginning any optimisation steps, a preliminary analysis for detection of cyt c was performed. The anti-cyt aptamer was immobilised onto a citrate reduced AgNP electrode, followed by incubation for 2 hours in ethanolic 1 mM 12-mercaptododecanoic acid (12-MDA) alkanethiol spacer, followed by light rinsing with ethanol and water. The purpose of the 12-MDA is to prevent non-specific interaction of cyt c and other non-target molecules with bare areas of the AgNP electrode surface where a monolayer of DNA aptamer has not been formed via a Ag-S bond. Additionally, the 12-MDA promotes an upright orientation of the anti-cyt aptamer, which may help bind the protein [131]. The aptasensor was then treated with 20 μL of 10 μM cyt c protein in phosphate buffer, and left to incubate for 1 hour, followed by light rinsing with phosphate buffer and water. EC-SERS spectra were collected in 0.1 M NaF in an identical manner to the previous analyses.

Preliminary results (Figure 22) suggested that the aptasensor was able to detect cyt c protein. After treatment with cyt c, bands for both the DNA aptamer (anti-cyt) and the cyt c protein were observed. For example, the diagnostic cyt c band at 748 cm^{-1} was observed at potentials more negative than -0.6 V in the cathodic and anodic scans.
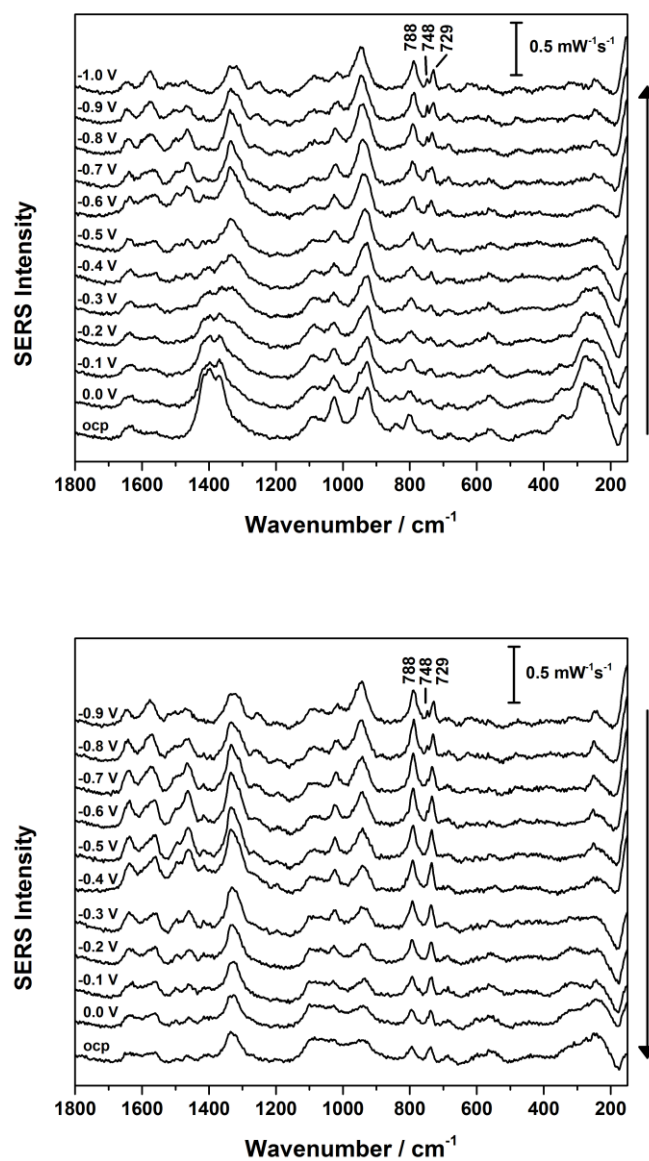
Figure 22. EC-SERS spectra (Top: cathodic scan; bottom: anodic scan) anti-cyt + 12-MDA modified AgNP electrode after treatment with 20 μL of 1 mM cyt c protein for 1 hour. Laser power = 3 mW, collection time = 30 s, wavelength = 532 nm.

5.12 Non-specific adsorption onto alkanethiol spacer

The 12-MDA alkanethiol spacer was originally used for the initial IgE studies and other DNA hybridisation work in our lab. One concern; however, was that the cyt c may be electrostatically interacting with the 12-MDA alkanethiol spacer, and not specifically bonding to the anti-cyt aptamer. Specifically, positively charged amino acid residues may be interacting with the carboxyl group of the 12-MDA. A search of the literature revealed that this interaction may indeed be a problem [86].

Shown in Figure 23 are EC-SERS spectra recorded at -0.7 V of self-assembled monolayers (SAM) of 6-mercaptohexanoic acid (6-MHA) and 6-mercapto-1-hexanol (6-MH) on AgNPs. (Full cathodic EC-SERS spectra shown in the Appendix Figures A2 and A3). Spectra have been collected for each alkanethiol SAM before and after treatment with cyt c protein (incubation in 7 mL of 7 μM cyt c in phosphate buffer for 1 hour, followed by light rinsing with phosphate buffer and ultrapure water). 6-MHA and 6-MH were chosen as shorter substitutes for 12-MDA and 11-mercapto-1-undecanol (11-MUD), respectively, since any cyt c present on the SAM would be closer to the Ag metal surface on the shorter alkanethiol chain, thereby giving it increased SERS enhancement compared to the longer alkanethiol. Based on the characteristic cyt c band at 750 cm^{-1}, the protein was clearly detected on the 6-MHA SAM, but not on 6-MH. Accordingly, the use of 12-MDA was discontinued for all future analyses, and 11-MUD was used instead. Note that the longer 11-MUD was used for the aptasensor, instead of the shorter 6-MH, because previous work in our lab found that longer alkanethiols exhibit better long-term stability. Additionally, confirmation of a lack of adsorption onto 11-MUD could perhaps

not give an accurate result, because any non-specifically adsorbed cyt c may be too far from the SERS-active AgNP surface, and simply not detected via SERS.
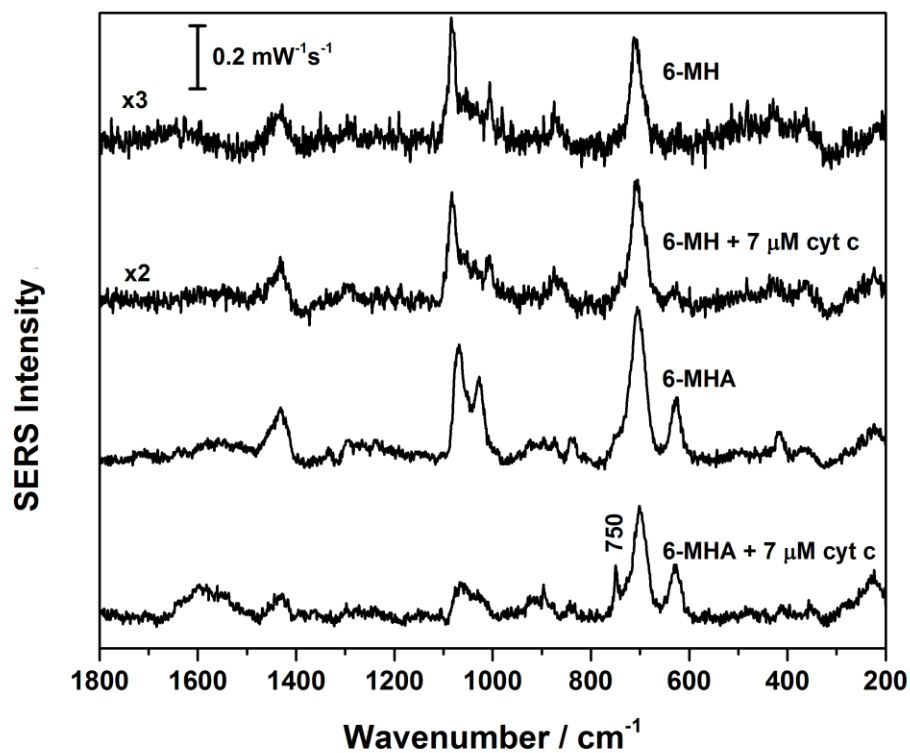
Figure 23. EC-SERS spectra of self-assembled monolayers of alkanethiol (6-MHA or 6-MH, 20 hour incubation) with and without 7 μM cyt c (1 hour incubation in 7 mL) on citrate/borohydirde reduced AgNPs recorded at -0.7 V. Full cathodic EC-SERS spectra shown in the Appendix Figures A2 and A3. Laser excitation = 532 nm, time = 30 s, power = 5 mW.

5.13 Dilution of anti-cyt aptamer

The previous results had shown that cyt c could be detected using the anti-cyt aptamer. Furthermore, the issue of non-specific adsorption of cyt c onto 12-MDA had been resolved by substituting it with a different alkanethiol spacer, 11-MUD. Using 1 mM aptamer is relatively wasteful and cost-prohibitive. For example, one order of laptamer contained 7.35 mg (379.8 nmol) DNA for a price of about $370 CAD. Preparing a 1 mM solution gives 379.8 μL of solution. If 10 μL of this solution is used per electrode, that means each order of aptamer can only be used to prepare 37 electrodes. If each electrode costs about $10 for the DNA aptamer, in addition to the costs for the screen printed electrode, AgNPs and the alkanethiol spacer, the cost for producing these aptasensors could be prohibitively expensive for use in limited resource settings. Accordingly, a lower concentration of aptamer was desired.

The 1 mM aptamer was diluted to 0.1, 0.01 and 0.001 mM, and 10 μL aliquots of these solutions were drop-coated onto AgNP electrodes. Furthermore, the aptamer functionalised electrodes were prepared separately with and without 1 mM 11-MUD for 2 hours using the usual procedure. EC-SERS spectra were collected in 0.1 M NaF. Good EC-SERS spectra could be collected using 0.1 mM anti-cyt, and the result was found to be reproducible for all three trials. Three EC-SERS spectra recorded at -0.7 V for 0.1 mM anti-cyt are shown in Figure 24. When 11-MUD was used (also shown in Figure 24), it was possible to detect anti-cyt for all three trials. Shown in Figure 25, it was possible to detect anti-cyt at concentrations of 0.01 and 0.001 mM. However, after incubation in 1 mM 11-MUD, it was not possible to detect the DNA aptamer. For all trials, the spectra

recorded at -0.7 V show just the 11-MUD alkanethiol spacer characteristic bands, such as the ν(C-S)$_{trans}$ around 705 cm^{-1} and the ν(C-O) at 1105 cm^{-1}. Note that the ν(C-S)$_{gauche}$ band at 656 cm^{-1} of the aptamer is no longer observed [150, 154-155]. Accordingly, 0.1 mM anti-cyt aptamer was chosen as the concentration for all future analyses. The cost was minimised, while still achieving a good signal.
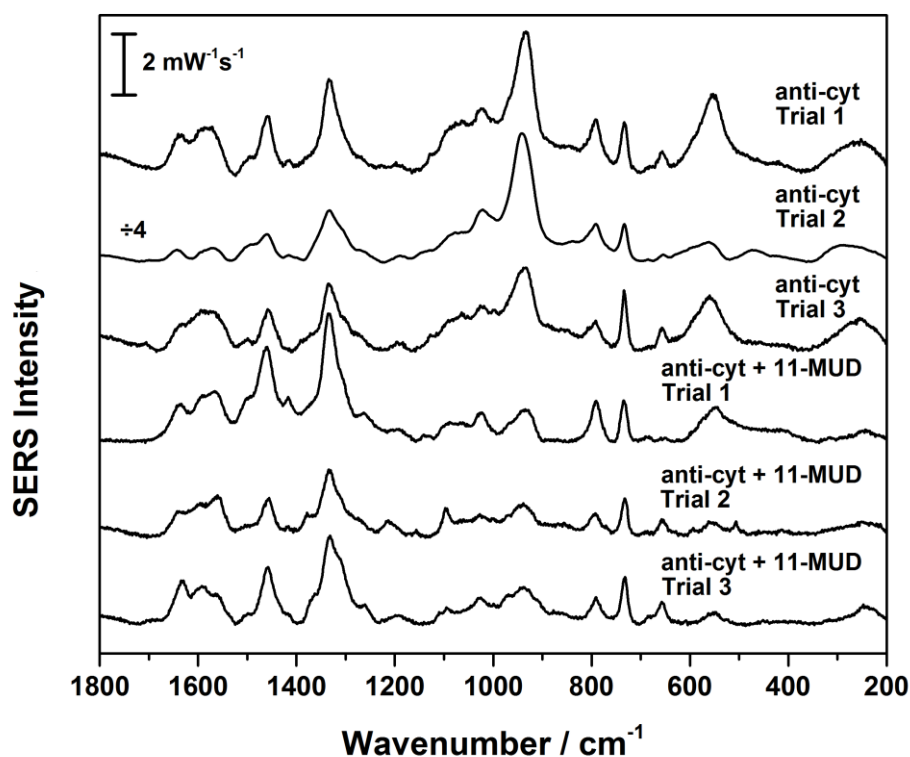
Figure 24. EC-SERS spectra recorded at -0.7 V (cathodic) of 10 μL for 0.1 mM anti-cyt aptamer with and without 1mM 11-MUD for three trails each on citrate reduced AgNP electrodes in 0.1 M NaF Laser power = 3 mW, collection time = 30 s, wavelength = 532 nm.
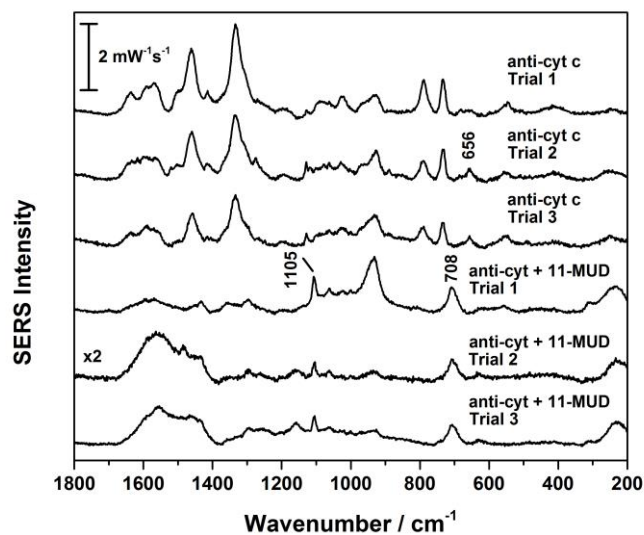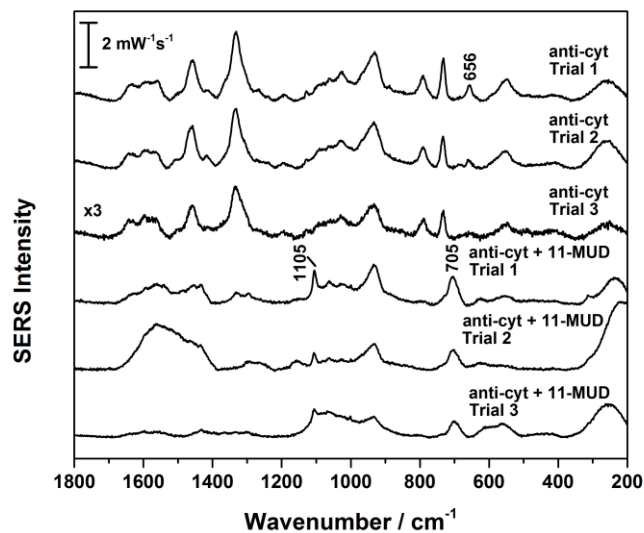
Figure 25. EC-SERS spectra recorded at -0.7 V (cathodic) for 10 µL of 0.01 mM (top) and 0.001 mM (bottom) anti-cyt aptamer with and without 1mM 11-MUD for three trails each on citrate reduced AgNP electrodes in 0.1 M NaF. Laser power = 3 mW, collection time = 30 s, wavelength = 532 nm.

5.14 Averaging of multiple spectra method

The previous results of this study have shown that the best signal intensity for detection of cyt c using this aptasensor method is at potentials more negative than -0.7 V vs. Ag/AgCl. Furthermore, slight signal intensity decreases were observed at more negative potentials. Accordingly, -0.7 V was chosen as the best potential for analysis. It had been observed in some analyses (data not shown) that there were often significant spot-to-spot variations in relative band signal intensity. In some instances, the anti-cyt aptamer would dominate the EC-SERS spectra. In other cases, there would be more significant contributions from the 11-MUD. This result suggests an uneven distribution of aptamer on the surface [156], followed by uneven backfilling of alkanethiol spacer, which gives rise to differing EC-SERS spectra at different spots on the surface. To account for this variation, multiple EC-SERS spectra could be collected at different spots on the electrode surface while the potential is held constant at -0.7 V, and then averaged to give one spectrum. Not only will this method account for variations in the monolayer of aptamer and/or alkanethiol spacer, but it also ought to account for variations in SERS enhancement, also known as "hotspots".

Instead of jumping directly from ocp (no applied potential) to -0.7 V, linear sweep voltammetry (LSV) was used to gradually alter the potential from 0.0 to -0.7 V at a sweep rate of 2.3 mVs^{-1}, after which it was held constant at -0.7 V while 30 spectra were collected at various spots on the electrode. These spectra were then averaged. This method was used for three trials of 0.1 mM anti-cyt aptamer. The three averaged spectra

are highly reproducible, although some slight differences are observed. These averaged

spectra are shown in Figure 26.
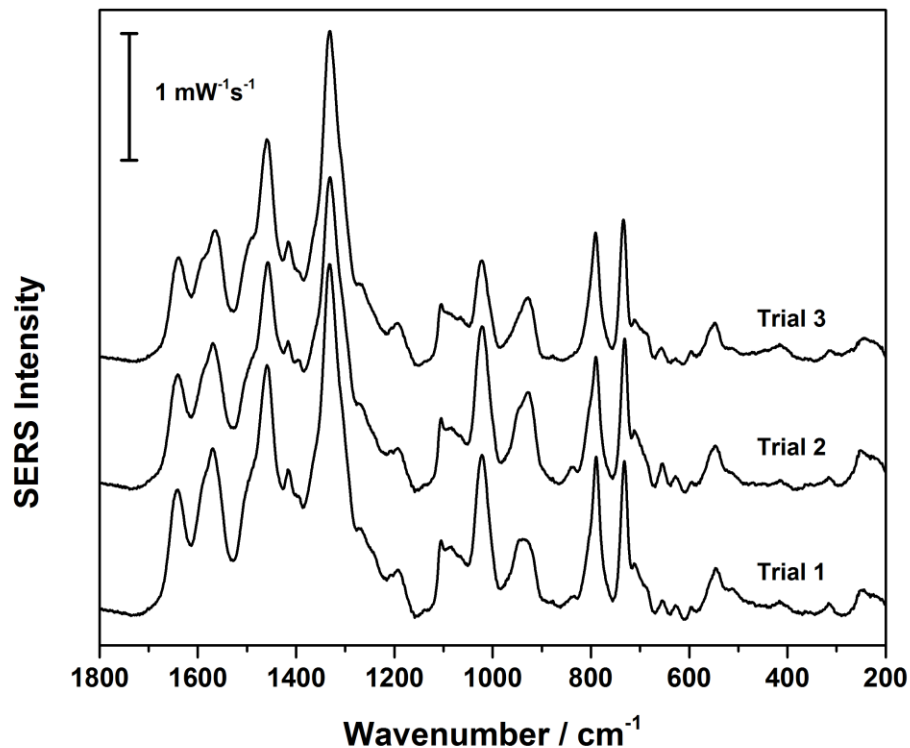
Figure 26. Three trials of averaged EC-SERS spectra (30 spots) recorded at -0.7

V of 10 µL of 0.1 mM anti-cyt aptamer + 1 mM 11-MUD on citrate reduced

AgNP electrodes in 0.1 M NaF. Laser power = 3 mW, collection time = 30 s,

wavelength = 532 nm.

The same method was then used for five trials of the aptasensor after treatment with 10 μL of 10 μM cyt c protein, shown in Figure 27. Looking at two cyt c bands, 1168 and 748 cm^{-1}, shows wide variation between each trial. In trials 1 and 2, the signal is very intense, but the 748 cm^{-1} band is more intense in trial 1. Trials 3 and 4 were much weaker in intensity, both for the cyt c bands and for the DNA aptamer bands. In trial 5, the 1168 cm^{-1} band is comparable to trials 1 and 2, but the 748 cm^{-1} is comparable to trials 3 and 4. Additionally, the DNA bands in trial 5 are comparable to trials 1 and 2. The 1107 cm^{-1} band from 11-MUD also shows a lot of variation; from relatively weak in trials 2 and 3, stronger in trial 5, and then even more intense in trials 1 and 4. What can be said from these results is that there appears to be no relationship between DNA aptamer (anti-cyt) and 11-MUD band intensity, and the cyt c band intensity. Furthermore, the variation in anti-cyt and 11-MUD band intensities of the averaged spectra suggests that an uneven monolayer may be formed on the surface. The variation in cyt band intensity may be a result of different orientations of cyt c in the aptamer-cyt c complex [162], or simply from an unequal adsorption of cyt c from one spot or one trial to the next.

5.14 Detection of lower concentrations of cyt c

The next step involved using the aptasensor to detect diluted cyt c protein. Figure 28 shows the EC-SERS method with 30 averaged spectra used for detection of cyt c in 10 μL aliquots samples of 10 μM and 1 μM cyt c. For the 1 μM sample, it was not possible to detect the cyt c protein. There may be a small cyt band around 1170 cm^{-1}, but the signal-to-noise ratio is certainly too low, moreover it would not seem unlikely that cyt c

could be detected at even lower concentrations, due to the already very weak signal intensity.
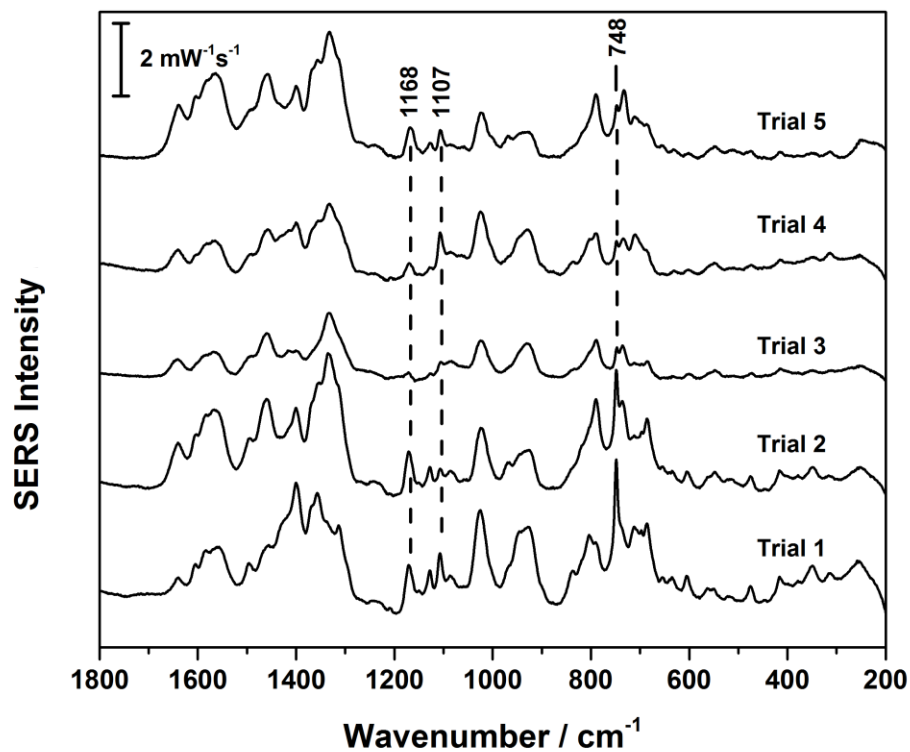
Figure 27. Five trials of averaged EC-SERS spectra (30 spots) recorded at -0.7 V of 10 μL of 0.1 mM anti-cyt aptamer + 1 mM 11-MUD + 10 μL of 10 μM cyt c on citrate reduced AgNP electrodes in 0.1 M NaF. Laser power = 3 mW, collection time = 30 s, wavelength = 532 nm.
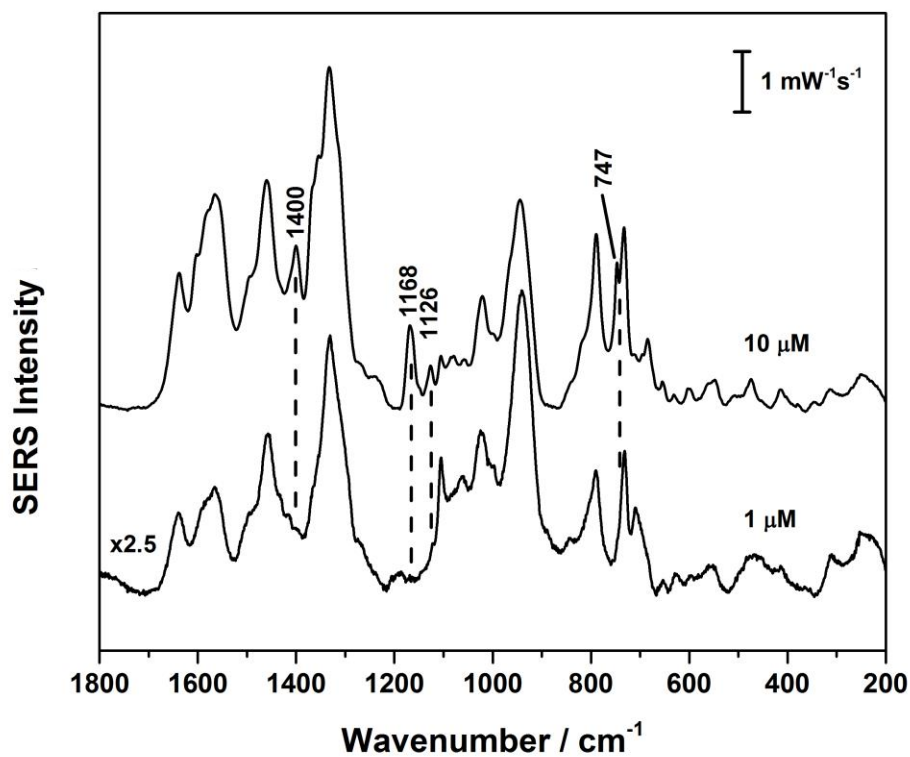
Figure 28. Averaged EC-SERS spectra (30 spots) recorded at -0.7 V of 10 μL of
0.1 mM anti-cyt aptamer + 1 mM 11-MUD for detection of 10 μL of 10 μM and 1
μM cyt c on citrate reduced AgNP electrodes in 0.1 M NaF. Laser power = 3 mW,
collection time = 30 s, wavelength = 532 nm.

It was decided that instead of trying to detect cyt c in a 10 μL aliquot, the aim should be to detect it in several milliliters of solution. In a real clinical analysis for detection of cyt c in urine, there would be no requirement to have such a microliter sized sample volume. Therefore, it was decided to immerse the aptasensor into several milliliters of protein / phosphate buffer solution for 1 hour, instead of just treating it with a small 10 μL droplet. This method was used to detect cyt c over the concentration range of 1000 nM (1 μM) to 10 nM, shown in Figure 29. The signal for cyt c was strong at 1000 and 100 nM, but it could not be detected at 10 nM. To encourage binding of cyt c to the anti-cyt aptamer, the 10 nM cyt c solution with the aptasensor immersed in it was heated to 37 °C using a water bath for 1 hour. The other method involved an 18 hour incubation at room temperature, instead of the usual 1 hour wait time. Unfortunately, neither of these methods led to successful detection of cyt c at a concentration of 10 nM. The usual method (room temperature, 1 hour incubation) was used for a 50 nM sample, and a weak signal was detected for the protein. A proper limit of detection (LOD) was not determined, but these results suggest that the LOD lies somewhere between 100 and 10 nM.
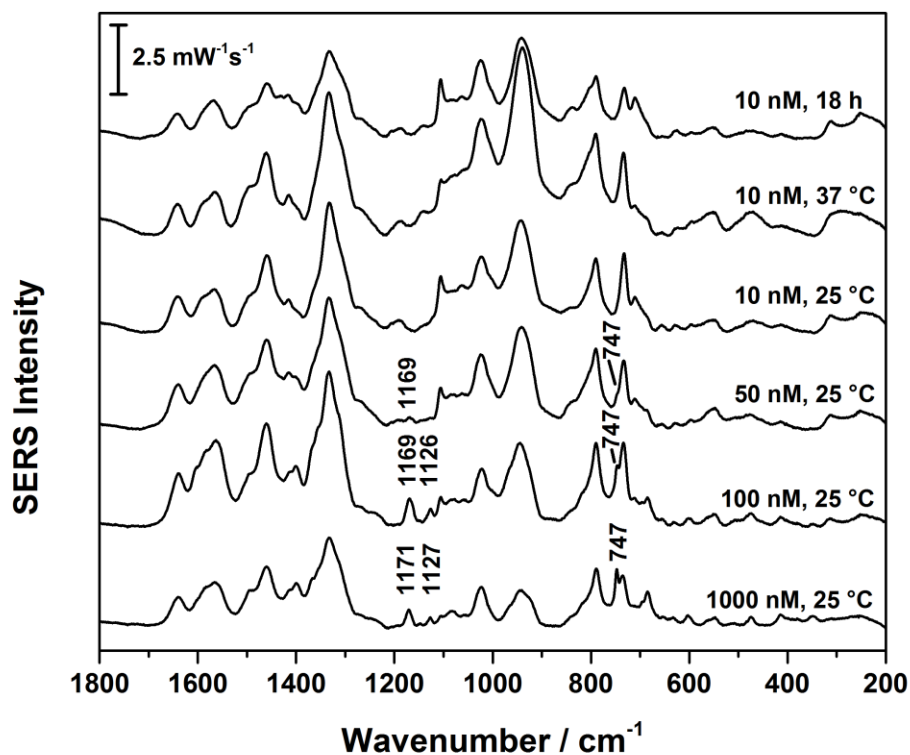
Figure 29. Averaged EC-SERS spectra (30 spots) recorded at -0.7 V for 10 μL of 0.1 mM anti-cyt aptamer + 1 mM 11-MUD for the detection of cyt c in 10 mL of phosphate buffer using solution at concentrations of 1000, 100, 50 and 10 nM at room temperature, 10 nM at 37 °C, and 10 nM after an 18 hour incubation at room temperature. EC-SERS on citrate reduced AgNP electrodes in 0.1 M NaF electrolyte. Laser power = 3 mW, collection time = 30 s, wavelength = 532 nm.

5.15 Change of electrolyte

Around this time in the project, it was realised that the fluoride ion of the NaF electrolyte may be interacting with the protein [157-159]. NaF had originally been chosen instead of NaCl or KCl because of the low affinity of F^- for the Ag surface, whereas Cl^- would easily bind to the AgNP surface, potentially displacing the aptamer. In fact, the high affinity of Cl^- for the Ag surface is sometimes used in our lab to displace citrate ion from the AgNP surface. Na_2SO_4 is an ideal electrolyte for this analysis, since the SO_4^{2-} ought not to interfere with the cyt c, nor will it have a strong interaction with the Ag surface. EC-SERS spectra were collected at 10 different spots while the potential was held at -0.7 V for the standard aptasensor setup. The analysis was done in 0.1 M NaF, 0.1 M NaCl and 0.03 M Na_2SO_4 (equal ionic strength), shown in Figure 30. Interestingly, when NaCl was used, the chloride ion had no significant impact on the SERS averaged spectrum. Some small changes were observed in the 1400-1300 cm^{-1} range, and a new band was observed at 996 cm^{-1}. Nonetheless, the chloride ion did not displace the anti-cyt aptamer from the surface. Favourable results were also obtained when Na_2SO_4 was used, and no significant differences were observed compared to NaF. One study using sum frequency generation (SFG) spectroscopy reported differences at the surface for aqueous solutions of NaF and Na_2SO_4 [160], but no significant differences were observed in the EC-SERS spectra. Accordingly, it was decided that Na_2SO_4 should be used for future analyses. At this point, several previous experiments were repeated, such as cyt c protein in NaF and Na_2SO_4. Experiments for detection of catalase-peroxidase (KatG) in Chapter 6 were also conducted at this time, and 0.03 M Na_2SO_4 was used for nearly all analyses in that phase of the project.
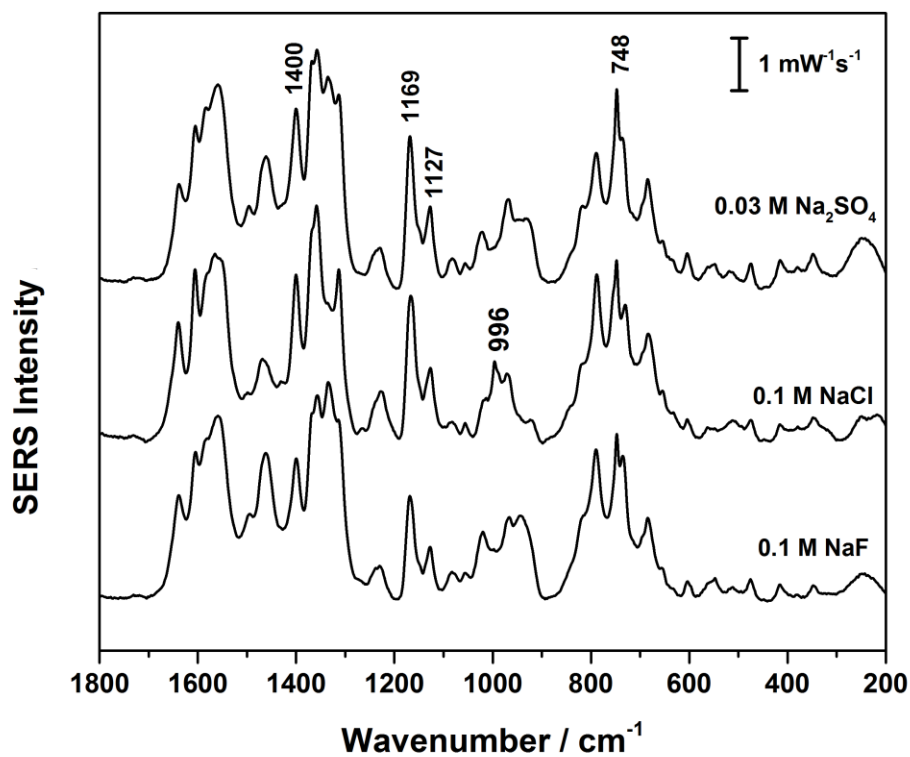
Figure 30. Averaged EC-SERS spectra (10 spots) recorded at -0.7 V for 10 μL of 0.1 mM anti-cyt aptamer + 1 mM 11-MUD for detection of 10 mL of 100 nM cyt c on citrate reduced AgNP electrodes in 0.1 M NaF, 0.1 M NaCl and 0.03 M Na$_2$SO$_4$. Laser power = 3 mW, collection time = 30 s, wavelength = 532 nm.

5.17 Note regarding change of 11-MUD concentration

At this stage of the project, it was decided to change the 11-MUD concentration from 1 mM to 0.1 mM. The effect of lowering the concentration is shown in Chapter 6. In summary, a high concentration of 11-MUD results in significant band intensities for the alkanethiol, at the expense of DNA aptamer. Therefore, for all of the following experiments, 0.1 mM 11-MUD was used for the 2 hour incubation.

5.18 Binding buffer to induce protein binding

By immersing the aptasensor in 10 mL of cyt c in phosphate buffer, it was possible to detect cyt c as low as 50 nM. The phosphate buffer containing KH_2PO_4 and K_2HPO_4 keeps the solution pH at 7.4, which maintains physiological pH and prevents cyt c from denaturing. However, this buffer may not be ideal for inducing binding of the cyt c protein to the anti-cyt aptamer. When Sen *et al*. originally developed the anti-cyt aptamer, a binding buffer consisting of 50 mM Tris-HCl, 120 mM NaCl, 50 mM KCl, 1% DMSO, 0.03% Triton X-100, 10 μM $K_3Fe(CN)_6$ was used. They also reported that the affinity of cyt c for the aptamer increased if the binding buffer contained 10 μM hemin. When only hemin was bound to the aptamer, no $K_3Fe(CN)_6$ was used.

Shown in Figure 31 are the results obtained when the binding buffer was used to detect cyt c. Ten EC-SERS spectra were collected at different spots on the electrode while the potential was held at -0.7 V, and the spectra were then averaged. The aptasensor was immersed in 7 mL of cyt c solution. The bottom spectrum shows an improvement in the detection of cyt c. In phosphate buffer (Figure 29), the band intensity

for 50 nM cyt c was very weak. In binding buffer, the cyt c band was very strong. When the aptasensor was used to bind hemin (middle spectrum) in binding buffer (no cyt c), a similar spectrum was obtained. This result is expected because hemin essentially *is* a Heme B group plus a chloride ligand, and the resonance enhancement of the heme group of cyt c gives the most intense contributions to the spectrum. In the case of hemin, the 748 cm^{-1} band shifts to 756 cm^{-1}. The EC-SERS spectra of hemin alone in NaF show that this band is indeed found at 756 cm^{-1}, which is shown in Figure 32. When the binding buffer with hemin (Figure 31, top) was used to bind 50 nM cyt c, it was possible to distinguish the cyt c and hemin bands. Even though the concentration of hemin is several orders of magnitude higher than cyt c, the 748 cm^{-1} cyt c band was most intense, whereas the hemin band at 756 cm^{-1} was observed as a shoulder.
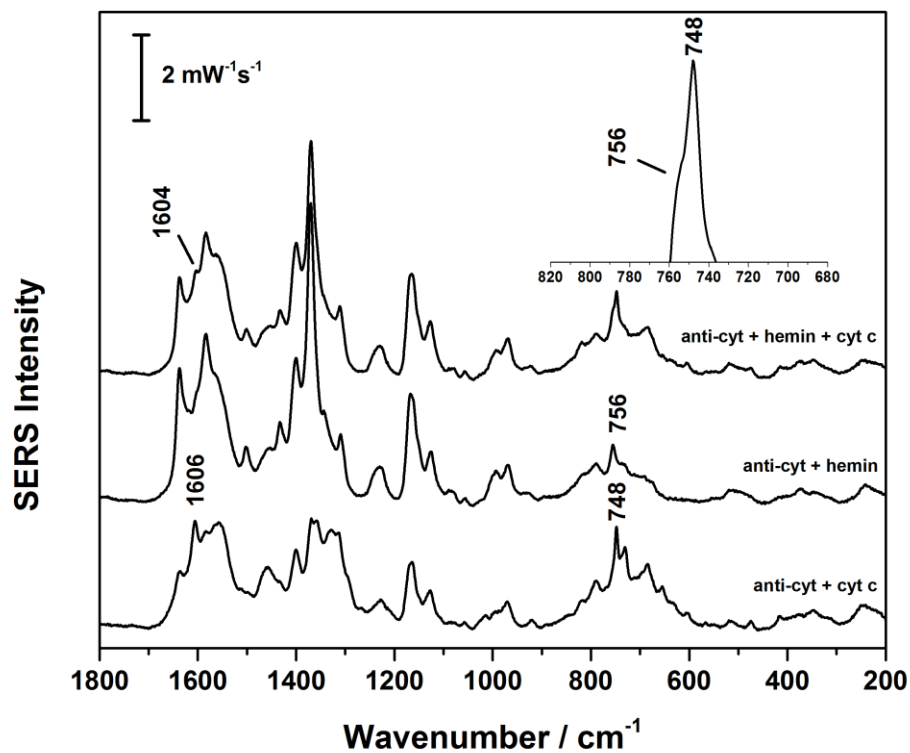
Figure 31. Averaged EC-SERS spectra (10 spots) recorded at -0.7 V of 10 µL of 0.1 mM anti-cyt aptamer + 0.1 mM 11-MUD for detection of 7 mL of 50 nM cyt c and/or 10 µM hemin in binding buffer on citrate/borohydride reduced AgNP electrodes in 0.1 M NaF. Laser power = 3 mW, collection time = 30 s, wavelength = 532 nm. The inset shows a close-up view of the aptamer-hemin-cyt c spectrum in the spectral range of 820 to 680 cm^{-1}.

Using the binding buffer to induce binding of cyt c to the anti-cyt aptamer has obvious benefits. However, even though it was possible to distinguish aptamer/cyt vs. aptamer/hemin/cyt spectra, detection of cyt in the presence of hemin may not be ideal for SERS-based methods. For example, the bands near 1170 and 1128 cm^{-1}, which appear in the spectra of hemin and cyt c, are indistinguishable. Even though the 748/756 cm^{-1} bands could be distinguished, the intensity of the 748 cm^{-1} band shows high variability (Figure 27), so an overlapping band may cause problems for quantitative analysis. The binding buffer without hemin was chosen for further analyses; however, the use of hemin for binding of cyt c does merit further investigation. Additionally, it is likely just a SERS-specific problem, as the same issues may not arise using other methods of detection.
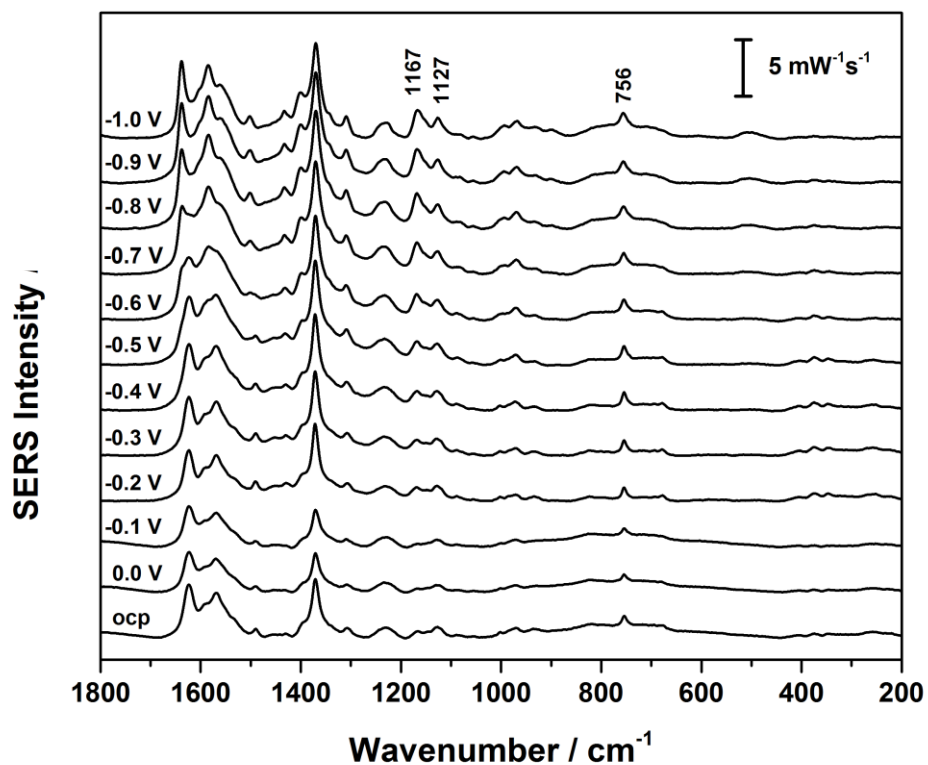
Figure 32. EC-SERS 0.025 mM porcine hemin in 0.075 M NaF solution recorded on a citrate reduced AgNP electrode. Hemin dissolved in aqueous 0.8 mM NaOH solution before addition to NaF for EC-SERS. Laser power = 3 mW, collection time = 30 s, wavelength = 532 nm.

The same method was then used to detect cyt c in binding buffer (no hemin) after a tenfold dilution to 5 nM protein. At room temperature (25 °C), the cyt c band intensities were very weak (Figure 33). When the experiment was repeated by heating the solution in a water bath to 37 °C during the 1 hour binding, no improvement in detection of cyt c was observed. However, when the experiment was repeated at room temperature under magnetic stirring, most of the cyt c bands (1398, 1166, and 1131 cm^{-1}) were strong, along with the 748 cm^{-1} observed as a shoulder. Due to the very dilute concentration (5 nM), the result suggests that detection of nanomolar cyt c simply requires more kinetic collisions (mass transport limitation). One significant difference in the spectra after treatment with binding buffer is that the adenine band near 730 cm^{-1} typically increases significantly in intensity relative to the cytosine/thymine band near 790 cm^{-1}. This result is consistent with previous findings, where the adenine ring breathing mode band intensity increased in the presence of Cl$^-$ [163].
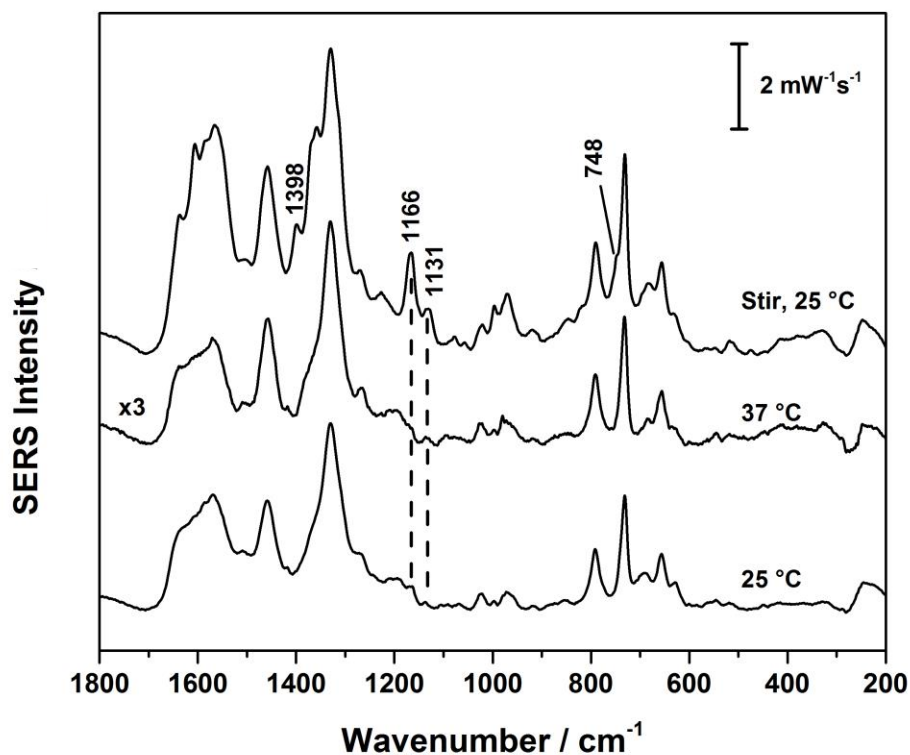
Figure 33. Comparison of averaged spectra (n=10) at -0.7 V for 10 μL of 0.1 mM anti-cyt + 0.1 mM 11-MUD + 5 nM cyt c under differing binding conditions. Incubation in 7 mL solution (binding buffer + protein) without stirring at 25 and 37 °C, and 25 °C with magnetic stirring. EC-SERS in 0.03 M Na_2SO_4 on citrate/borohydride reduced AgNP. Laser power = 3 mW, collection time = 30 s, wavelength = 532 nm.

5.19 Cyclic voltammetry of cyt c aptasensor

Cyclic voltammetry (CV) was also used as an additional method to show changes in surface chemistry after cyt c had bound to the aptamer-modified electrode. Two redox probes were used: $K_3Fe(CN)_6$ and $Ru(NH_3)_6Cl_3$. In both cases, each addition to the electrode surface had an insulating effect and prevented electron transfer between the redox probe to the electrode surface. Using CV, it was possible to detect the presence of cyt c at a concentration of 10 nM, as shown in Figure 34.
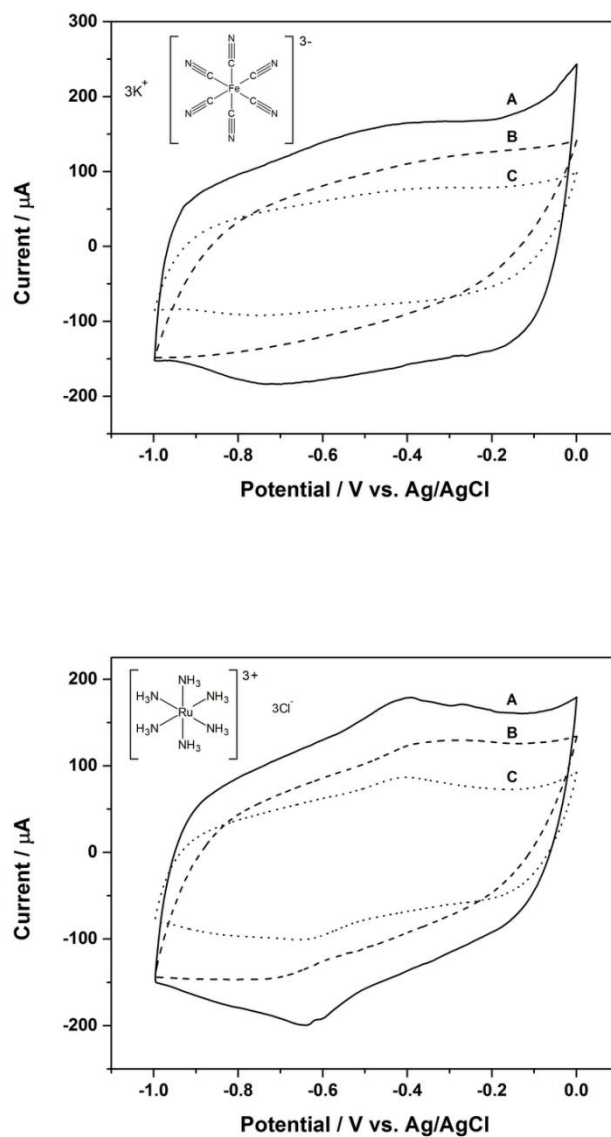
Figure 34. Cyclic voltammograms of A: anti-cyt, B: anti-cyt + 11-MUD, C: anti-cyt + 11-MUD + 10 nM cyt c (in binding buffer) recorded in 0.1 mM $K_3Fe(CN)_6$ (top) and 50 μM $Ru(NH_3)_6Cl_3$ (bottom) in pH 7.4 phosphate buffer on AgNP modified screen printed electrode. Scan rate 100 mVs^{-1}.

5.20 Control studies

5.20.1 Control Study: anti-cyt + 3 nM hemoglobin

Human hemoglobin (Hb) was chosen as a control protein for use with the cyt c aptasensor. Hb is significantly larger than cyt c; these proteins have molecular masses of about 64 kDa and 12 kDa, respectively. However, Hb is a good control protein because it is abundant in the body and relatively cheap. Most importantly, cyt c and Hb are both heme proteins. Hb was chosen because both proteins have the same heme prosthetic group, and non-specifically adsorbed Hb ought to give a similar spectrum to cyt c. Additionally, Hb and cyt c would both give rise to resonance Raman spectra when the 532 nm laser is used, so any Hb present on the aptamer functionalised surface should be fairly easy to detect.

The established EC-SERS method (-0.7 V, average of 10 spots, 7 mL binding buffer with magnetic stirring) was used to detect 3 nM Hb using the anti-cyt aptamer. Figure 35 shows the results of three trials for this study, along with a Hb spectrum for comparison. For all three trials, no non-specific interaction of Hb with the aptasensor was observed.
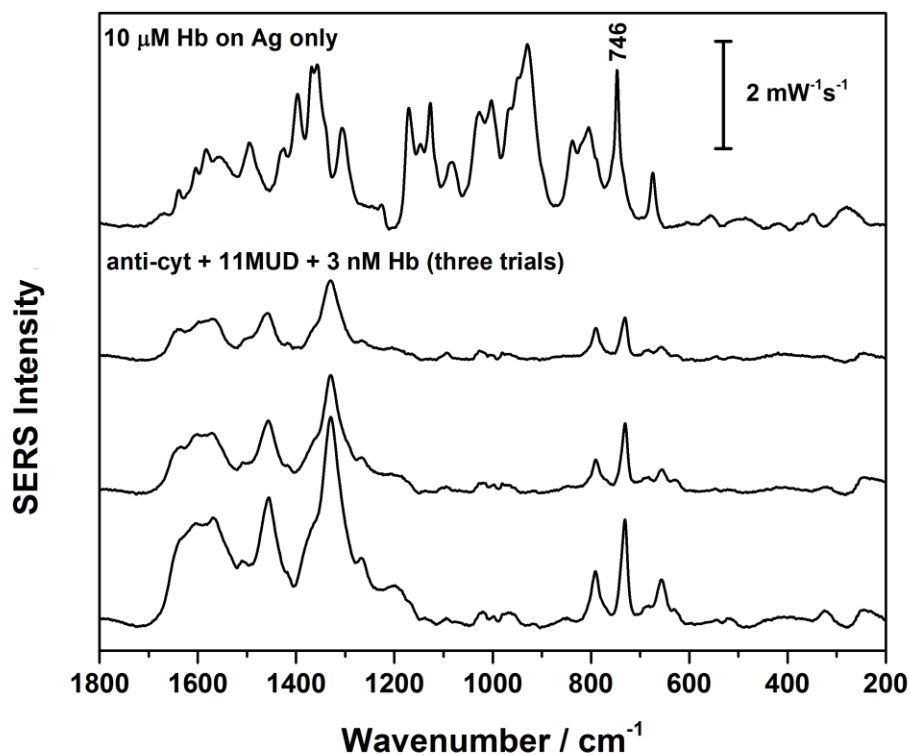
Figure 35. Averaged spectra (n=10) at -0.7 V of 10 μL of 0.1 mM anti-cyt + 0.1 mM 11-MUD + 3 nM human hemoglobin (Hb). Incubation in 7 mL solution (binding buffer + protein) with magnetic stirring. EC-SERS in 0.03 M Na_2SO_4 on citrate/borohydride reduced AgNP. Shown for comparison is a spectrum of Hb recorded at -0.7 V. Laser power = 3 mW, collection time = 30 s, wavelength = 532 nm.

5.20.2 Control Study: Anti-IgE / anti-KatG + 3 nM cyt c

The previous findings showed that the cyt c aptamer does not detect the control protein hemoglobin. Another useful study is to see if cyt c interacts with control aptamers. For this experiment, the two control aptamers were the other two used for this project: anti-IgE and anti-KatG. The anti-IgE aptamer (40 mer) is smaller than anti-cyt (63 mer), and anti-KatG is larger (89 mer). With regards to their target proteins, KatG is a heme protein, but IgE is not.

Figure 36 shows the results of three trials for detection of 3 nM cyt c on anti-KatG (top) and anti-IgE (bottom). The data show that cyt c *does* non-specifically adsorb onto these other aptamers. While this result was at first somewhat alarming, since it suggests that cyt c could potentially adsorb omto any aptamer, or perhaps even any random DNA sequence, it does not present a major problem. So long as the anti-cyt aptamer *only* binds cyt c, it is still useful for clinical detection. The interaction of cyt c with control aptamers, or a scramble sequence anti-cyt aptamer, under non-ideal binding conditions (i.e. very high ionic strength) deserves further attention, and some work has in this area previously been conducted [164].
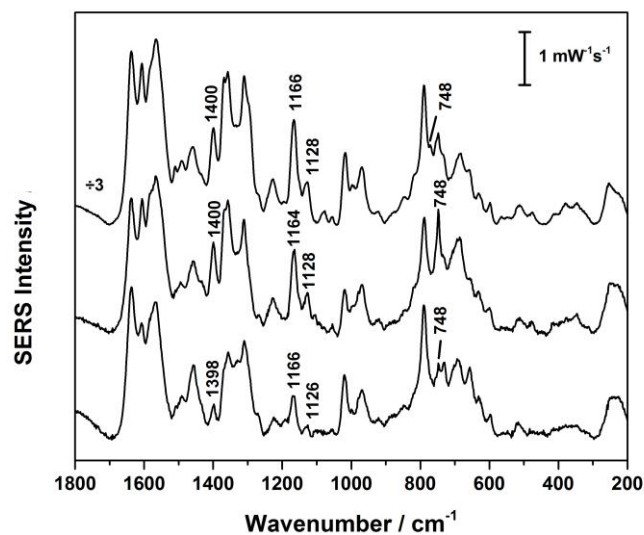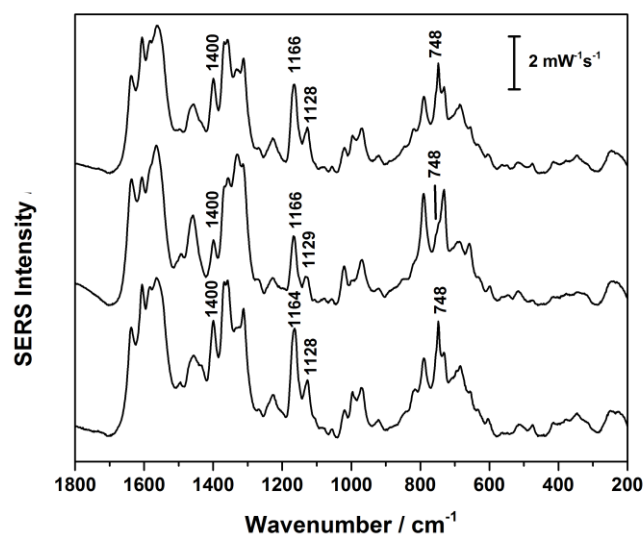
Figure 36. Averaged spectra (n=10) recorded at -0.7 V for three trials of 10 μL of 0.1 mM anti-KatG (top) / anti-IgE (bottom) + 0.1 mM 11-MUD + 3 nM cyt c. Incubation in 7 mL solution (binding buffer + protein) with magnetic stirring. EC-SERS in 0.03 M Na_2SO_4 on citrate/borohydride reduced AgNP. Laser power = 3 mW, collection time = 30 s, wavelength = 532 nm.

5.21 Quantitative detection of cyt c

The cyt c aptasensor was next tested to see if it is able to detect cyt c quantitatively over the concentration range of 1 to 7 nM. Ten spectra were collected at different spots on each electrode as the potential was held at -0.7 V. The ν(pyr half ring)$_{sym}$ band at 1170 cm^{-1} was chosen for cyt c. The average intensity for the 1170 cm^{-1} band at each concentration is plotted with its standard deviation (error bars) in Figure 37.

The plot of the average signal intensity of the cyt c band shows somewhat of a linear trend, with an R^2 value of 0.77. However, the standard deviation for some samples was very large, particularly for the 6 and 7 nM solutions. This result suggests that this EC-SERS aptamer-based method shows potential for quantitative detection of cyt c in the nanomolar concentration range, but it nonetheless needs to be improved.
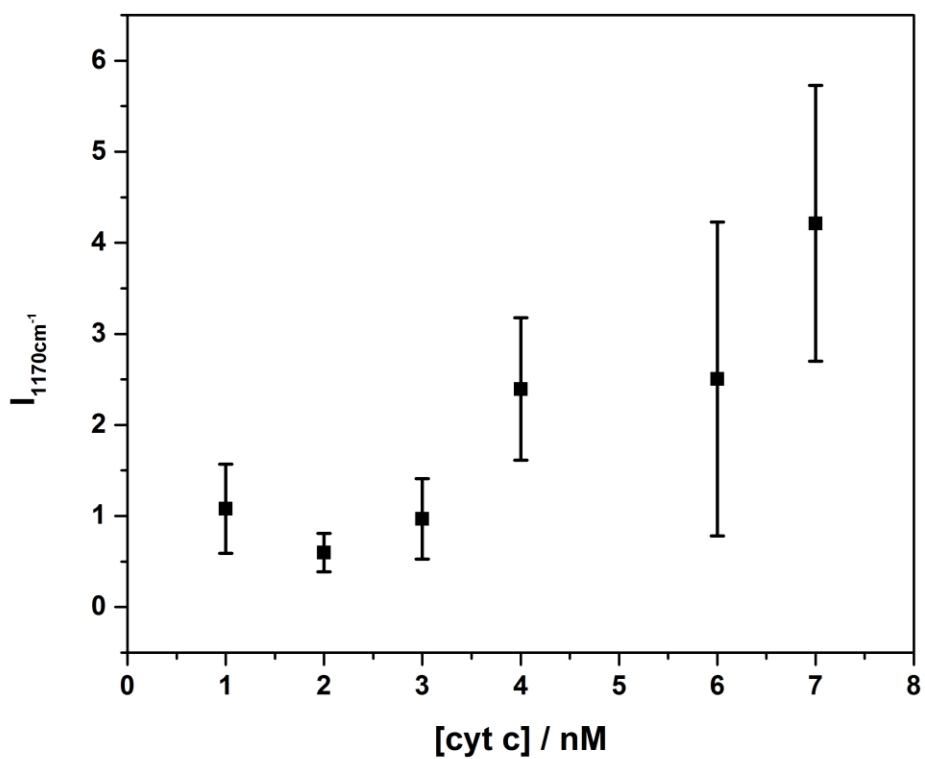
Figure 37. Average 1170 cm^{-1} band intensity from 10 spectra at each concentration with standard deviation (error bars) for detection of cyt c over the range of 1 to 7 nM.

One motivation for collecting multiple spectra and then averaging them was to avoid spot to spot variations on the electrode surface. This problem is exemplified in the analysis when 10 spectra were collected at -0.7 V for 3 nM cyt c (Figure 38). The signal intensity of the anti-cyt DNA bands at 790 and 732 cm^{-1} are relatively uniform, whereas the cyt c bands, such as 1606, 1401, 1167 and 1127 cm^{-1} show a large degree of variability. Since the aptamer bands are relatively uniform, it suggests that the SERS enhancement has minimal spot to spot differences and the aptamer SAM is relatively homogenous. The variability of the cyt c bands suggest either a difference in orientation of adsorbed cyt c in the aptamer-protein complex, or simply differences in amount of bound protein at each spot on the electrode surface. Either way, the difference in signal intensity for the cyt c bands at each spot on the electrode highlights the need for collecting multiple spectra to obtain an averaged spectrum representative of the entire surface.
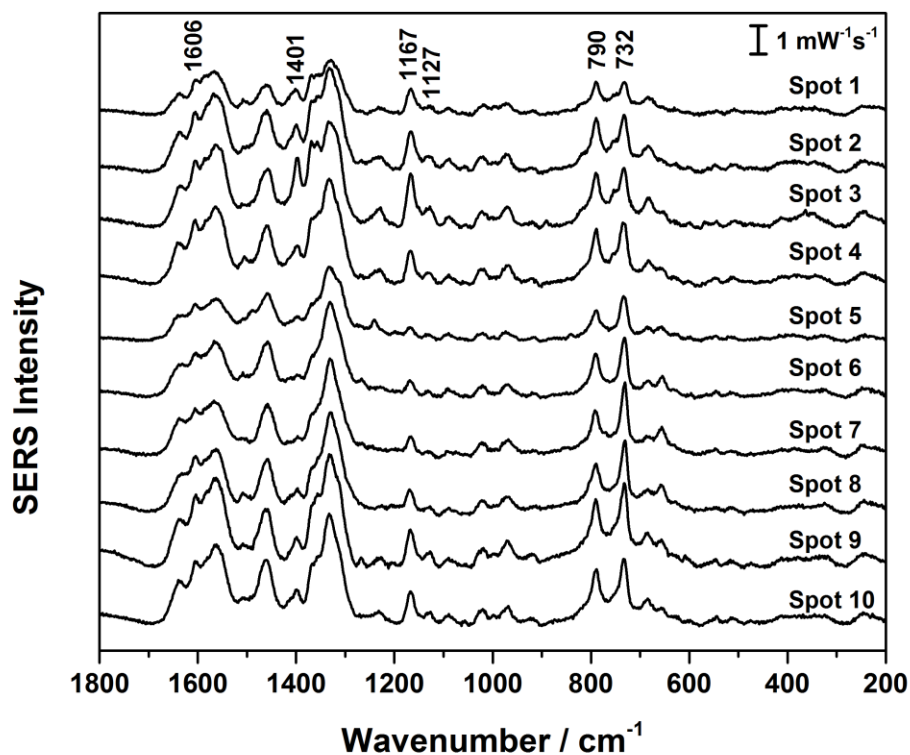
Figure 38. Ten spectra recorded at different spots on the modified electrode at -0.7 V of 10 μL of 0.1 mM anti-cyt + 0.1 mM 11-MUD + 3 nM cyt c. Incubation in 7 mL solution (binding buffer + protein) with magnetic stirring. EC-SERS in 0.03 M Na_2SO_4 on citrate/borohydride reduced AgNP. Laser power = 3 mW, collection time = 30 s, wavelength = 532 nm.

Despite the relatively low linearity of the data in Figure 38, a better fit with an acceptable range of error could potentially be obtained if the data were collected in triplicate trials. The experiment was repeated in triplicate for 3 nM cyt c, as shown in Figure 39. For comparison, the averaged spectrum of the data from Figure 38 is shown in spectrum A, and the results of the triplicate analysis are shown in B-D. It is clear that quantitative reproducibility is a major issue for this method. The aptamer spectrum is much more intense in A, but B-D show significant differences in intensity as well. Note that spectra B-D were much weaker, but have been normalised using the 732 cm^{-1} band intensity. In spectrum A, the 1168 and 1128 cm^{-1} cyt c bands are very intense. In trials B and C, these bands are much weaker, and not even observed in trial D. Coincidently, trial D has more intense aptamer bands than trials B-C. Relative to the DNA bands, the 748 cm^{-1} cyt c band is strongest in B, even when compared to spectrum A. This result shows that the method must be further refined before quantitative analyses can be reasonably considered. Improvements in the uniformity of the SERS signal obtained on the AgNP substrate could help improve this EC-SERS biosensing method. It should be noted that while quantitative detection is important for diseases such as HIV/AIDS (viral load) and conditions of the liver (see Table 2), it is not necessary for diagnosis of tuberculosis, which is the overall goal of this project.
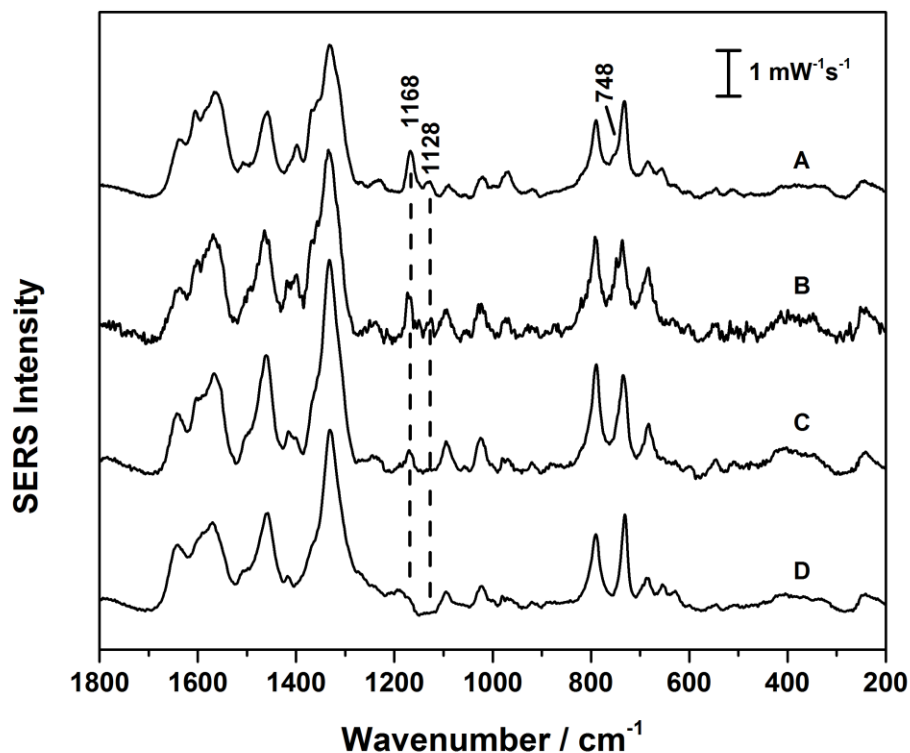
Figure 39. Averaged spectra (n=10) recorded at -0.7 V for of 10 µL of 0.1 mM anti-cyt + 0.1 mM 11-MUD + 3 nM cyt c. Incubation in 7 mL solution (binding buffer top, synthetic urine bottom) with magnetic stirring. EC-SERS in 0.03 M Na_2SO_4 on citrate/borohydride reduced AgNP. Laser power = 3 mW, collection time = 30 s, wavelength = 532 nm. Spectrum A is the average from Figure C38, and spectra B-D from the second round of trials done in triplicate using the same procedure. Spectra normalised to the 732 cm^{-1} band intensity.

5.22 Detection in binding buffer vs. synthetic urine

A standard procedure for detection of cyt c has now been established. The anti-cyt aptamer and 11-MUD alkanethiol spacer concentrations had been determined, the best applied potential (-0.7 V) for detection had been established, averaging spectra from collection at multiple spots was found to be useful, and the best conditions for binding had been determined (binding buffer and magnetic stirring). Using the optimised conditions, it was possible to detect cyt c in binding buffer as low as 1 nM concentration while still having reasonably good bands, shown in Figure 40 (top). For several trials at 0.5 nM concentration, it was not possible to detect cyt c protein. Cyt c is a biomarker in urine for various diseases of the kidney and liver, as outlined in Chapter 2. When the aptasensor was incubated in 7 mL synthetic urine (magnetic stirring) instead of binding buffer, it was possible to detect cyt c at 10 nM, but not 1 nM. These results suggest that the LOD lies between 1 nM and 500 pM in binding buffer, and 10 and 1 nM in synthetic urine. For detection of various liver conditions (Table 2), the LOD will need to be improved to the pM range.
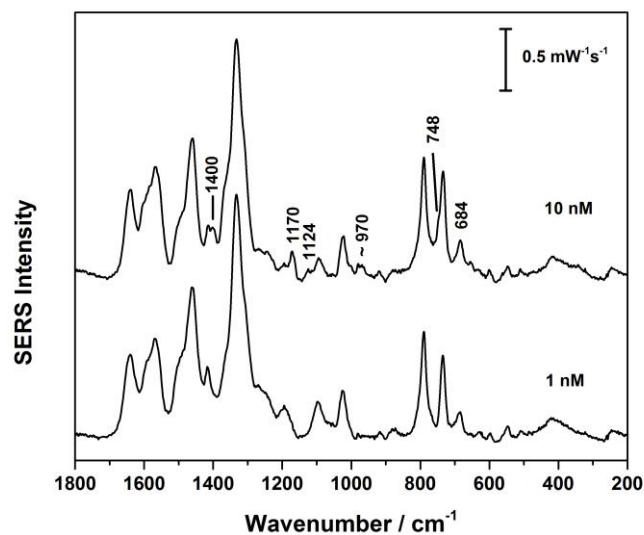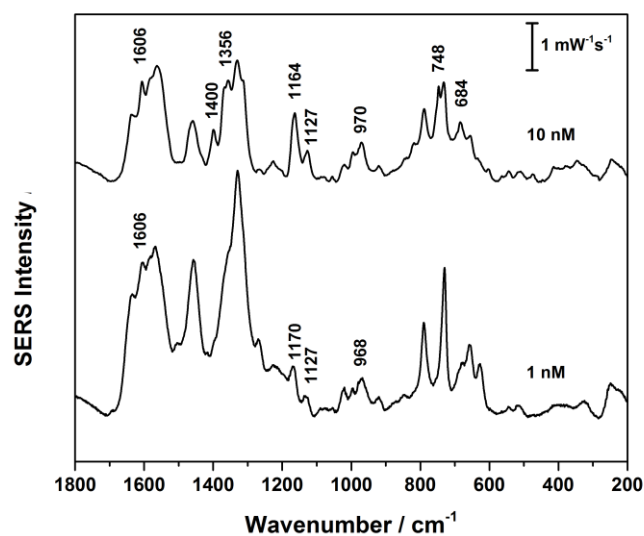
Figure 40. Averaged spectra (n=10) recorded at -0.7 V for of 10 µL of 0.1 mM anti-cyt + 0.1 mM 11-MUD + 10 and 1 nM cyt c. Incubation in 7 mL solution (binding buffer top, synthetic urine bottom) with magnetic stirring. EC-SERS in 0.03 M Na_2SO_4 on citrate/borohydride reduced AgNP. Laser power = 3 mW, collection time = 30 s, wavelength = 532 nm.

5.23 Conclusion for cytochrome c aptamer studies

Much preliminary work toward the eventual development of an EC-SERS KatG aptasensor for tuberculosis has been accomplished by this investigation of cyt c. Aptamer and alkanethiol concentrations have been established, along with which alkanethiol spacer best prevents non-specific interaction. The importance of the binding buffer has been established, in which it is possible to detect cyt c as low as 1 nM. Crucially, this method has been demonstrated to work in a clinically relevant solution, namely, synthetic urine, and a concentration that is very near being clinically useful (10 nM), which is close to the goal of 1 nM detection in urine. By comparison with the IgE studies, the heme cyt c protein was relatively easy to detect, while non-heme IgE remains a challenge. While EC-SERS detection of cyt c has been successful, other avenues may need to be explored for non-heme proteins like IgE.

Chapter 6 – Tuberculosis biomarker: catalase-peroxidase

6.1 Introduction

Catalase-peroxidase (KatG) is a biomarker protein for tuberculosis found in the sputum of infected patients. It is a relatively large protein, with a mass of approximately 160 kDa. Like cytochrome c, it is a heme protein. For this study, purified non-infectious *Mycobacterium tuberculosis* KatG protein was provided by the Blackburn laboratory at the University of Cape Town, South Africa. Our collaborators also developed several aptamers specific for KatG. For this thesis, the sequence with the highest affinity was chosen. The aptamer sequence is given in Chapter 4.

6.2 EC-SERS of KatG protein

The first step was to collect EC-SERS spectra for KatG protein in order to identify marker bands. It is worth bearing in mind that the cytochrome c (cyt c) protein EC-SERS spectra were very rich in vibrational information, but most of the bands did not appear in the spectra for the aptamer-cyt c complex. It was anticipated that the same result might be observed for the aptamer-KatG complex.

Figure 41 shows the EC-SERS spectra of 6.25 µM KatG in 0.05 M NaF on a Ag nanoparticle (AgNP) modified electrode. The EC-SERS spectra shown are over the applied potential range of -0.5 to -1.0 V vs. Ag/AgCl. The full cathodic EC-SERS spectra are shown in the Appendix. At potentials more positive than -0.7 V, very few spectral features are observed. Moreover, closer to 0.0 V (Appendix Figure A4), the spectra are dominated by the citrate reducing agent used to prepare the AgNPs. The behaviour of

KatG is similar to that of cyt c in that there are some changes in the spectra between -0.7 and -1.0 V, but these changes are minimal.
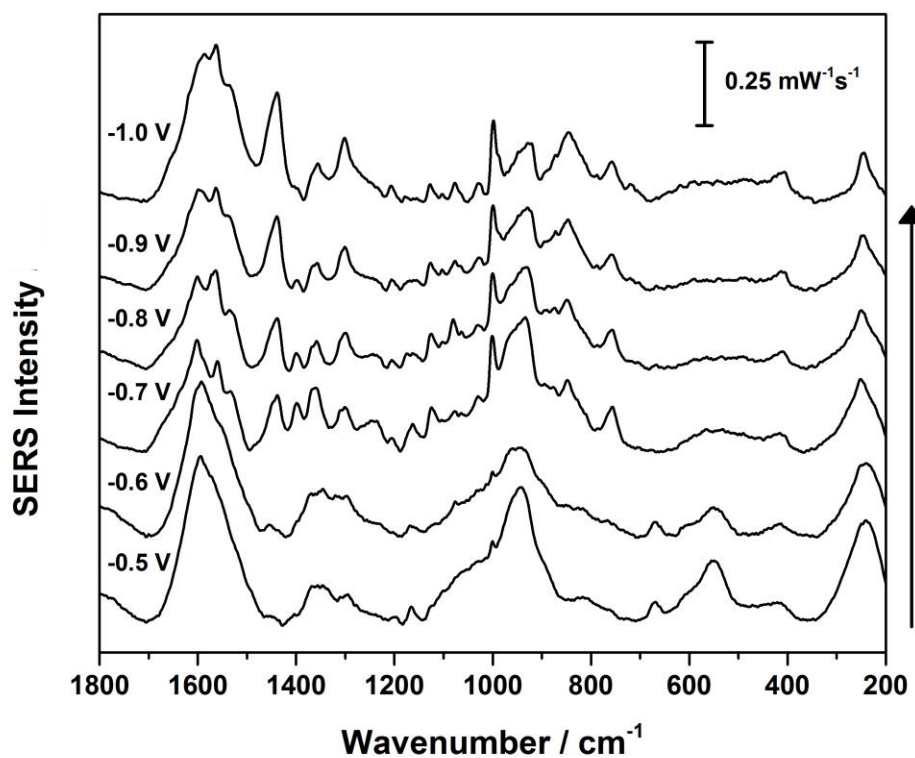
Figure 41. EC-SERS spectra of 6.25 µM KatG on AgNPs in 0.05 M NaF over the potential range of -0.5 to -1.0 V at -0.1 V increments, laser power = 7 mW, collection time = 30 s, laser wavelength = 532 nm. More positive potentials are shown in the Appendix Figure A4.

Shown in Figure 42 is the spectrum recorded at -0.7 V, with all significant bands labelled. At the time of writing and to the best of our knowledge, there have been no previous electrochemical SERS studies of KatG. There have been several resonance Raman studies [95-98], but these spectra are significantly different than those recorded for this project. Three factors that could explain this discrepancy are: 1) SERS spectra are not simply enhanced Raman spectra of the analyte molecule. Interaction with the Ag surface creates an adsorbed species, and the spectra will reflect this newly formed species. 2) SERS is a localised effect. A normal Raman spectrum of a bulk sample may give rise to bands for all the vibrations of a molecule, but SERS may give only bands for vibrations that are near the Ag surface, particularly for very large molecules. Collection of Raman spectra of KatG was attempted using the 532 and 780 nm lasers. Unfortunately, it was not possible to obtain normal Raman spectra for the KatG protein. Moreover, due to limited sample availability (12 x 1 mg tubes), it was decided that these samples could be better used for detection studies, rather than characterisation.

Despite the difficulties in assigning the modes of vibration that give rise to the bands in the EC-SERS spectra of KatG, there are several similarities with the cyt c EC-SERS spectra. Many of these bands are from the heme moiety; likely a result of the resonance effect. Similar bands (see Tables 7-8 for cyt c) include: $\nu(C_\alpha\text{-}C_m)$ indicating Fe^{2+} at 1601 cm^{-1}, ν(pyr quarter-ring) at 1399 cm^{-1}, ν(pyr half ring)$_{sym}$ at 1163 cm^{-1}, $\nu(C_\alpha N)$ at 1124 cm^{-1}, and ν(pyr breathing); $\nu(C_\alpha C_\beta)$ at 756 cm^{-1}. Other bands, such as 786, 566 and 416 cm^{-1}, have not been assigned, but nonetheless are observed in both the cyt c and KatG EC-SERS spectra. The 1438 cm^{-1} band can be assigned to $\delta(C=CH_2)_{sym}$, based

on comparison with EC-SERS spectra of hemin available in the literature [88]. The $\nu(C_\alpha C_\beta)$ band at 756 cm^{-1} is found at the same position as for hemin (Figures 31-32), which is expected since KatG contains a heme B, and hemin is essentially a heme B with a chloride ligand attached. By comparison, cyt c contains a heme C, and the $\nu(C_\alpha C_\beta)$ band is observed near 748 cm^{-1} throughout this project in the EC-SERS spectra. Lastly, the intense band at 252 cm^{-1} could be assigned to ν(Ag-Cl), possibly due to small amounts of chloride ion present in the KatG sample [161].
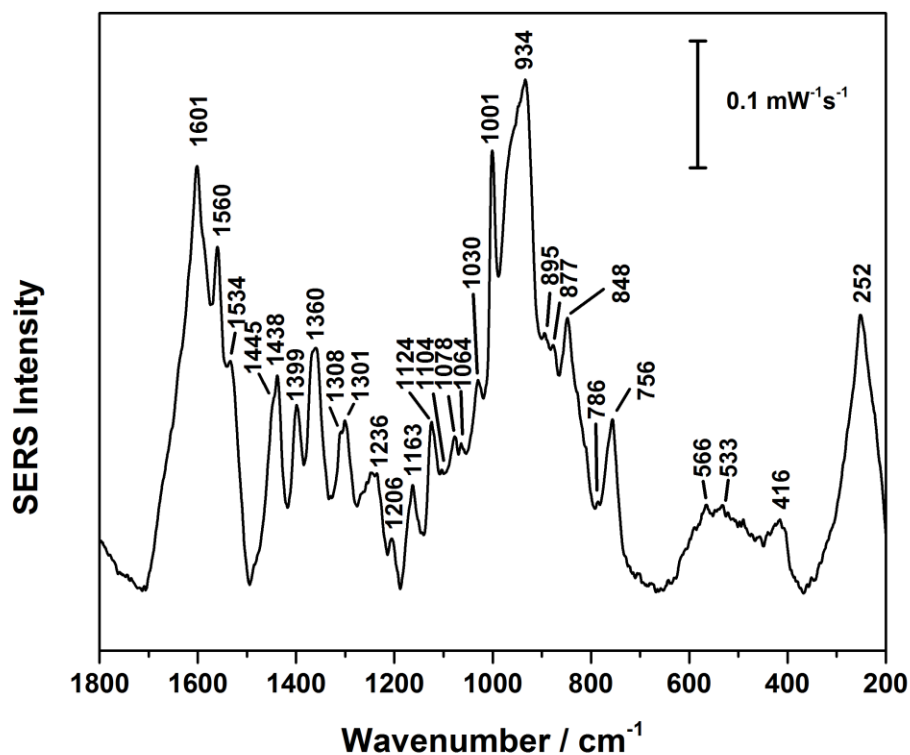
Figure 42. EC-SERS spectrum of 6.25 μM KatG on AgNPs in 0.05 M NaF, Applied potential = -0.7 V, laser power = 7 mW, collection time = 30 s, laser wavelength = 532 nm.

6.3 Concentration of Anti-KatG Aptamer

It was initially assumed that immobilisation of anti-KatG aptamer onto AgNPs would be similar to immobilisation of anti-cyt during the model studies. This assumption turned out to be true. Preparation of aptamer at a concentration of 1 mM for 10 µL per electrode means that each batch of aptamer is good for 30-50 electrodes, depending on the batch size received from the manufacturer. Dilution to 0.1 mM aptamer accordingly increases the number of uses per batch tenfold. Similar to the anti-cyt aptamer, 10 µL of 0.1 mM anti-KatG on AgNPs gives a very intense EC-SERS signal. For the anti-cyt aptamer, 0.1 mM aptamer spectra are not significantly weaker than those recorded using 1 mM aptamer. Accordingly, a 1 mM anti-KatG aptamer spectrum was not collected. Averaged EC-SERS spectra (n=10) at -1.0 V vs. Ag/AgCl of 0.1, 0.01 and 0.001 mM anti-KatG are shown in Figure 43, with band assignment given in Table 10. Many of the bands can still be seen in the 0.01 and 0.001 mM spectra, but the minor reduction in monetary cost of aptamer used does not justify the significant reduction in signal intensity. For the remainder of the project, 0.1 mM aptamer was used for all studies.
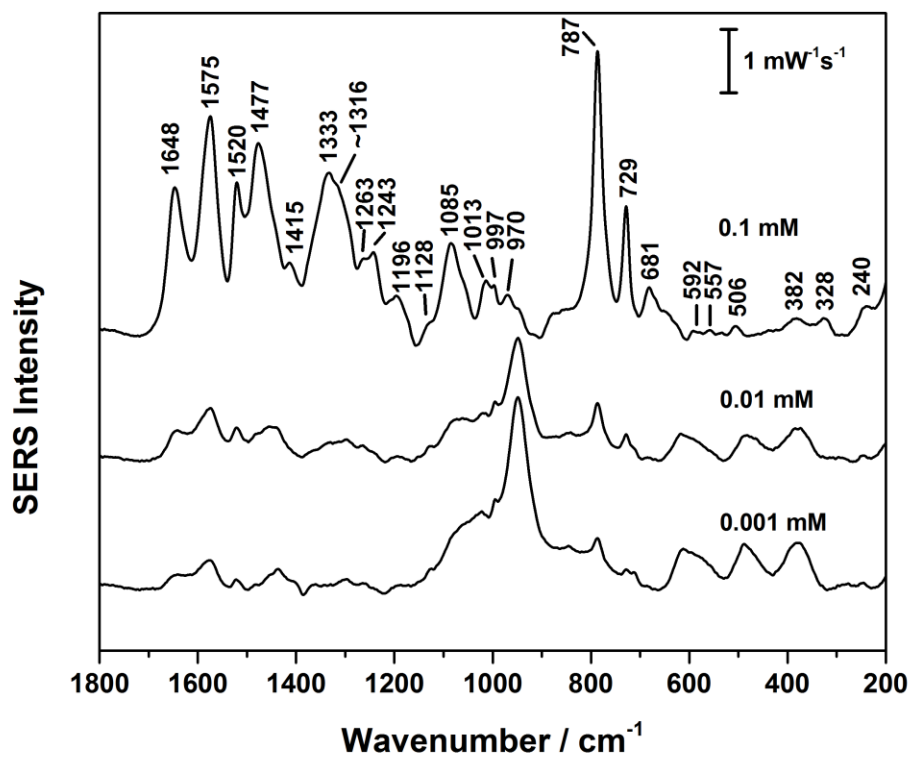
Figure 43. Averaged spectra (n=10) comparing the effects of anti-KatG aptamer concentration in a 10 µL aliquot drop coated onto a AgNP modified electrode. Applied potential = -1.0 V, laser power = 3 mW, collection time = 30 s, 0.1 M NaF electrolyte. Laser wavelength = 532 nm.

Table 10. Band assignment for the anti-KatG aptamer on AgNPs.

Wavenumber / cm⁻¹	Assignment	Reference
1648	ν(C=O) thymine and cytosine	[132]
1575	Ring stretching of adenine and guanine	[134]
1520	Guanine ring stretching	[132]
1477	Adenine, cytosine, thymine	[133]
1415	CH2 deformation	[48]
1333	Adenine (mixed modes)	[34, 134, 146]
1316 sh	ν(C-NH$_2$) of adenine	[34]
1263	Adenine (mixed modes)	[132]
1243	?	-
1196	Cytosine and adenine (mixed modes)	[132]
1128	?	-
1085	DNA backbone (PO$_2^-$ stretch)	[133, 148]
1013	NH$_2$ rock of adenine	[146]
997	?	-
970	?	-
787	Ring breathing of cytosine and thymine	[34, 133]
729	Ring breathing of adenine	[34, 132-133, 146-147]
681	Guanine or ν(C-S)	[34, 133, 148]
592	Ag-S-C-C$_{trans}$	[152]
557	Ag-S-C-C$_{gauche}$ or cytosine	[132, 152]
506	Guanine (mixed modes)	[132]
382	Guanine δ(C-NH$_2$)	[132]
328	Adenine ip-δ(C-NH$_2$)	[132, 146]
240	ν(Ag-S)	[130, 151-152]

6.4 Annealing of anti-KatG aptamer

Some aptamer studies involve heating the aptamer before immobilisation, while others do not use this step. The anti-KatG aptamer used in this study was prepared with an annealing step, so this step is also required for protein binding. The procedure is covered in Chapter 4, but briefly, it involves boiling the aptamer solution for 5 minutes, followed by rapid freezing. Once the frozen aptamer solution has been thawed, it can be immobilised onto the AgNP substrate. The annealing procedure was carried out using 85 and 100 °C water, and compared with aptamer that was immobilised onto AgNPs without the annealing procedure. These spectra are shown in Figure 44. No significant spectral differences were observed. It remains to be determined whether the annealing process helps the binding of KatG protein or not. Nonetheless, these results show that the annealing process apparently does not lead to any sort of thermal degradation or other detriment to the anti-KatG aptamer. For all proceeding analyses, the 100 °C annealing procedure was used.
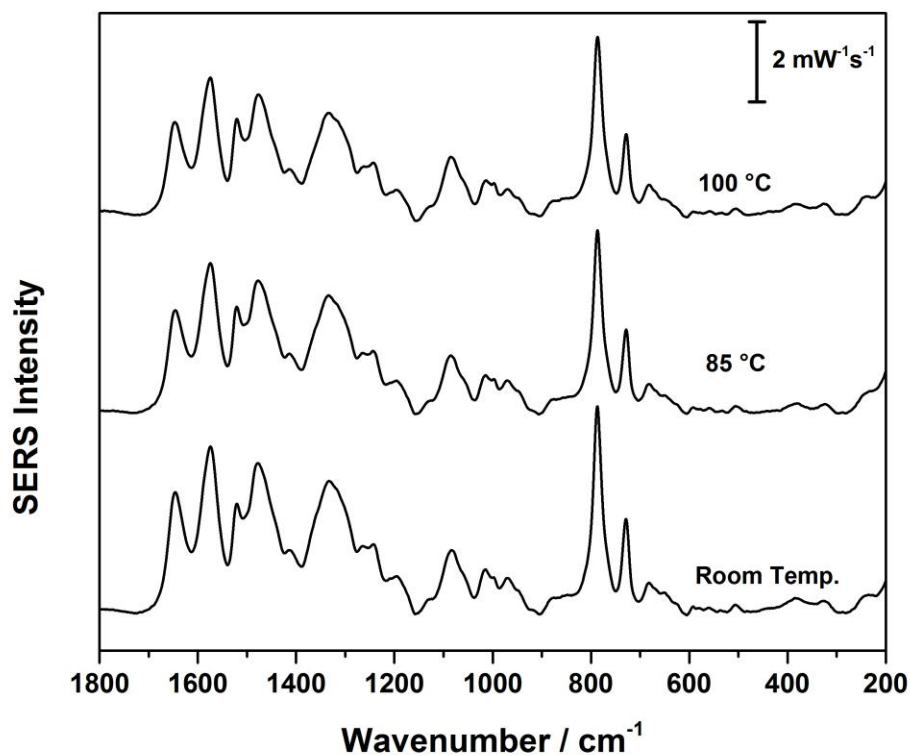
Figure 44. Averaged spectra (n=10) comparing the effects of immobilisation of the anti-KatG aptamer onto AgNPs at room temperature, heating to 85 °C for 5 minutes followed by rapid cooling in an ice water bath, and boiling at 100 °C for 5 minutes followed by rapid cooling in an ice water bath. Applied potential = -1.0 V, laser power = 3 mW, collection time = 30 s, 0.1 M NaF electrolyte. Laser wavelength = 532 nm.

6.5 Concentration of 11-MUD

The alkanethiol spacer molecule used with the anti-KatG aptamer was 11-mercapto-1-undecanol (11-MUD). It is important to determine the optimal concentration of 11-MUD on the AgNP-aptamer surface for binding of KatG protein. Figure 45 shows 10 EC-SERS spectra of anti-KatG in the absence of 11-MUD recorded at different spots on an AgNP electrode while the potential was held at -1.0 V vs. Ag/AgCl. There is a high degree of spectral reproducibility, both in terms of band position and band intensity.
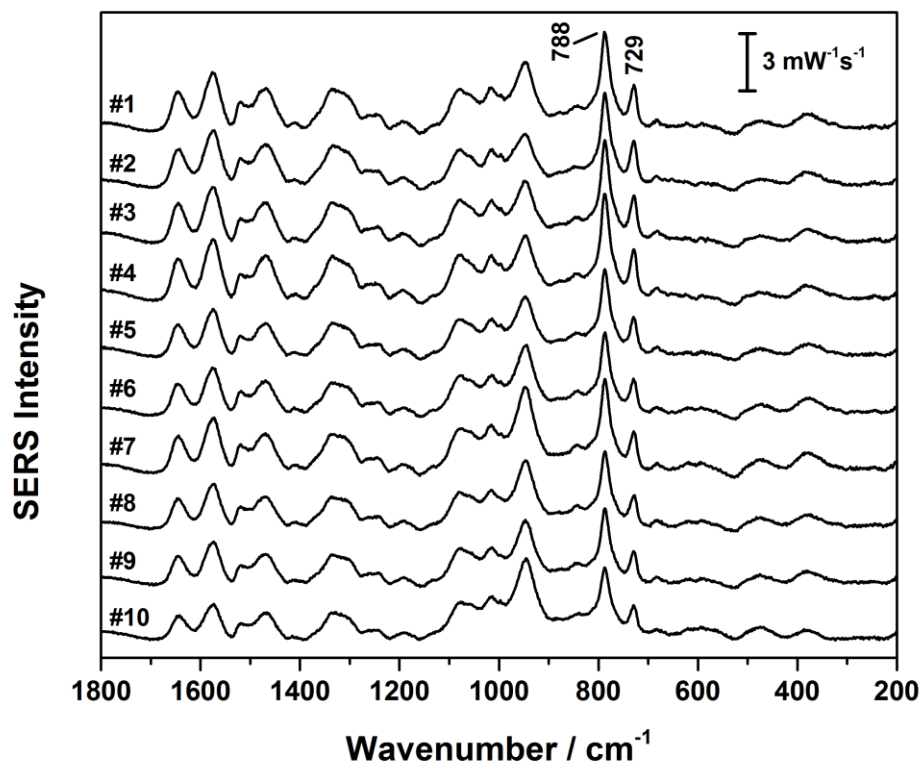
Figure 45. Ten EC-SERS spectra of 0.1 mM anti-KatG recorded at different spots on a AgNP-modified electrode. Applied potential = -1.0 V, laser power = 3 mW, collection time = 30 s, 0.1 M NaF electrolyte. Laser wavelength = 532 nm.

Figure 46 shows EC-SERS spectra for a SAM of 11-MUD immobilised onto AgNPs from a 1 mM ethanolic solution. Ten spectra were recorded at different spots on the electrode while the potential was held at -1.0 V. The 11-MUD spectra are also reproducible, with two diagnostic bands observed at 1106 and 709 cm^{-1}.
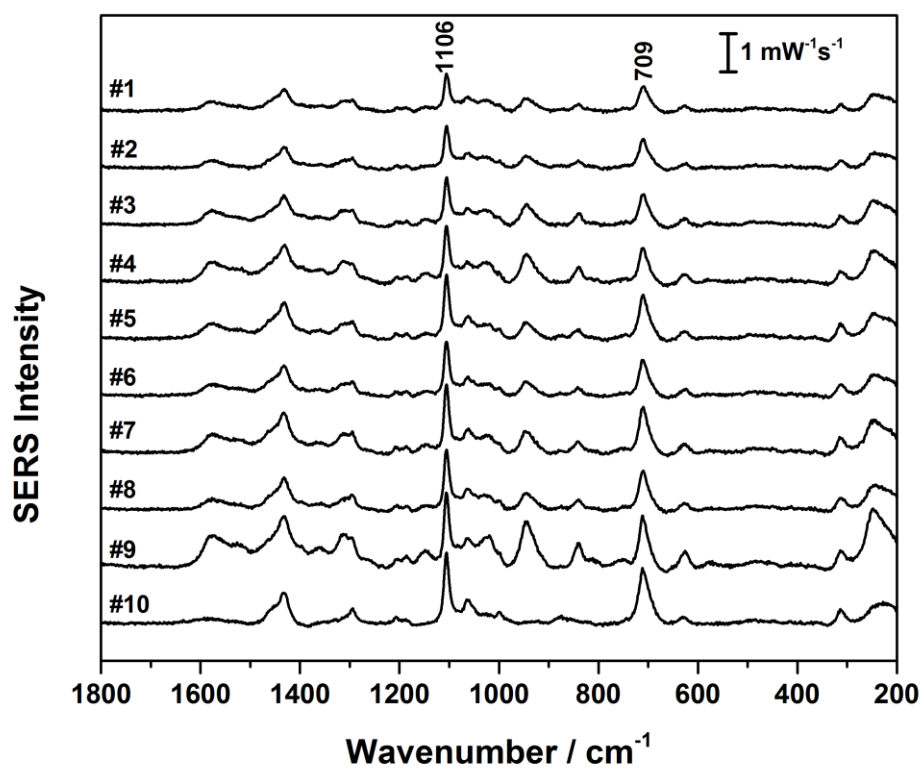
Figure 46. Ten EC-SERS spectra of 1.0 mM 11-MUD recorded at different spots on a AgNP-modified electrode. Applied potential = -1.0 V, laser power = 3 mW, collection time = 30 s, 0.1 M NaF electrolyte. Laser wavelength = 532 nm.

Figure 47 shows 10 spectra recorded in a similar manner for anti-KatG after incubation of the aptamer-modified electrode in 1 mM 11-MUD solution. In some spectra, for example #7, the spectral features of the spacer molecule (1105 and 708 cm^{-1}) are stronger than those of the aptamer (789 and 731 cm^{-1}). Figure 48 shows the 10 spectra recorded when 0.1 mM 11-MUD was used. Minimal interference from 11-MUD was observed when this lower concentration was used.
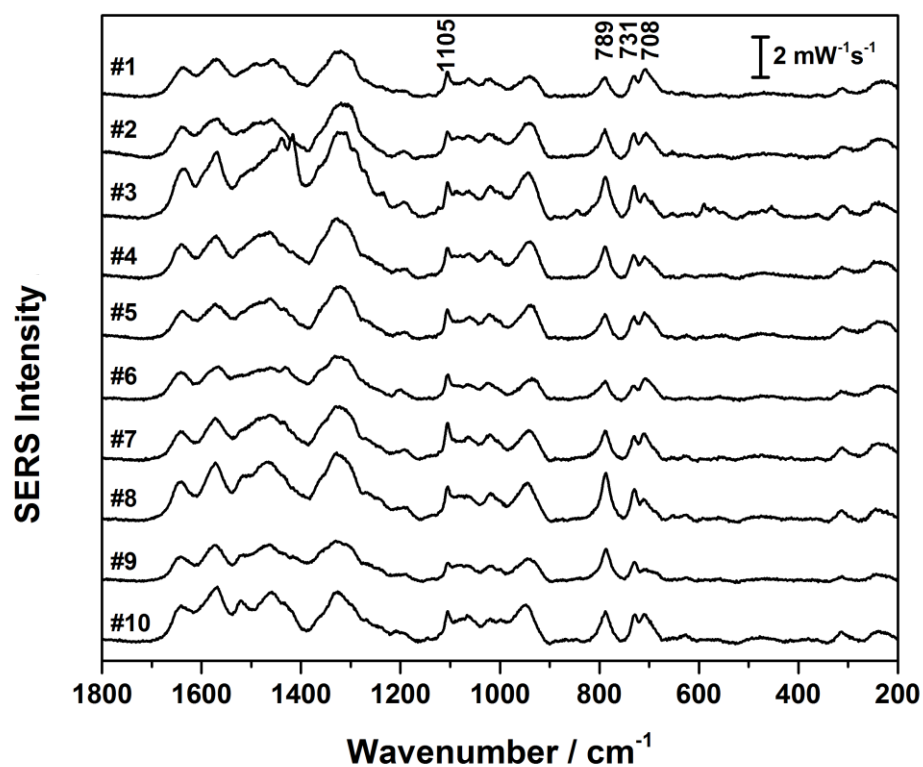
Figure 47. Ten EC-SERS spectra of 0.1 mM anti-KatG + 1.0 mM 11-MUD recorded at different spots on a AgNP-modified electrode. Applied potential = -1.0 V, laser power = 3 mW, collection time = 30 s, 0.1 M NaF electrolyte. Laser wavelength = 532 nm.
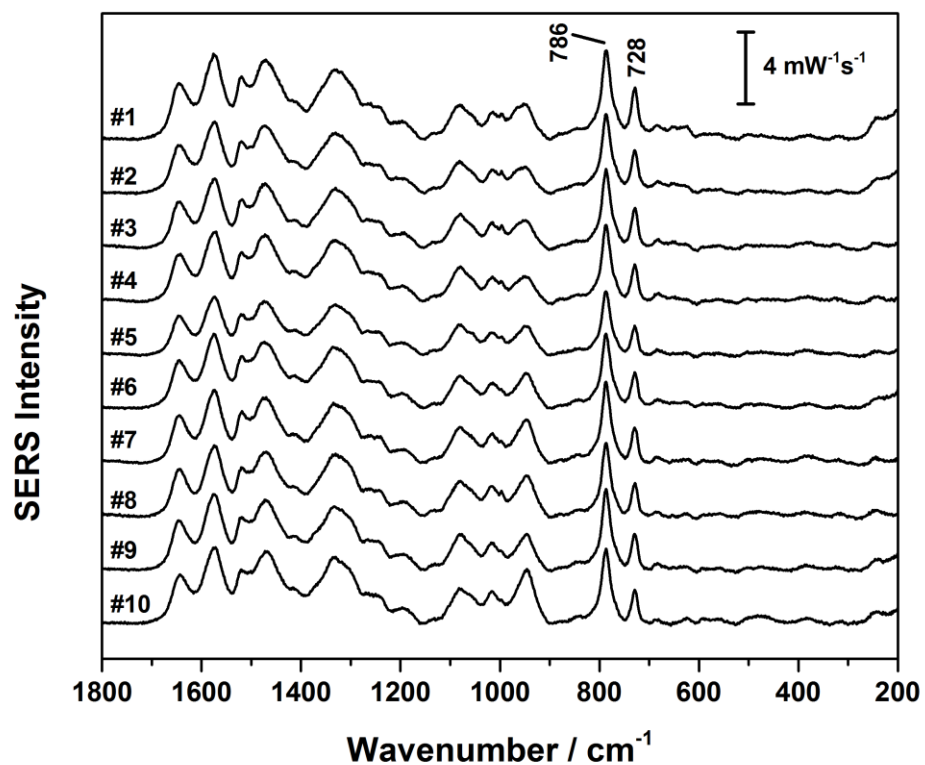
Figure 48. Ten EC-SERS spectra of 0.1 mM anti-KatG + 0.1 mM 11-MUD recorded at different spots on a AgNP-modified electrode. Applied potential = -1.0 V, laser power = 3 mW, collection time = 30 s, 0.1 M NaF electrolyte. Laser wavelength = 532 nm.

Averages of these spectra (Figures 45-48) plus data for 0.01 and 0.001 mM 11-MUD are shown in Figure 49. Since cyt c could be detected at a similar concentration, initial studies for detection of KatG at 100 nM seemed reasonable. Figure 50 depicts the results of the the same procedure used to compile the averaged spectra in Figure 49, except in this case, the aptasensor was immersed in 7.0 mL of 100 nM KatG in phosphate buffer under magnetic stirring. Unfortunately, KatG was not detected in any of the recorded spectra. After consultation with our colleagues at the University of Cape Town, it was determined that the lack of a proper binding buffer may have contributed to the problem. A HEPES/NaCl/KCl/MgCl$_2$/CaCl$_2$ binding buffer is needed for binding of the KatG protein to the aptamer. Accordingly, the studies would need to be repeated at a later date. While the optimal 11-MUD concentration was not explicitly determined, since 0.1 mM was the highest concentration at which spectral interference was not observed, it was chosen as the working concentration of 11-MUD for all future analyses.
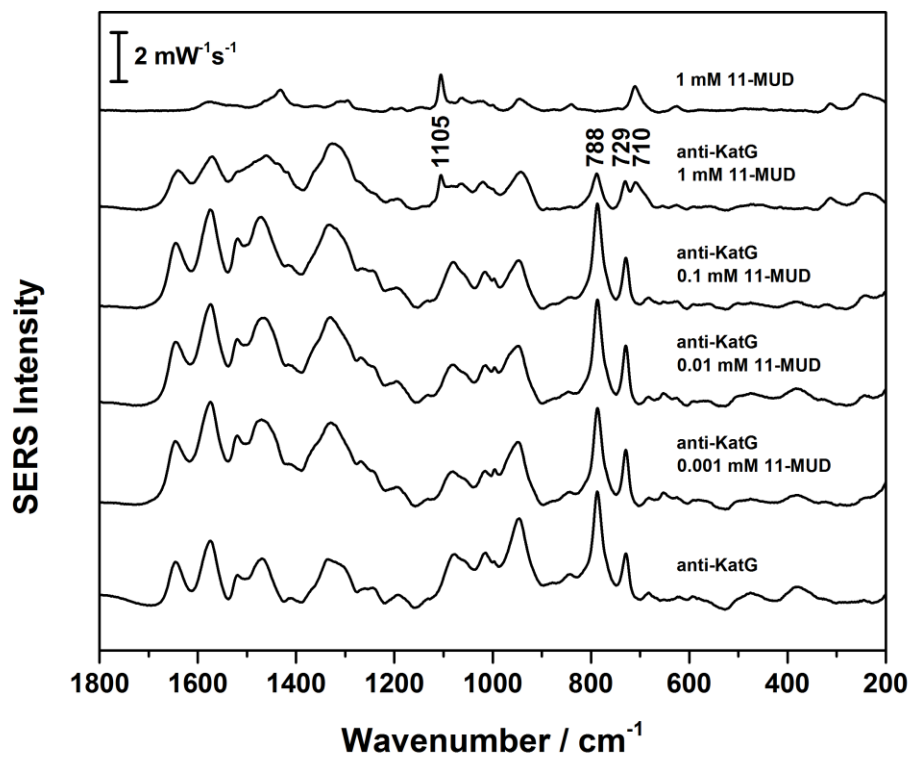
Figure 49. Averaged spectra (n=10) comparing the effects of differing concentrations of 11-MUD with anti-KatG aptamer on a AgNP-modified electrode. Applied potential = -1.0 V, laser power = 3 mW, collection time = 30 s, 0.1 M NaF electrolyte. Laser wavelength = 532 nm.
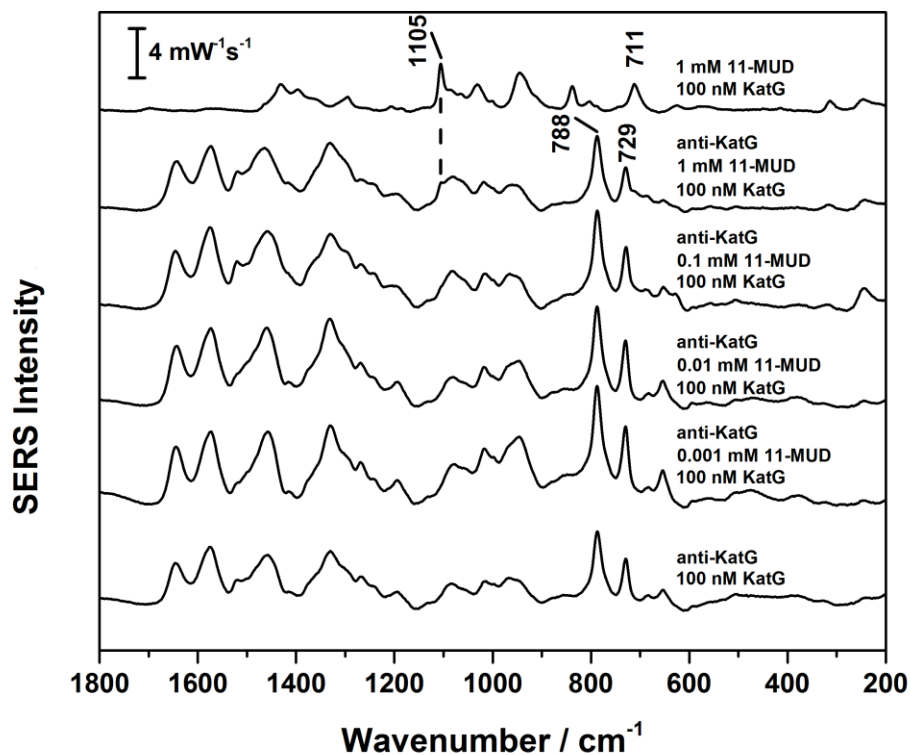
Figure 50. Averaged spectra (n=10) comparing the effects of differing concentrations of 11-MUD with anti-KatG aptamer on a AgNP-modified electrode after incubation with magnetic stirring in 7.0 mL solution of 100 nM KatG in phosphate buffer (pH 7.4). Applied potential = -1.0 V, laser power = 3 mW, collection time = 30 s, 0.1 M NaF electrolyte. Laser wavelength = 532 nm.

6.6 Change of electrolyte from NaF to Na_2SO_4

At a relatively late point in the project, it was realised that fluoride ion can form a Fe-F bond with the iron centre of a heme protein [157-159]. It is not known if this will affect the detection binding of KatG to the aptamer, but to be safe, Na_2SO_4 was used as the electrolyte for all subsequent analyses.

6.7 Reductive desorption of thiols

While repeating the anti-KatG aptamer studies in 0.03 M Na_2SO_4, EC-SERS spectra were collected as negative as -1.5 V instead of stopping at -1.0 V in order to determine the stability of the aptasensor at and more negative than -1.0 V. It was found that the Ag-S bond breaks at these more negative potentials, and the aptamer desorbs from the surface. The EC-SERS spectra are shown in Figure 51. Incubation in 0.1 mM 11-MUD does not prevent desorption of the aptamer, as shown in Figure 52. Curiously, the alkanethiol spacer molecule remains on the surface even at -1.5 V, while the aptamer does not. Note that in both cases, the closest part of the adsorbed species near the Ag surface consists of Ag-S-$(CH_2)_n$- (where n = 6 for the aptamer, and 11 for 11-MUD). The EC-SERS procedure was repeated for just a SAM of 11-MUD from 0.1 mM solution, which is shown in Figure 53. The spectral results do indeed show that 11-MUD remains on the surface at -1.5 V. The normal Raman spectrum of solid 11-MUD is also shown in Figure 53 for comparison.
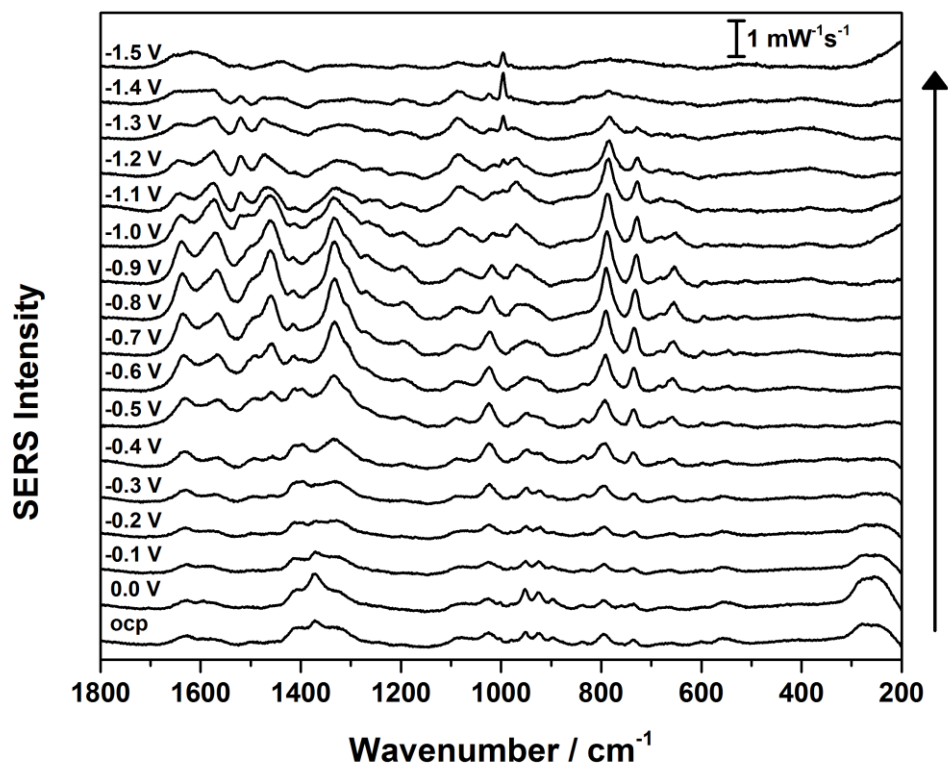
Figure 51. EC-SERS spectra of anti-KatG aptamer on a AgNP-modified electrode recorded at ocp, and applied potentials of 0.0 to -1.5 V at -0.1 V increments. Laser power = 7 mW, collection time = 30 s, 0.03 M Na_2SO_4 electrolyte. Laser wavelength = 532 nm.
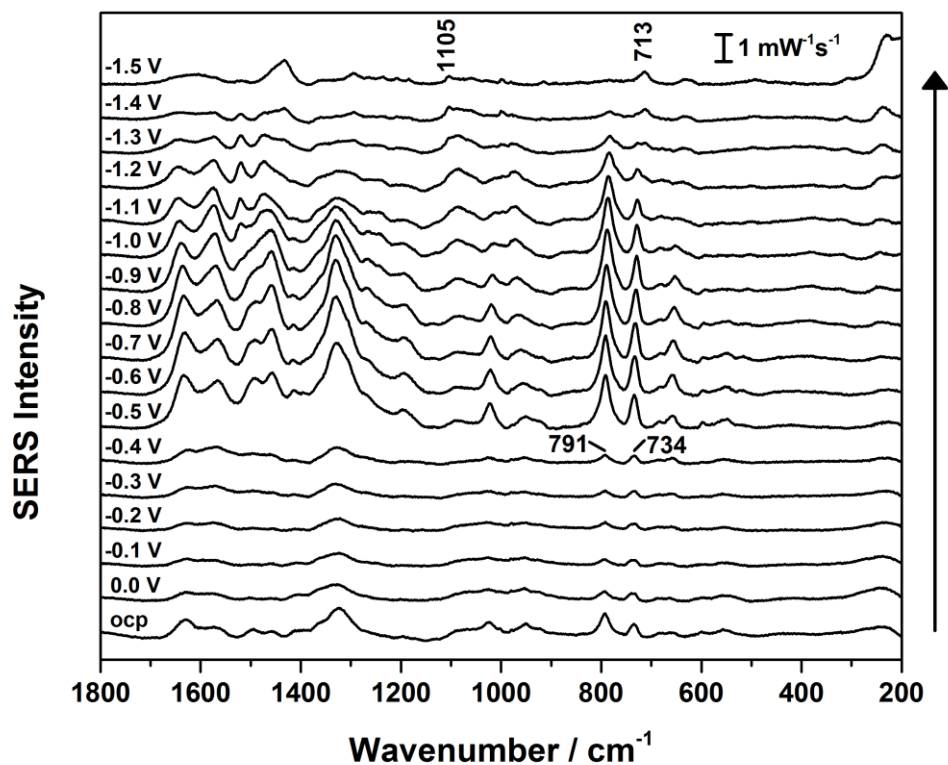
Figure 52. EC-SERS spectra of anti-KatG aptamer + 0.1 mM 11-MUD on AgNP-modified electrode recorded at ocp, and applied potentials of 0.0 to -1.5 V at -0.1 V increments. Laser power = 7 mW, collection time = 30 s, 0.03 M Na$_2$SO$_4$ electrolyte. Laser wavelength = 532 nm.
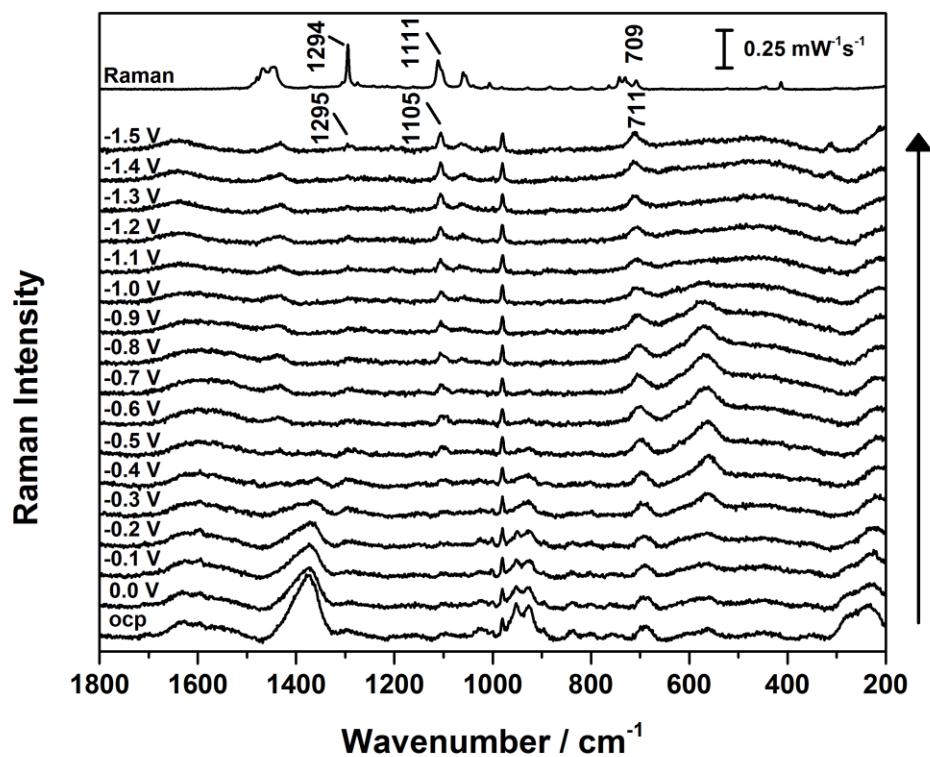
Figure 53. EC-SERS spectra of 0.1 mM 11-MUD on AgNP-modified electrode recorded at ocp, and applied potentials of 0.0 to -1.5 V at -0.1 V increments. Laser power = 7 mW, collection time = 30 s, 0.03 M Na_2SO_4 electrolyte. Raman spectrum of solid 11-MUD. Laser power = 10 mW, collection time = 120 s. Laser wavelength = 532 nm.

6.8 Preliminary detection of KatG and associated problems

Figure 54 shows the EC-SERS spectra recorded at ocp and between 0.0 and -1.5 V for the aptasensor (AgNP + 0.1 mM anti-KatG + 0.1 mM 11-MUD) after treatment for 1 hour with 10 μL of HEPES/NaCl/KCl/MgCl$_2$/CaCl$_2$ binding buffer (without KatG). After 1 hour, the electrode was rinsed gently with ultrapure water. It was fortunate, that in this case, spectra were collected as negative as -1.5 V and not just -1.0 V. Until about -1.3 V, the spectral behavior is very similar to what is observed for an unused (no protein) aptasensor: increase in aptamer signal intensity after -0.3 V, desorption after ca. -1.0 V and 11-MUD still observed at more negative potentials. Interestingly however, several new bands in the 1400-1200 cm^{-1} range were observed at -1.5 V. The importance of these bands is discussed in later pages.
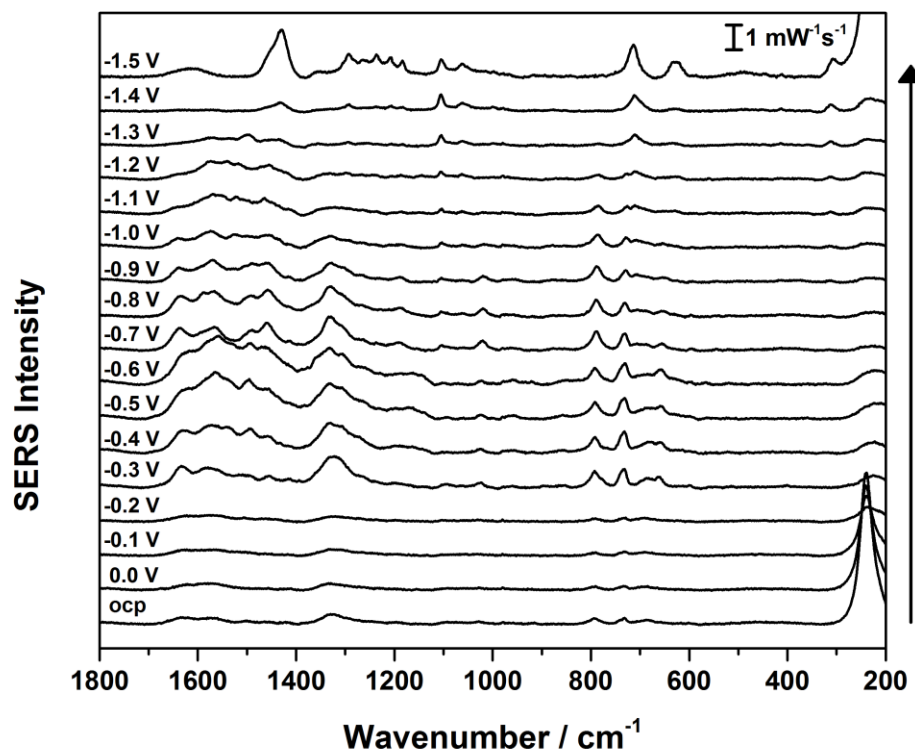
Figure 54. EC-SERS spectra of anti-KatG + 0.1 mM 11-MUD on AgNP-modified electrode after 1 hour of reaction with 10 µL binding buffer (blank) recorded at ocp, and applied potentials of 0.0 to -1.5 V at -0.1 V increments. Laser power = 7 mW, collection time = 30 s, 0.03 M Na_2SO_4 electrolyte.

Figure 55 shows a summary of the EC-SERS spectra recorded at -0.6 V for anti-KatG (A, from Figure 51), anti-KatG+ 11-MUD (B, from Figure 52), anti-KatG + 11-MUD treated with 10 µL blank binding buffer (C, from Figure 54) and anti-KatG + 11-MUD treated with 10 µL of 10 µM KatG in binding buffer (D, from Trial #2, see Appendix). The EC-SERS spectrum of 6.25 µM KatG protein at -0.7 V (Figures 41 and 42) is shown for comparison. It can be seen that 11-MUD has no negative effect on the aptamer spectrum (A&B). Treatment with blank binding buffer results in a decrease in band intensity, but no new bands appear (C). Treatment with 10 µL of 10 µM KatG in binding buffer gives rise to many new bands (D), several of which match the KatG reference spectrum (E). These preliminary results suggest that KatG is indeed binding to the aptamer, and is remaining bound after gentle rinsing with binding buffer and ultrapure water.

This experiment (Figure 55D) was repeated in triplicate, and as shown in Figure 56, these spectra were certainly not reproducible. While there are similarities, there are also many differences observed in the three trials for detection of KatG. One possible explanation is based on previous studies by Neumann *et al*. [41]. This report showed that while aptamer spectra are very reproducible, the same cannot be said for the spectra of the aptamer-target complexes, which could be influenced by the orientation of the target molecule on the aptamer-modified surface.
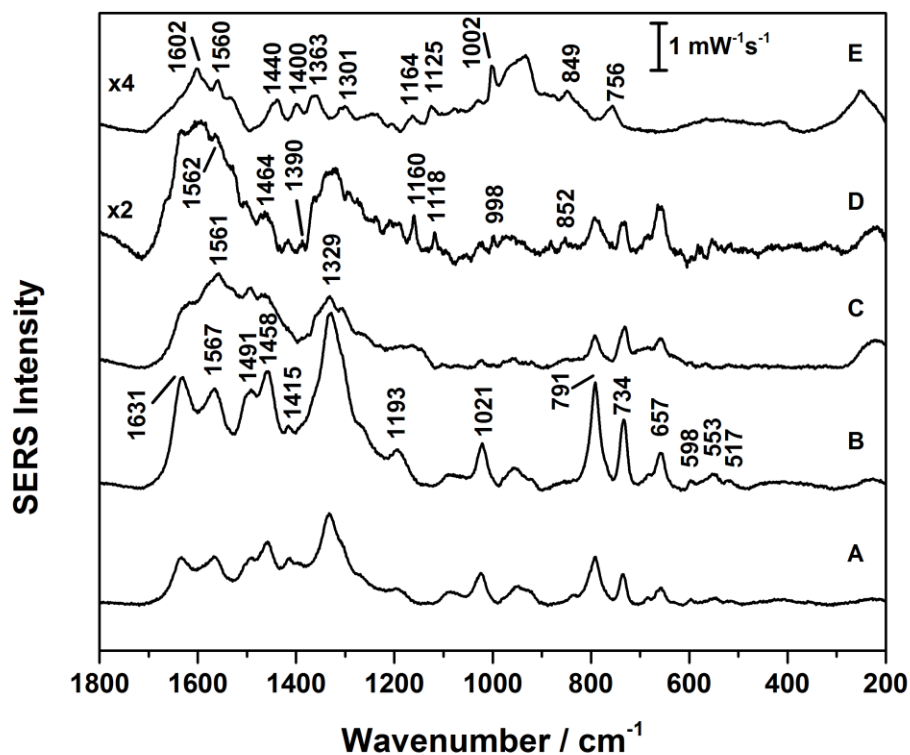
Figure 55. EC-SERS spectra on AgNP-modified electrode of anti-KatG aptamer (A); anti-KatG aptamer + 11-MUD (B); anti-KatG aptamer + 11-MUD reacted with binding buffer (blank) for 1 hour (C); anti-KatG aptamer + 11-MUD reacted with 10 μL of 10 μM KatG in binding buffer for 1 hour (D); spectra A-D with an applied potential of -0.6 V in 0.03 M Na$_2$SO$_4$ electrolyte. For comparison, the EC-SERS spectrum of 6.25 μM KatG in 0.05 M NaF recorded on AgNPs with an applied potential of -0.7 V (E). Laser power = 7 mW, collection time = 30 s, laser wavelength = 532 nm.
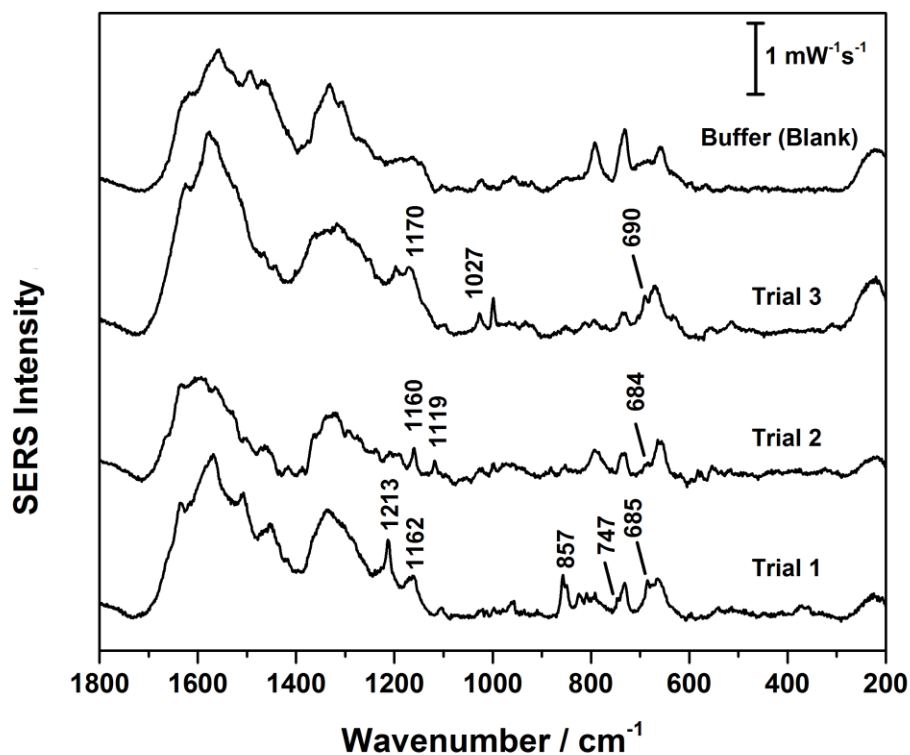
Figure 56. Averaged spectra (n=10) on AgNP-modified electrode of anti-KatG aptamer + 11-MUD reacted with blank binding buffer and three trials 10 μL of 10 μM KatG in binding buffer for 1 hour. Applied potential = -0.6 V, 0.03 M Na_2SO_4 electrolyte, Laser power = 7 mW, collection time = 30 s, laser wavelength = 532 nm. Full EC-SERS in Appendix Figures A5-A7.

The band appearing in all three trials around 1160-1170 cm^{-1} likely corresponds to the 1163 cm^{-1} band of KatG protein, which may be from the same mode of vibration giving rise to the ν(pyr half ring)$_{sym}$ band in cyt c. Similarly, the 1119 cm^{-1} band may be the 1124 cm^{-1} band of KatG, also seen in cyt c as ν(C$_α$N). The intense bands in trial 1 at 1213 and 857 cm^{-1} may correspond to the 1206, and 848 cm^{-1} bands for KatG protein. The 747 cm^{-1} band in trial 1 is assigned to the ν(pyr breathing) mode of vibration. Similarly, the 1027 cm^{-1} band in trial 3 may correspond to the 1030 cm^{-1} band of KatG. A band around 690 cm^{-1} appears in all three spectra, but this band was no observed in the analyses of KatG protein without aptamer.

It was also observed in Trial 3 (Full EC-SERS in the Appendix Figure A7) at -1.5 V that the new bands observed in the blank binding buffer spectrum (Figure 54) at the same potential were observed again. The two spectra are compared in Figure 57. By comparison with the normal Raman spectrum of HEPES powder, it was determined that these bands at -1.5 V are brought about by HEPES adsorbed on the AgNP surface.
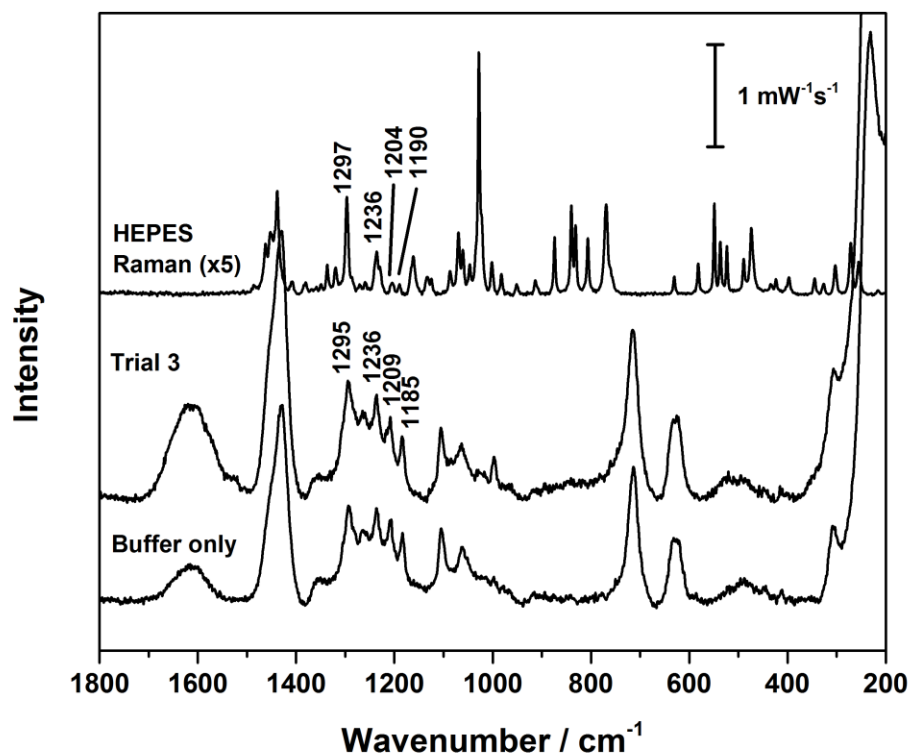
Figure 57. EC-SERS spectra of anti-KatG + 11-MUD after 1 hour reaction with blank binding buffer and 10 µL of 10 µM KatG in binding buffer (trial 3), applied potential = -1.5 V, 0.03 M Na_2SO_4 electrolyte, Laser power = 7 mW, collection time = 30 s. For comparison, the Raman spectrum (x5) of HEPES powder is shown. Laser power = 10 mW, collection time = 120 s. Laser wavelength = 532 nm.

The ramifications of this observation may be significant. The anti-KatG aptamer was selected under conditions such that it requires the HEPES molecule to be present in the buffer. However, the data shows that HEPES may be penetrating the aptamer/alkanethiol SAM, and interacts with or adsorbs onto the surface. This surface reaction may also explain why the spectrum after treatment with blank buffer (Figure 55) is significantly weaker than without buffer (B). These findings might suggest that the HEPES molecule may be displacing some of the anti-KatG aptamer from the AgNP surface. It is possible that the HEPES molecule may be bonding to the surface via its hydroxyl or sulfonic groups, but further studies are needed. In order to test this hypothesis, EC-SERS spectra were collected for an AgNP electrode that had been incubated in 7 mL of 20 mM HEPES solution for 1 hour, but no HEPES bands were observed over the potential range of 0.0 to -1.5 V. As such, how HEPES interacts with the surface and if this interaction negatively affects the binding of protein remains unclear.

6.9 Attempted detection in salt solution without HEPES

The KatG binding buffer contains 20 mM HEPES, 75 mM NaCl, 2 mM KCl, 2 mM $CaCl_2$ and 2 mM $MgCl_2$. The effect of not using HEPES, but still using the other salts was investigated in triplicate. Other than the removal of HEPES from the solution the analyses were conducted in an identical manner to those done previously. For two trials it was simply not possible to detect KatG (Appendix Figure A8), but for one trial, a KatG band was observed (Figure 58).

For the trials where KatG was not detected (Appendix Figure A8), diagnostic bands for KatG were not observed. However, at an applied potential of -1.5 V, weak bands for HEPES may have been observed in the spectrum. These HEPES bands are not likely from a contamination from the salt solution, but instead because the KatG protein was lyophilised in 5 mM HEPES buffer. The concentration of HEPES present in the solution used for the present analysis would have been much lower, but nonetheless HEPES was detected in the spectrum. In the successful trial (Figure 58), a weak band for the ν(pyr half ring)$_{sym}$ at 1162 cm^{-1} was detected at the applied potential of -0.6 V but this same band was not observed in the other trials. These results suggest that it is not possible to detect KatG in a reproducible manner without using the HEPES binding buffer.
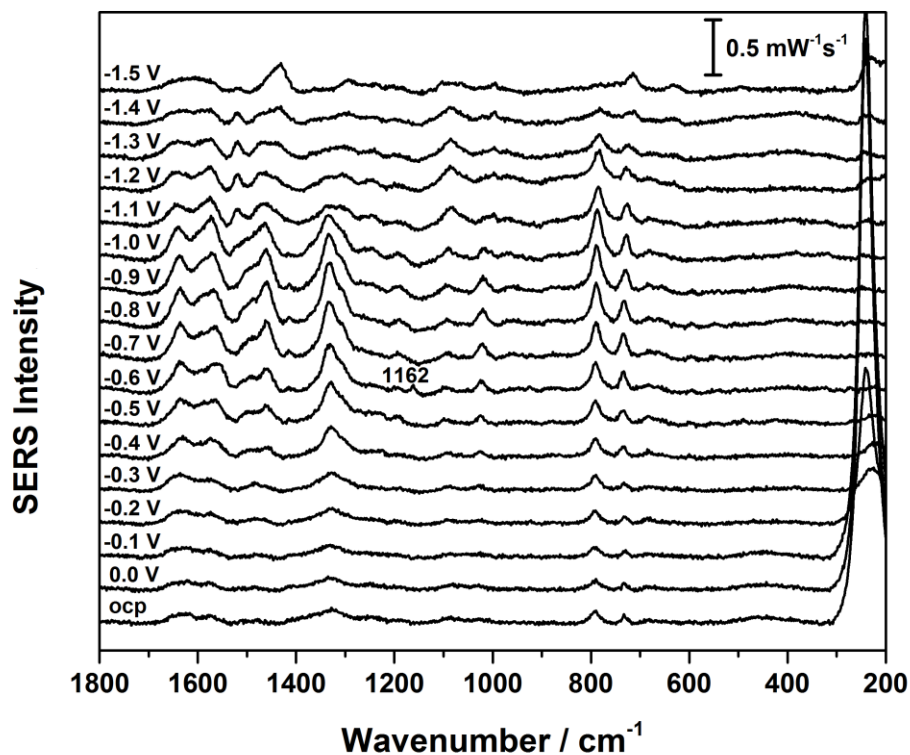
Figure 58. EC-SERS spectra of anti-KatG + 0.1 mM 11-MUD on AgNP-modified electrode after 1 hour of reaction with 10 µL of 10 µM KatG in 75 mM NaCl, 2 mM KCl, 2 mM CaCl$_2$ and 2 mM MgCl$_2$ recorded at ocp, and applied potentials of 0.0 to -1.5 V at -0.1 V increments. Laser power = 7 mW, collection time = 30 s, 0.03 M Na$_2$SO$_4$ electrolyte.

6.10 Conclusion for KatG aptamer studies

This study was the first EC-SERS analysis of KatG protein. Based on comparison with EC-SERS of cytochrome c and resonance Raman studies of KatG in the literature, it was possible to assign many of the bands for KatG protein. The anti-KatG aptamer developed at the University of Cape Town was found to bind KatG at a concentration of 10 μM, although the signal was not very reproducible. Lastly, the role of HEPES in the binding buffer has been investigated. HEPES is needed for binding the KatG protein to the aptamer, but it may also have a negative effect whereby it displaces the aptamer from the AgNP surface.

Chapter 7 – Conclusions

This project involved EC-SERS aptamer-based detection of three target proteins: immunoglobulin E (IgE), cytochrome c (cyt c) and catalase-peroxidase (KatG). As with any project, there were both successes and failures.

For the IgE phase of the project, the anti-IgE aptamer has been characterised using EC-SERS, but it was not possible to detect IgE protein using this method. Nonetheless, it was possible to detect IgE with the anti-IgE aptamer using cyclic voltammetry, which demonstrated that the aptamer does bind the protein, but the IgE could not be detected by EC-SERS Additionally, it was possible to collect a vibrational spectrum for IgE using ATR-FTIR spectroscopy.

The next phase of the project involved two heme proteins: cyt c and KatG. Cyt c and its aptamer served as a model system for the tuberculosis biomarker KatG. However, detection of cyt c is important in its own right, because it is a urine biomarker for diseases of the liver. Optimisation steps for the aptasensor were accomplished in this project, including concentration of DNA aptamer and alkanethiol spacer, choice of alkanethiol spacer (carboxylic acid or alcohol) to prevent non-specific interaction, and choice of an optimal electrolyte for EC-SERS analysis. Small spectral differences were observed for when the aptamer had bound cyt c compared to when it bound hemin. Using the EC-SERS aptamer method, it was possible to detect cyt c in binding buffer at a concentration of 1 nM, and in synthetic urine, at 10 nM. Small improvements may make this a clinically viable method for diagnosis of disease.

For the detection of KatG, preliminary results have shown that that it is possible to detect the TB biomarker protein at a concentration of 10 μM using the anti-KatG aptamer, although much work remains for the eventual development of an EC-SERS aptasensor for detection of TB at the point of care. Uniform spectra were not obtained in each trial, although some similarities were observed. The interaction of HEPES in the binding buffer with the aptamer SAM is not yet clear, so this area merits further investigation in case it is a reason for concern. Despite this possible problem, it was found that HEPES is necessary for binding KatG, because the anti-KatG aptamer will not bind its target protein in phosphate buffer, nor a solution of NaCl/KCl/CaCl$_2$/MgCl$_2$.

In summary, EC-SERS detection was successful only for the heme proteins, cyt c and KatG, but not the non-heme protein IgE. Quantitative analysis of cyt c in the nanomolar range shows some promise, although the methodology needs to be refined in order to generate a more reproducible signal.

Chapter 8 – Future Work

For the IgE aptasensor, future research could explore indirect methods, such as using a Raman reporter molecule, for indirect EC-SERS detection. Further voltammetric studies, such as square wave voltammetry could also be used. The solution in which the aptamer-protein binding is carried out (binding buffer) could also have been a factor, as was the case in detecting cyt c at lower concentrations. However, at this point in the project the IgE studies were concluded and the focus had moved on to cyt c and KatG, and there simply was not enough time to reconsider the IgE detection methodology.

This project developed an EC-SERS aptasensor for cyt c. Future work could involve improving the reproducibility of the system, especially so that reliable quantitative analysis could be conducted. This goal could be achieved by using more uniform SERS substrates. A lower limit of detection in the pM range would also be more desirable, particularly for clinical use of the aptasensor. The use of hemin to improve binding should be explored, although quantitative detection may be an issue when both cyt c and hemin around bound to the aptamer.

For the KatG aptasensor, there remains a lot of work to be done. Firstly, there were issues involving solubility of the KatG protein that need to be resolved. The interaction of HEPES with the aptasensor should be explored further. It may turn out to not be a problem, but it does merit more attention. Detection of KatG ought to be achieved at lower concentrations than 10 μM, so that the goal of developing an EC-SERS aptasensor for detection of tuberculosis at the point of care can be achieved. Control

studies with a large heme protein such as hemoglobin should be conducted, as well as detection of KatG in synthetic sputum. In addition to EC-SERS, electrochemical methods such as CV and SWV also ought to be explored.

For both of the heme proteins (cyt c and KatG), laser excitation of ~409 nm could be used to see if it improves the resonance Raman contribution, and therefore increases signal intensity. Statistical methods such as principal component analysis (PCA) ought also to be used to see if computer software can reliably determine if the aptamer has bound the target protein. Once both aptasensors have been optimised, the possibility for use with real clinical samples should be considered.

Appendix
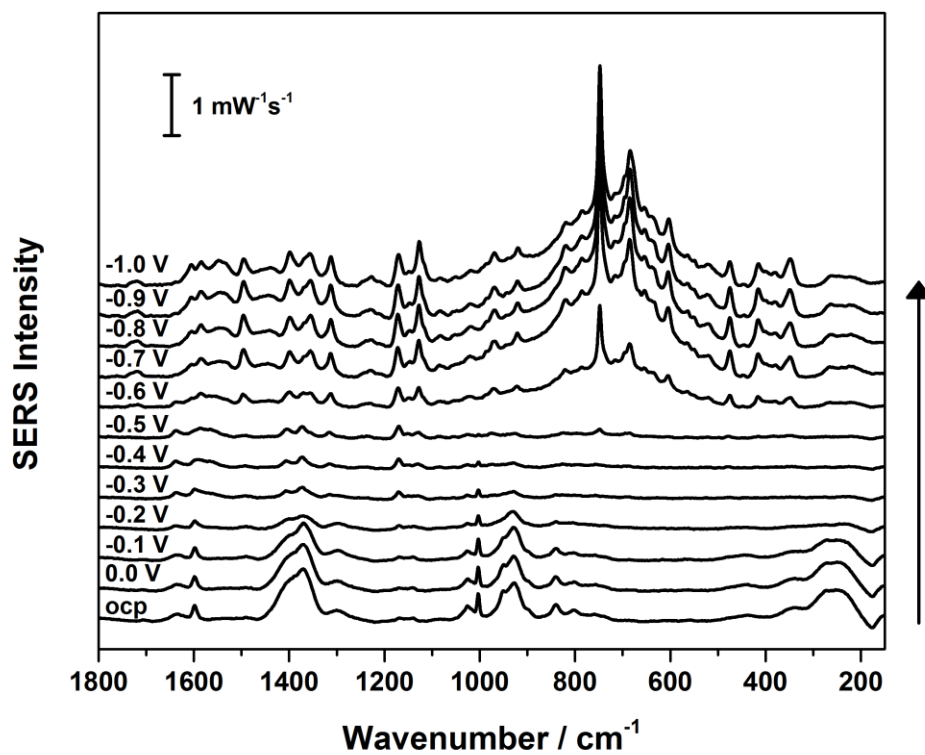
Figure A1. EC-SERRS 5 μM cyt c solution in 0.1 M NaF at a citrate reduced AgNP electrode collected at ocp, and over the cathodic potential range of 0.0 to -1.0 V vs Ag/AgCl. Laser power = 10 mW, collection time = 30 s, wavelength = 532 nm.
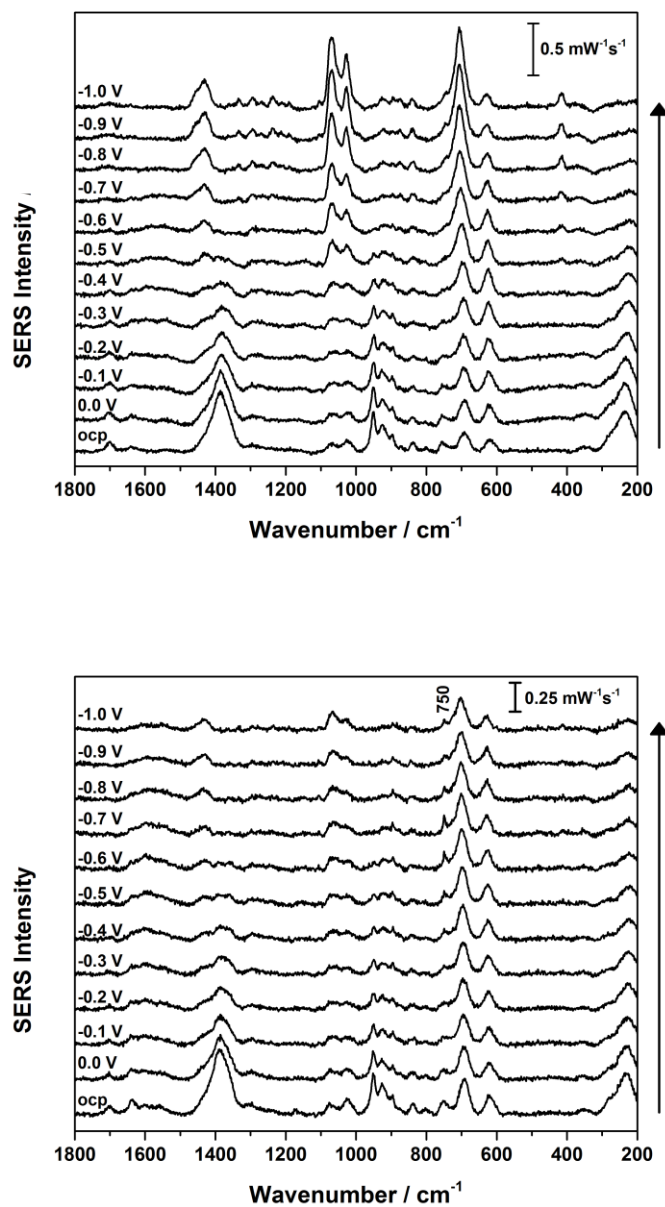
Figure A2. EC-SERS spectra of self-assembled monolayers of 6-MHA (20 hour incubation) with (bottom) and without (top) 7 μM cyt c (1 hour incubation in 7 mL) on citrate/borohydirde reduced AgNPs recorded at ocp and over the cathodic potential range of 0.0 to -1.0 V. Laser excitation = 532 nm, time = 30 s, power = 5 mW.
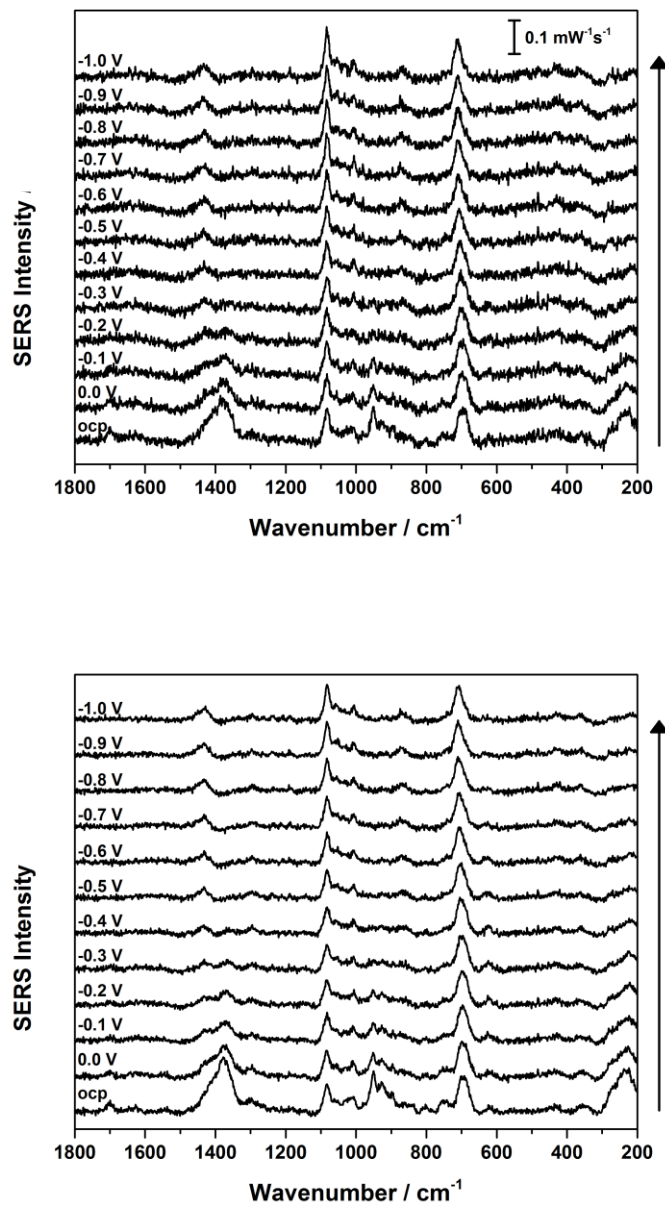
Figure A3. EC-SERS spectra of self-assembled monolayers of 6-MH (20 hour incubation) with (bottom) and without (top) 7 μM cyt c (1 hour incubation in 7 mL) on citrate/borohydirde reduced AgNPs recorded at ocp and over the cathodic potential range of 0.0 to -1.0 V. Laser excitation = 532 nm, time = 30 s, power = 5 mW.
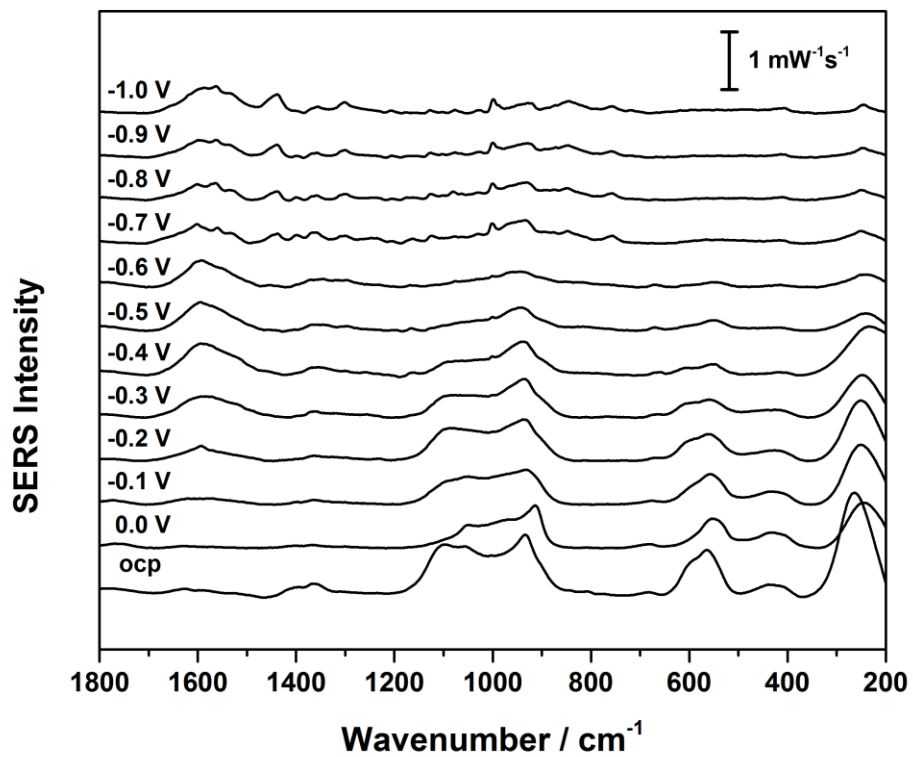
Figure A4. EC-SERS spectra of 6.25 μM KatG on AgNPs in 0.05 M NaF over the potential range of ocp, 0.0 to -1.0 V at -0.1 V increments, laser power = 7 mW, collection time = 30 s, laser wavelength = 532 nm.
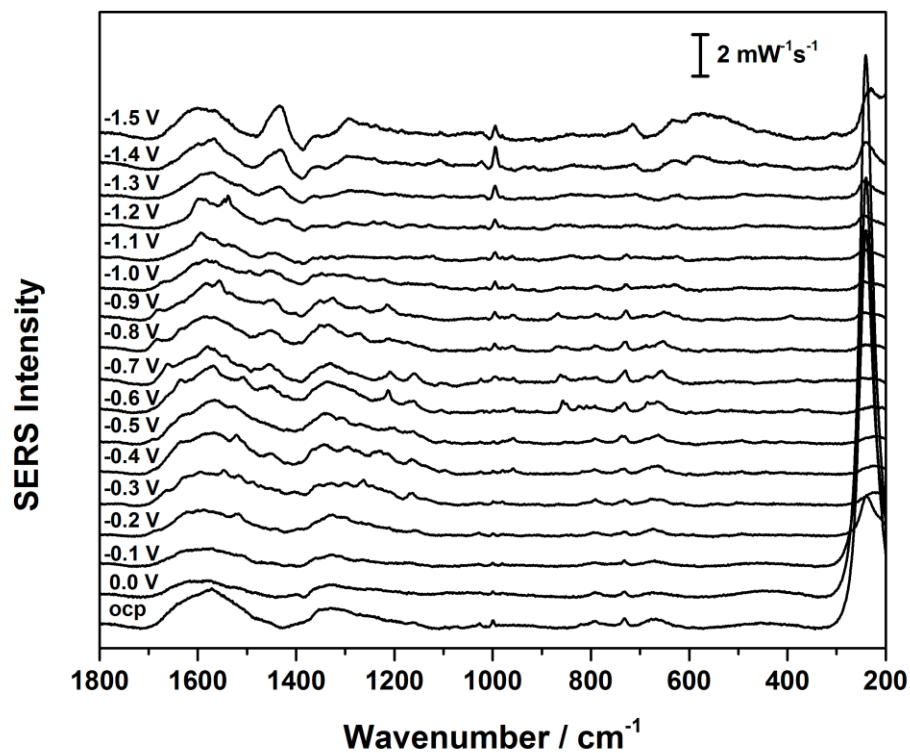
Figure A5. Trial 1 of EC-SERS spectra of 0.1 mM anti-KatG + 0.1 mM 11-MUD on AgNP-modified electrode after 1 hour of reaction with 10 μL of 10 μM KatG in binding buffer recorded at ocp, and applied potentials of 0.0 to -1.5 V at -0.1 V increments. Laser power = 7 mW, collection time = 30 s, 0.03 M Na_2SO_4 electrolyte.
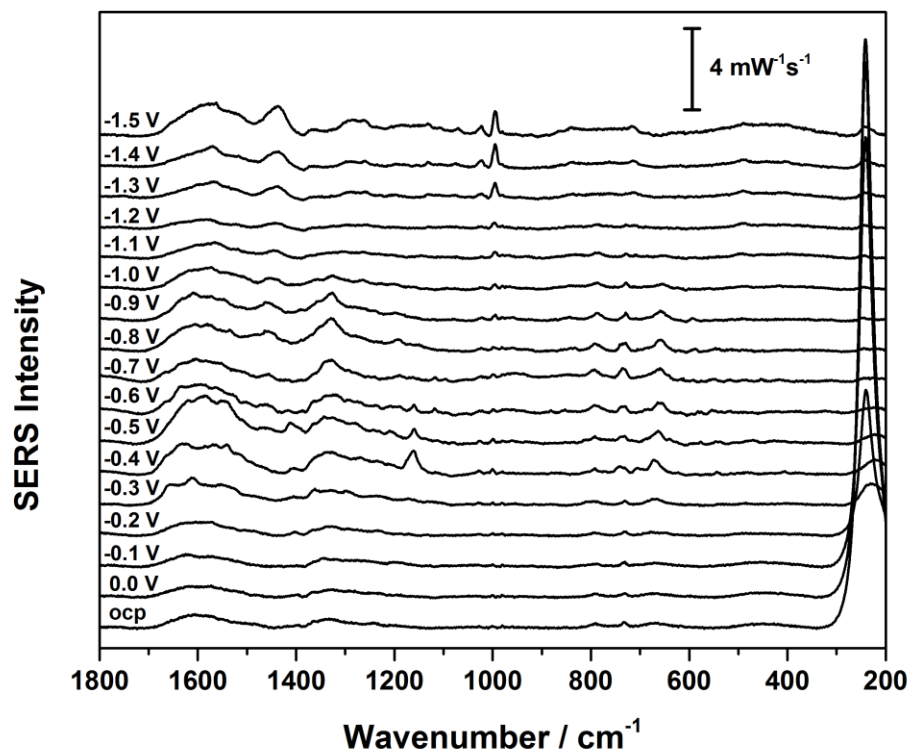
Figure A6. Trial 2 of EC-SERS spectra of 0.1 mM anti-KatG + 0.1 mM 11-MUD on AgNP-modified electrode after 1 hour of reaction with 10 μL of 10 μM KatG in binding buffer recorded at ocp, and applied potentials of 0.0 to -1.5 V at -0.1 V increments. Laser power = 7 mW, collection time = 30 s, 0.03 M Na_2SO_4 electrolyte.
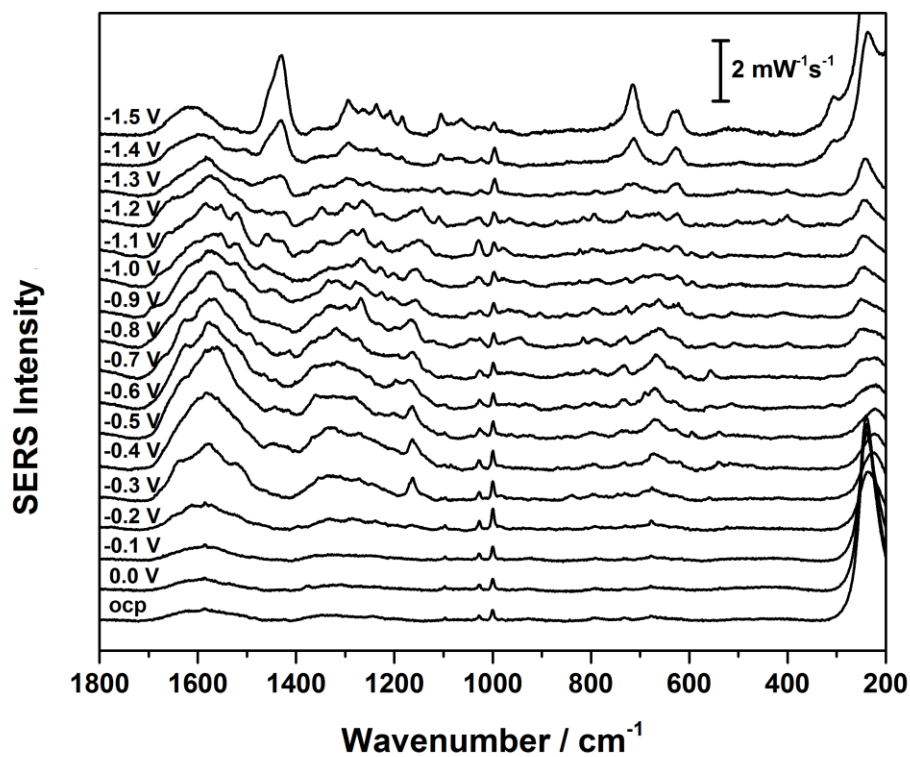
Figure A7. Trial 3 of EC-SERS spectra of 0.1 mM anti-KatG + 0.1 mM 11-MUD on AgNP-modified electrode after 1 hour of reaction with 10 μL of 10 μM KatG in binding buffer recorded at ocp, and applied potentials of 0.0 to -1.5 V at -0.1 V increments. Laser power = 7 mW, collection time = 30 s, 0.03 M Na_2SO_4 electrolyte.
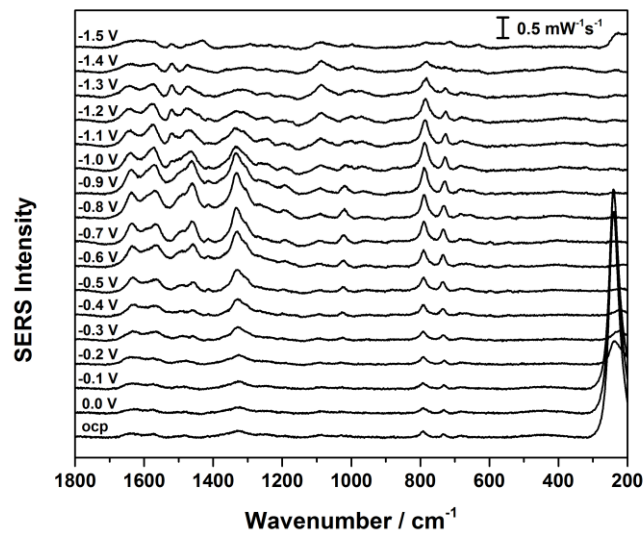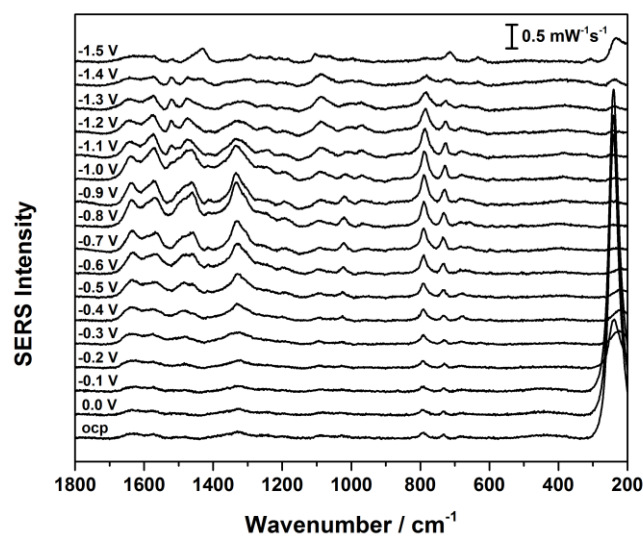
Figure A8. EC-SERS spectra of anti-KatG + 0.1 mM 11-MUD on AgNP-modified electrode after 1 hour of reaction with 10 μL of 10 μM KatG in 75 mM NaCl, 2 mM KCl, 2 mM $CaCl_2$ and 2 mM $MgCl_2$ recorded at ocp, and applied potentials of 0.0 to -1.5 V at -0.1 V increments. Laser power = 7 mW, collection time = 30 s, 0.03 M Na_2SO_4 electrolyte. Two trials shown.

References

[1] Centers for Disease Control and Prevention. Tuberculosis: Basic TB facts. 1 April 2014. http://www.cdc.gov/tb/topic/basics/default.htm

[2] World Health Organization. Tuberculosis fact sheet. 1 April 2014. http://www.who.int/mediacentre/factsheets/fs104/en/

[3] P. Yager, G. J. Domingo, J. Gerdes. *Annu. Rev. Biomed. Eng.,* **2008,** *10,* 107-144.

[4] United Nations. The Millennium Goals Development Report 2013. 1 April 2014. http://www.un.org/millenniumgoals/pdf/report-2013/mdg-report-2013-english.pdf

[5] D. Coetzee, K. Hilderbrand, E. Goemaere, F. Matthys, M. Boelaert. *Trop. Med. Int. Health*, **2004,** *9,* A11-A15.

[6] V. Gubala, L. F. Harris, A. J. Ricco, M. X. Tan, D. E. Williams. *Anal. Chem.,* **2012,** *84,* 487-515.

[7] N. P. Pai, C. Vadnais, C. Denkinger, N. Engels M. Pai. *PLOS Med.,* **2012,** *9,* e1001306.

[8] K. Dheda, M. Ruhwald, G. Theron, J. Peter, W. C. Yam. *Respirology,* **2013,** *18,* 217-232.

[9] S. B. Squire, A. K. Belaye, A. Kashoti, F. M. L. Salaniponi, C. J. F. Mundy, S. Theobald, J. Kemp. *Int. J. Tuberc. Lung Dis.,* **2005,** *9,* 25-31.

**[10]** G. Theron, L. Zijenah, D. Chanda, P. Clowes, A. Rachow, M. Lesosky, W. Bara, S. Mungofa, M. Pai, M. Hoelscher, D. Dowdy, A. Pym, P. Mwaba, P. Mason, J. Peter, K. Dheda. *Lancet,* **2014,** *383,* 424-435.

[11] C. Wejse. *Lancet,* **2014,** *383,* 388-390.

[12] Point-of-Care Diagnostics Meeting, Bill and Melinda Gates Foundation, Seattle, Washington, United States. May 2012.

[13] S. Wang, F. Inci, G. De Libero, A. Singhal, U. Demirci. *Biotechnol. Adv.,* **2013,** *31,* 438-449.

[14] P. K. Drain, E. Losina, S. M. Colemann, J. Giddy, D. Ross, J. N. Katz, R. P. Walensky, K. A. Freedberg, I. V. Bassett. *BMC Infect. Dis.,* **2014,** 14:110.

[15] A. B. Iliuk, L. Hu, W. A. Tao. *Anal. Chem.,* **2011,** *83,* 4440-4452.

[16] W. Zhou, P.-J. J. Huang, J. Ding, J. Liu. *Analyst,* **2014,** *139,* 2627-2640.

[17] A. D. Ellington, J. W. Szostak. *Nature,* **1990,** *346,* 818-822.

[18] A. K. H. Cheng, D. Sen, H.-Z. Yu. *Bioelectrochemistry,* **2009,** *77,* 1-12.

[19] C. K. O'Sullivan. *Anal. Bioanal. Chem.,* **2002,** *372,* 44-48.

[20] P. J. Vikesland, K. R. Wigginton. *Environ. Sci. Technol.,* **2010,** *44,* 3656-3669.

[21] J. J. Gooding, N. Darwish. *Chem. Rec.,* **2012,** *12,* 92-105.

[22] Y.-X. Wang, Z.-Z. Ye, C.-Y. Si, Y.-B. Ying. *Chin. J. Anal. Chem.,* **2012,** *40,* 634-642.

[23] J. Chen, J. Jiang, X. Gao, G. Liu, G. Shen, R. Yu. *Chem. Eur. J.,* **2008,** *14,* 8374-8382.

[24] N. H. Kim, S. J. Lee, M. Moskovits. *Nano Lett.,* **2010,** *10,* 4181-4185.

[25] M. Li, J. Zhang, S. Suri, L. J. Sooter, D. Ma, N. Wu. *Anal. Chem.,* **2012,** *84,* 2837-2842.

[26] J. Yang, M. Palla, F. G. Bosco, T. Rindzevicius, T. S. Alstrom, M. S. Schmidt, A. Boisen, J. Ju, Q. Lin. *ACS Nano,* **2013,** *7,* 5350-5359.

[27] H. Cho, B. R. Baker, S. Wachsmann-Hogiu, C. V. Pagba, T. A. Laurence, S. M. Lane, L. P. Lee, J. B.-H. Tok. *Nano Lett.,* **2008,** *8,* 4386-4390.

[28] H. Kim, T. Kang, H. Lee, H. Ryoo, S. M. Yoo, S. Y. Lee, B. Kim. *Chem. Asian J.,* **2013,** *8,* 3010-3014.

[29] J. Hu, P.-C. Zheng, J.-H. Jiang, G.-L. Shen, R.-Q. Yu, G.-K. Liu. *Anal. Chem.,* **2009,** *81,* 87-93.

[30] E. Temur, A. Zengin, I. H. Boyaci, F. C. Dudak, H. Torul, U. Tamer. *Anal. Chem.,* **2012,** *84,* 10600-10606.

[31] Y. Wang, H. Wei, B. Li, W. Ren, S. Guo, S. Dong, E. Wang. *Chem. Commun.,* **2007,** *48,* 5220-5222.

[32] Y. Wang, K. Lee, J. Irudayaraj. *Chem. Commun.,* **2010,** *46,* 613-615.

[33] J. Yoon, N. Choi, J. Ko, K. Kim, S. Lee, J. Choo. *Biosens. Bioelectron.,* **2013,** *47,* 62-67.

[34] P. Negri, G. Chen, A. Kage, A. Nitsche, D. Naumann, B. Xu, R. A. Dluhy. *Anal. Chem.,* **2012,** *84,* 5501-5508.

[35] C. V. Pagba, S. M. Lane, H. Cho, S. Wachsmann-Hogiu. *J. Biomed. Opt.,* **2010,** *15,* 047006-1-047006-8.

[36] M. A. Ochsenkuhn, C. J. Campbell. *Chem. Commun.,* **2010,** *46,* 2799-2801.

[37] P. D. Howes, S. Rana, M. M. Stevens. *Chem. Soc. Rev.* **2014,** *43,* 3835-3853.

[38] M. Citartan, S. C. B. Gopinath, J. Tominaga, T.-H. Tang. *Analyst,* **2013,** *138,* 3576-3592.

[39] W. Xie, S. Schlucker. *Phys. Chem. Chem. Phys.,* **2013,** *15,* 5329-5344.

[40] P. Negri, A. Kage, A. Nitsche, D. Naumann, R. A. Dluhy. *Chem. Commun.,* **2011,** *47,* 8635-8637.

[41] O. Neumann, D. Zhang, F. Tam, S. Lal, P. Wittung-Stafshede, N. J. Halas. *Anal. Chem.,* **2009,** *81,* 10002-10006.

[42] L. He, E. Lamont, B. Veeregowda, S. Sreevatsan, C. L. Haynes, F. Diez-Gonzalez, T. P. Labuza. *Chem. Sci.,* **2011,** *2,* 1579-1582.

[43] E. A. Lamont, L. He, K. Warriner, T. P. Labuza, S. Sreevatsan. *Analyst,* **2011,** *136,* 3884-3895.

[44] L. He, B. D. Deen, A. H. Pagel, F. Diez-Gonzalez, T. P. Labuza. *Analyst,* **2013,** *138,* 1657-1659.

[45] S. Pang, T. P. Labuza, L. He. *Analyst,* **2014,** *139,* 1895-1901.

[46] F. Barahona, C. L. Bardliving, A. Phifer, J. G. Bruno, C. A. Batt. *Ind. Biotech.,* **2013,** *9,* 42-50.

[47] B. C. Galarreta, M. Tabatabaei, V. Guieu, E. Peyrin, F. Lagugni-Labarthet. *Anal. Bioanal. Chem.,* **2013,** *405,* 1613-1621.

[48] C. V. Pagba, S. M. Lane, S. Wachsmann-Hogiu. *J. Raman. Spectrosc.,* **2010,** *41,* 241-247.

[49] A. K. H. Cheng, B. Ge, H.-Z. Yu. *Anal. Chem.,* **2007,** *79,* 5158-5164.

[50] L. Li, H. Zhao, Z. Chen, X. Mu, L. Guo. *Biosens. Bioelectron.,* **2011,** *30,* 261-266.

[51] M. C. Rodriguez, A.-N. Kawde, J. Wang. *Chem. Commun.,* **2005,** 4267-4269.

[52] H. J. Gould, B. J. Sutton. *Nat. Rev. Immunol.,* **2008,** *8,* 205-217.

[53] H. J. Gould, B. J. Sutton, A. J. Beavil, R. L. Beavil, N. McCloskey, H. A. Coker, D. Fear, L. Smurthwaite. *Annu. Rev. Immunol.,* **2003,** *21,* 579-628.

[54] T. W. Wiegand, P. B. Williams, S. C. Dreskin, M.-H. Jouvin, J.-P. Kinet, D. Tasset. *J. Immunol.,* **1996,** *157,* 221-230.

[55] E. Katilius, C. Flores, N. W. Woodbury. *Nucleic Acids Res.,* **2007,** *35,* 7626-7635.

[56] M. Liss, B. Petersen, H. Wolf, E. Prohaska. *Anal. Chem.,* **2002,** *74,* 4488-4495.

[57] C. Yao, Y. Qi, Y. Zhao, Y. Xiang, Q. Chen, W. Fu. *Biosens. Bioelectron.,* **2009,** *24,* 2499-2503.

[58] Y. Jiang, C. Zhu, L. Ling, L. Wan, X. Fang, C. Nai. *Anal. Chem.,* **2003,** *75,* 2112-2116.

[59] Y. H. Kim, J. P. Kim, S. J. Han, S. J. Sim. *Sensor Actuat. B-Chem.,* **2009,** *139,* 471-475.

[60] J.-L. He, Z.-S. Wu, S.-B. Zhang, G.-L. Shen, R. Q. Yu. *Analyst,* **2009,** *134, 1003-1007.*

[61] K. Feng, C. Sun, J. Jiang, R. Yu. *Anal. Lett.,* **2011,** *44,* 1301-1309.

[62] D. Xu, D. Xu, X. Yu, Z. Liu, W. He, Z. Ma. *Anal. Chem.,* **2005,** *77,* 5107-5113.

[63] E. J. Nam, E. J. Kim, A. W. Wark, S. Rho, H. Kim, H. J. Lee. *Analyst,* **2012,** *137,* 2011-2016.

[64] J. Wang, A. Munir, Z. Li, H. S. Zhou. *Talanta,* **2010,** *81,* 63-67.

[65] S. Khezrian, A. Salimi, H. Teymourian, R. Hallaj. *Biosens. Bioelectron.,* **2013,** *43,* 218-225.

[66] C.-Y. Lee, K.-Y. Wu, H.-L. Su, H.-Y. Hung, Y.-Z. Hsieh. *Biosens. Bioelectron.,* **2013,** *39,* 133-138.

[67] Z.-S. Wu, F. Zhang, G.-L. Shen, R.-Q. Yu. *Biomaterials,* **2009,** *30,* 2950-2955.

[68] H. Li, C. Wang, Z. Wu. L. Lu, L. Qiu, H. Zhou, G. Shen, R. Yu. *Anal. Chim. Acta,* **2013,** *758,* 130-137.

[69] Y.-L. P. Ow, D. R. Green, Z. Hao, T. W. Mak. *Nat. Rev. Mol. Cell Biol.,* **2008,** *9,* 532-542.

[70] D. R. Green, J. C. Reed. *Science,* **1998,** *281,* 1309-1312.

[71] T. J. Miller, A. Knapton, O. Adeyemo, L. Noory, J. Weaver, J. P. Hanig. *J. Appl. Toxicol.,* **2008,** *28,* 815-828.

[72] A. Parfieniuk-Kowerda, T. W. Lapinski, M. Rogalska-Plonska, M. Swizderska, A. Panasiuk, J. Jaroszewicz, R. Flisiak. *Liver Int.,* **2014,** *34,* 544-550.

[73] I. Sakaida, T. Kimura, T. Yamasaki, Y. Fukomoto, K. Watanabe, M. Aoyama, K. Okita. *J. Gastroenterol.,* **2005,** *40,* 179-185.

[74] B. Killinger, M. Shah, A. Moszczynska. *J. Neurochem.,* **2014,** *128,* 764-775.

[75] R. A. Zager, A. C. M. Johnson, S. Y. Hanson. *Kidney Int.,* **2004,** *65,* 2123-2134.

[76] K. C. Zimmermann, N. J. Waterhouse, J. C. Goldstein, M. Schuler, D. R. Green. *Neoplasia,* **2000,** *2,* 505-513.

[77] T. M. Cotton, S. G. Schultz, R. P. Van Duyne. *J. Am. Chem. Soc.,* **1980,** *102,* 7962-7965.

[78] M. Collinson, E. F. Bowden. *Anal. Chem.,* **1992,** *64,* 1470-1476.

[79] J. F. Cerda, C. X. Guzman, H. Zhang, E. J. Amendola, J. D. Castorino, N. Millet, A. L. Fritz, D. N. Houchins, M. H. Roeder. *Electrochem. Commum.,* **2013,** *33,* 76-79.

[80] S. Hu, I. K. Morris, J. P. Singh, K. M. Smith, T. G. Spiro. *J. Am. Chem. Soc.,* **1993,** *115,* 12446-12458.

[81] G. Niaura, A. K. Gaigalas, V. L. Vilker. *J. Electroanal. Chem.,* **1996,** *416,* 167-178.

[82] G. Liu, C. A. Grygon, T. G. Spiro. *Biochemistry,* **1989,** *28,* 5046-5050.

[83] A. Krolikowska, J. Bukowska. *J. Raman. Spectrosc.,* **2010,** *41,* 1621-1631.

[84] M. J. Tarlov, E. F. Bowden. *J. Am. Chem. Soc.,* **1991,** *113,* 1847-1849.

[85] M. Collinson, E. F. Bowden. *Langmuir,* **1992,** *8,* 1247-1250.

[86] D. H. Murgida, P. Hildebrandt. *J. Phys. Chem. B,* **2001,** *105,* 1578-1586.

[87] D. J. F. Chinnapen, D. Sen. *Biochemistry,* **2002,** *41,* 5202-5212.

[88] Q. Shi, W.-B. Cai, D. A. Scherson. *J. Phys. Chem. B,* **2004,** *108,* 17281-17284.

[89] Q. Zhao, X.-F. Li, X. C. Le. *Anal. Chem.,* **2008,** *80,* 3915-3920.

[90] J.-M. Liu, X.-P. Yan. *J. Anal. At. Spectrom.,* **2011,** *26,* 1191-1197.

[91] J. F. C. Loo, P. M. Lau, H. P. Ho, S. K. Kong. *Talanta,* **2013,** *115,* 159-165.

[92] C. Ocana, E. Arcay, M. del Valle. *Sensor Actuat. B-Chem.,* **2014,** *191, 860-865.*

[93] Y. Xia, P. Gao, X. Qiu, Q. Xu, S. Gan, H. Yang, S. Huang. *Analyst,* **2012,** *37,* 5705-5709.

[94] K. Gupta, I. Verma, G. Khuller, R. Mahajan. *Indian J. Med. Microbiol.,* **2010,** *28,* 221-226.

[95] G. S. Lukat-Rodgers, N. L. Wengenack, F. Rusnak, K. R. Rodgers. *Biochemistry,* **2000,** *39,* 9984-9993.

[96] S. Kapetanaki, S. Chouchane, S. Girotto, S. Yu, R. S. Magliozzo, J. P. M. Schelvis. *Biochemistry,* **2003,** *42,* 3835-3845.

[97] S. M. Kapetanaki, S. Chouchane, S. Yu, R. S. Magliozzo, J. P. M. Schelvis. *J. Inorg. Biochem.,* **2005,** *99,* 1401-1406.

[98] G. Smulevich, C. Jakopitsch, E. Droghetti, C. Obinger. *J. Inorg. Biochem.,* **2006,** *100, 568-585.*

[99] N. L. Wengenack, H. Lopes, M. J. Kennedy, P. Tavares, A. S. Pereira, I. Moura, J. J. G. Moura, F. Moura. *Biochemistry,* **2000,** *39,* 11508-11513.

[100] L. S. Rotherham, C. Maserumule, K. Dheda, J. Theron, M. Khati. *PLOS One,* **2012,** *7,* e46862.

[101] L. Qin, R. Zheng, Z. Ma, Y. Feng, Z. Liu, H. Yang, J. Wang, R. Jin, J. Lu, Y. Ding, Z. Hu. *Clin. Chem. Lab. Med.,* **2009,** *47,* 405-411.

[102] Y. Kang, M. Si, R. Liu, S. Qiao. *J. Raman Spectrosc.,* **2010,** *41,* 614-617.

[103] Y. Kang, M. Si, Y. Zhu, L. Miao, G. Xu. *Spectrochim. Acta A,* **2013,** *108,* 177-180.

[104] D. Drescher, T. Buchner, D. McNaughton, J. Kneipp. *Phys. Chem. Chem. Phys.,* **2013,** *15,* 5364-5373.

[105] A. Smekal. *Naturwissenschaften,* **1923,** *11,* 873-875.

[106] C. V. Raman, K. S. Krishnan. *Nature*, **1928,** *121,* 501-502.

[107] G. Turrell. The Raman Effect. In *Raman microscopy: Developments and Applications.* Eds. G. Turrell, J. Corset; Academic Press Limited: London, 1996.

[108] M. Fleishmann, P. J. Hendra, A. J. McQuillan. *Chem. Phys. Lett.,* **1974,** *26,* 163-166.

[109] D. L. Jeanmaire, R. P. Van Duyne. *J. Electroanal. Chem.,* **1977,** *84,* 1-20.

[110] M. G. Albrecht, J. A. Creighton. *J. Am. Chem. Soc.,* **1977,** *99,* 5215-5217.

[111] E. C. Le Ru, E. Blackie, M. Meyer, P. G. Etchegoin. *J. Phys. Chem. C,* **2007,** *111,* 13794-13803.

[112] R. Aroca. *Surface-Enhanced Vibrational Spectroscopy.* John Wiley & Sons, Ltd.: Chichester, 2006.

[113] C. A. Murray, D. L. Allara. *J. Phys. Chem.,* **1982,** *76,* 751-752.

[114] A. Otto. *J. Raman. Spectroc.,* **2005,** *36,* 497-509.

[115] D.-Y. Wu, J.-F. Li, B. Ren, Z.-Q. Tian. *Chem. Soc. Rev.,* **2008,** *37,* 1025-1041.

[116] H. B. Aguiar, A. C. Sant'Ana, M. L. A. Temperini, P. Corio, F. Cunha. *Vib. Spectrosc.,* **2006,** *40,* 127-132.

[117] S. G. Harroun, T. J. Abraham, C. Prudhoe, Y. Zhang, P. J. Scammells, C. L. Brosseau, C. C. Pye, R. D. Singer. *Phys. Chem. Chem. Phys.,* **2013,** *15,* 19205-19212.

[118] J. Wang. *Analytical Electrochemistry,* 2nd ed.; John Wiley & Sons: New York, 2000.

[119] A. J. Bard, L. R. Faulkner. *Electrochemical Methods: Fundamentals and Applications,* 2nd ed.; John Wiley & Sons, Inc.: New York, 2001.

[120] R. Stoltenburg, C. Reinemann, B. Strehlitz. *Biomol. Eng.,* **2007,** *24,* 381-403.

[121] J. Feigon, T. Dieckmann, F. W. Smith. *Chem. Biol.,* **1996,** *3,* 611-617.

[122] C. Tuerk, L. Gold. *Science,* **1990,** *249,* 505-510.

[123] A. D. Ellington, J. W. Szostak. *Nature,* **1990,** *346,* 818-822.

[124] A D. Ellington, J. W. Szostak. *Nature,* **1992,** *355,* 850-852.

[125] C. J. Sandroff, D. R. Herschbach. *J. Phys. Chem.,* **1982,** *86,* 3277-3279.

[126] M. Venkataramanan, G. Skanth, K. Bandyopadhyay, K. Vijayamohanan, T. Pradeep. *J. Colloid Interface Sci.,* **1999,** *212,* 553-561.

[127] M. Takahashi, M. Fujita, M. Ito. *Surf. Sci.,* **1985,** *158,* 307-313.

[128] T. H. Joo, K. Kim, M. S. Kim. *J. Mol. Struct.,* **1987,** *162,* 191-200.

[129] Y.-S. Li, Y. Wang, J. S. Church, F. Garzena, Z. Zhang, D. An. *Spectrochim. Acta, Part A,* **2003,** *59,* 1791-1798.

[130] I. Matulaitiene, Z. Kuodis, O. Eicher-Lorka, G. Niaura. *J. Electroanal. Chem.,* **2013,** *700,* 77-85.

[131] M. I. Pividori, A. Merkoci, S. Alegret. *Biosens. Bioelectron.,* **2000,** *15,* 291-303.

[132] C. Otto, T. J. J. van den Tweel, F. F. M. de Mul, J. Greve. *J. Raman Spectrosc.,* **1986,** *17,* 289-298.

[133] A. Barhoumi, D. Zhang, F. Tam, N. J. Halas. *J. Am. Chem. Soc.,* **2008,** *130,* 5523-5529.

[134] L. Q. Dong, J. Z. Zhou, L. L. Wu, P. Dong, Z. H. Lin. *Chem. Phys. Lett.,* **2002,** *354,* 458-465.

[135] S. O. Kelley, J. K. Barton, N. M. Jackson, L. D. McPherson, A. B. Potter, E. M. Spain, M. J. Allen, M. G. Hill. *Langmuir,* **1998,** *14,* 6781-6784.

[136] A. Rygula, K. Majzner, K. M. Marzec, A. Kaczor, M. Pilarczyk, M. Baranska. *J. Raman Spectrosc.,* **2013,** *44,* 1061-1076.

[137] D. Kurouski, T. Postiglione, T. Deckert-Gaudig, V. Deckert, I. K. Lednev. *Analyst,* **2013,** *138,* 1665-1673.

[138] E. S. Grabbe, R. P. Buck. *J. Am. Chem. Soc.,* **1989,** *111,* 8362-8366.

[139] X. X. Han, B. Zhao, Y. Ozaki. *Anal. Bioanal. Chem.,* **2009,** *394,* 1719-1727.

[140] T. W. Wiegand, P. B. Williams, S. C. Dreskin, M.-H. Jouvin, J.-P. Kinet, D. Tasset. *J. Immunol.,* **1996,** *157,* 221-230.

[141] D. J. F. Chinnapen, D. Sen. *Biochemistry,* **2002,** *41,* 5202-5212.

[142] A. M. Robinson, S. G. Harroun, J. Bergman, C. L. Brosseau. *Anal. Chem.,* **2012,** *84,* 1760-1764.

[143] P. C. Lee, D. Meisel. *J. Phys. Chem.*, **1982**, *86*, 3391-3395.

[144] L. Zhao, K. Ding, X. Ji, J. Li, H. Wang, W. Yang. *Colloids Surf., A*, **2011,** *386,* 172-178.

[145] S. Basu, S. Jana, S. Pande, T. Pal. *J. Colloid Interface Sci.,* **2008,** *321,* 288-293.

[146] J. Kundu, O. Neumann, B. G. Janesko, D. Zhang, S. Lal, A. Barhoumi, G. E. Scuseria, N. J. Halas.

[147] J. S. Suh and M. Moskovits. *J. Am. Chem. Soc.,* **1986,** *108,* 4711-4718.

[148] P. Negri, R. A. Dluhy. *Analyst,* **2013,** *138,* 4877-4884.

[149] J. Duguid, V. A. Bloomfield, J. Benevides, G. J. Thomas, Jr. *Biophys. J.,* **1993,** *65,* 1916-1928.

[150] M. Rycenga, J. M. McLellan, Y. Xia. *Chem. Phys. Lett.,* **2008,** *463,* 166-171.

[151] T. Watanabe, H. Maeda. *J. Phys. Chem.,* **1989,** *93,* 3258-3260.

[152] Y. Chen, L. Wu, Y. Chen, N. Bi, X. Zheng, H. Qi, M. Qin, X. Liao, H. Zhang, Y. Tian. *Microchim Acta,* **2012,** *177,* 341-348.

[153] P. Hildabrandt, M. Stockburger. *J. Phys. Chem.*, **1986,** *90,* 6017-6024.

[154] G. Socrates, *Infrared and Raman Characteristic Group Frequencies*, John Wiley & Sons, Ltd., Chichester, 2001

[155] A. Kudelski. *Vib. Spectrosc.,* **2008,** *46,* 34-38.

[156] J. N. Murphy, A. K. H. Cheng, H.-Z. Yu, D. Bizzotto. *J. Am. Chem. Soc.,* **2009,** *131,* 4042-4050.

[157] F. P. Nicoletti, E. Droghetti, L. Boechi, A. Bonamore, N. Sciamanna, D. A. Estrin, A. Feis, A. Boffi, G. Smulevich. *J. Am. Chem. Soc.,* **2011,** *133,* 20970-20980.

[158] E. Droghetti, F. P. Nicoletti, A. Bonamore, N. Sciamanna, A. Boffi, A. Feis, G. Smulevich. *J. Inorg. Biochem.,* **2011,** *105,* 1338–1343.

[159] J. F. Cerda, M. H. Roeder, D. N. Houchins, C. X. Guzman, E. J. Amendola, J. D. Castorino, A. L. Fritz. *Anal. Biochem.,* **2013,** *443,* 75-77.

[160] T. Imamura, Y. Mizukoshi, T. Ishiyama, and A. Morita. *J. Phys. Chem. C,* **2012,** *116,* 11082-11090.

[161] E. J. Liang, C. Engert, W. Kiefer. *Vib. Spectrosc.,***1995,** *8,* 435-444.

[162] L. A. Dick, A. J. Haes, R. P. Van Duyne. *J. Phys. Chem. B,* **2000,** *104,* 11752-11762.

[163] L. A. Gearheart, H. J. Ploehn, C. J. Murphy. *J. Phys. Chem. B,* **2001,** *105,* 12609-12615.

[164] M. K. Beissenhirtz, E. Leupold, W. Stöcklein, U. Wollenberger, O. Pänke, F. Lisdat, F. W. Scheller. Aptamers: Hybrids Between Nature and Technology. In *Aptamers in Bioanalysis.* Ed. M. Mascini; Wiley: New Jersey, 2009.